

**AN INTERPRETATION OF THE
RESULTS OF A STUDY OF HEAVY MINERALS
IN MINNESOTA NORTHEASTERN-PROVENANCE
GLACIOFLUVIAL SEDIMENTS**

REPORT 284-1

1997

***A COOPERATIVE PROJECT
WITH THE UNITED STATES GEOLOGICAL SURVEY***



**MINNESOTA DEPARTMENT OF NATURAL RESOURCES
DIVISION OF MINERALS**

AN INTERPRETATION OF THE
RESULTS OF A STUDY OF HEAVY MINERALS
IN MINNESOTA NORTHEASTERN-PROVENANCE
GLACIOFLUVIAL SEDIMENTS

REPORT 284-1

1997

S.L. Nelson Russell*, P.K. Theobald**,
J.D. Lehr***, R.L. Johnson***, J.L. Ryder**, and T.L. Lawler*

* Minnesota DNR, Division of Minerals, Hibbing and *** St. Paul

** U.S.G.S., Geochemical Branch, Denver, Colorado

*A Cooperative Project
With the United States Department of the Interior
Geological Survey*

MINNESOTA DEPARTMENT OF NATURAL RESOURCES
DIVISION OF MINERALS
WILLIAM C. BRICE, DIRECTOR

This report is available at various libraries in Minnesota and at the U.S. Geological Survey library in Denver, Colorado. It may be purchased at the Hibbing office, DNR Minerals Division; for further information contact Mineral Resources Geologist at (218)262-6767.

Neither the State of Minnesota nor the Department of Natural Resources, nor any of their employees, nor any of their contractors, subcontractors, or their employees, makes any warranty, express or implied, or assumes any legal liability or responsibility for the accuracy, completeness or usefulness of any information, apparatus, product or process disclosed, or represents that its use would not infringe privately owned rights.

Reference to a Company or Product name does not imply approval or recommendation of the product by the State of Minnesota or the Department of Natural Resources to the exclusion of others that may meet specifications.

TABLE OF CONTENTS

ACKNOWLEDGMENTS	ix
INTRODUCTION	1
Geologic Setting	4
Precambrian Terranes	12
Middle Archean Gneiss Terrane	12
Late Archean Greenstone-Granite Terrane	12
Early Proterozoic Terrane	14
Middle Proterozoic Midcontinent Rift Terrane	15
Preglacial Setting	16
Quaternary Geology	17
Pre-late Wisconsinan Glaciations	17
Late Wisconsinan Glaciations	18
Genetic Types of Glaciofluvial Deposits	18
Late Wisconsinan Glacial History	19
General Lithology of Glacial Sediments	24
RESULTS	27
Interpretative Methods	27
Bulk Concentrate Geochemical Results	31
Paramagnetic and Nonmagnetic Fraction Sample Weight	39
Paramagnetic Fraction Geochemical Results	44
Single-element Data in the Paramagnetic Fraction	44
Paired-element Correlations in the Paramagnetic Fraction	52
Multi-element Associations in the Paramagnetic Fraction	55
Nonmagnetic Fraction Geochemical Results	59
Single-element Data in the Nonmagnetic Fraction	59
Paired-element Correlations in the Nonmagnetic Fraction	77
Multi-element Associations in the Nonmagnetic Fraction	78
Correlations Between the Geochemical Data Sets	84
Nonmagnetic Fraction Mineralogical Results	88
DISCUSSION	96
Variation	96
Variation in the Heavy Minerals Related to the Glacial Lobe	96
Patterns of Anomalous values	97
Individual Sites with Extreme Characteristics	100
SUMMARY AND SPECULATION	103

REFERENCES	105
APPENDICES	Overlay maps in back cover pocket
Appendix A. Generalized Bedrock Geology	
Appendix B. Generalized Quaternary Geology	

ILLUSTRATIONS

Figure 1.	General location of study area in Minnesota	1
Figure 2.	Reference map showing the locations of specific geographic and geologic areas in Minnesota referred to in this report	3
Figure 3.	Minnesota's geographic position on the southwestern margin of the exposed Canadian Shield of the North American Craton	4
Figure 4.	Areas in Minnesota in which bedrock is at the surface or beneath less than 15 meters of glacial sediments	4
Figure 5.	Generalized bedrock geology in Minnesota	6
Figure 6.	Simplified tectonic map of Minnesota	10
Figures 7-15.	Ice movements associated with late Wisconsinan glaciation in Minnesota	
Figure 7.	Early late-Wisconsinan advance from the northeast	21
Figure 8.	Early late-Wisconsinan advance from the northwest	21
Figure 9.	Alexandria phase	21
Figure 10.	Recession from the Alexandria moraine complex	21
Figure 11.	St. Croix phase	23
Figure 12.	St. Croix phase recession	23
Figure 13.	Superior lobe readvance to the Mille Lacs moraine, Rainy lobe recession, and readvance of the Des Moines lobe	23
Figure 14.	Recession of the Rainy and Superior lobes and readvance of the Des Moines lobe	23
Figure 15.	Recession of the Rainy and Superior lobes and advance of the St. Louis sublobe	24
Figure 16.	Geographic location of the sample sites for the heavy-mineral study	28
Figure 17.	Generalized Quaternary geology in Minnesota, with sample localities identified by the specific glacial sediment type collected	29

Figure 18.	Frequency and geographic distribution of gold in samples of the heavy-mineral concentrates	32
Figure 19.	Frequency and geographic distribution of platinum in samples of the heavy-mineral concentrates	34
Figure 20.	Frequency and geographic distribution of palladium in samples of the heavy-mineral concentrates	35
Figure 21.	Frequency distribution of platinum in samples of the heavy-mineral concentrates grouped by glacial sediment type	36
Figure 22.	Frequency distribution of palladium in samples of the heavy-mineral concentrates grouped by glacial sediment type	36
Figure 23.	Geographic distribution of ruthenium in samples of the heavy-mineral concentrates	37
Figure 24.	Geographic distribution of iridium, osmium and rhodium in samples of the heavy-mineral concentrates	38
Figure 25.	Geographic distribution of the sample weights of the paramagnetic-fraction (C2) samples shown in percent weight of the minus-20-mesh material	40
Figure 26.	Geographic distribution of the sample weights of the paramagnetic-fraction (C2) samples shown in percent weight of the heavy-mineral concentrate	41
Figure 27.	Geographic distribution of the sample weights of the nonmagnetic-fraction (C3) samples shown in parts-per-million of the minus-20-mesh material	42
Figure 28.	Geographic distribution of the sample weights of the nonmagnetic-fraction (C3) samples shown in percent weight of the heavy-mineral concentrate	43
Figure 29.	Geographic distribution of beryllium in samples of the paramagnetic fraction (C2) of the heavy-mineral concentrates	45
Figure 30.	Geographic distribution of silver, molybdenum, tin, and thorium in samples of the paramagnetic fraction (C2) of the heavy-mineral concentrates	46
Figure 31.	Frequency distribution of magnesium, nickel, cobalt, lanthanum, yttrium, lead, and boron in samples of the paramagnetic-fraction (C2) of the heavy-mineral concentrates	47
Figure 32.	Frequency distribution of gallium, barium, calcium, manganese, and strontium in samples of the paramagnetic fraction (C2) of the heavy-mineral concentrates	48
Figure 33.	Frequency distribution of chromium, scandium, copper, and zirconium in samples of the paramagnetic fraction (C2) of the heavy-mineral concentrates	49
Figure 34.	Paired-element correlation coefficients for 19 elements observed in samples of the paramagnetic fraction (C2) of the heavy-mineral concentrates	53

Figure 35.	Geographic distribution of the high and low normalized sum values of chromium and lanthanum in samples of the paramagnetic fraction (C2) of the heavy-mineral concentrates	54
Figure 36.	Frequency and geographic distribution of the high and low factor scores for Factor I of the two-factor model, which represents the multi-element associations among Mg, Ni, Co, -La, -Y, -Pb, and -B in samples of the paramagnetic fraction (C2) of the concentrates	56
Figure 37.	Frequency and geographic distribution of the high and low factor scores for Factor II of the two-factor model, which represents the multi-element associations among Ga, Ba, Ca, Mn, Sr, Y, Cr, B, Pb, and -Sc in samples of the paramagnetic fraction (C2) of the concentrates	57
Figure 38.	Geographic distribution of copper in samples of the paramagnetic fraction (C2) of the heavy-mineral concentrates	58
Figure 39.	Geographic distribution of nickel in samples of the nonmagnetic fraction (C3) of the heavy-mineral concentrates	60
Figure 40.	Geographic distribution of cobalt in samples of the nonmagnetic fraction (C3) of the heavy-mineral concentrates	61
Figure 41.	Geographic distribution of gold in samples of the nonmagnetic fraction (C3) of the heavy-mineral concentrates	62
Figure 42.	Geographic distribution of silver in samples of the nonmagnetic fraction (C3) of the heavy-mineral concentrates	63
Figure 43.	Geographic distribution of molybdenum in samples of the nonmagnetic fraction (C3) of the heavy-mineral concentrates	65
Figure 44.	Geographic distribution of tungsten in samples of the nonmagnetic fraction (C3) of the heavy-mineral concentrates	66
Figure 45.	Geographic distribution of bismuth in samples of the nonmagnetic fraction (C3) of the heavy-mineral concentrates	67
Figure 46.	Geographic distribution of zinc, copper, antimony, thorium, and associated element values in samples of the nonmagnetic fraction (C3) of the heavy-mineral concentrates	68
Figure 47.	Frequency and geographic distribution of lead in samples of the nonmagnetic fraction (C3) of the heavy-mineral concentrates	69
Figure 48.	Frequency distribution of tin, scandium, and boron in samples of the nonmagnetic fraction (C3) of the heavy-mineral concentrates	70
Figure 49.	Frequency distribution of phosphorus, calcium, yttrium, and lanthanum in samples of the nonmagnetic fraction (C3) of the heavy-mineral concentrates ...	71
Figure 50.	Frequency distribution of magnesium, manganese, and iron in samples of the nonmagnetic fraction (C3) of the heavy-mineral concentrates	72

Figure 51.	Frequency distribution of strontium, chromium, and gallium in samples of the nonmagnetic fraction (C3) of the heavy-mineral concentrates	72
Figure 52.	Frequency distribution of barium, sodium, niobium, vanadium, and beryllium in samples of the nonmagnetic fraction (C3) of the heavy-mineral concentrates	73
Figure 53.	Geographic distribution of tin in samples of the nonmagnetic fraction (C3) of the heavy-mineral concentrates	74
Figure 54.	Geographic distribution of beryllium in samples of the nonmagnetic fraction (C3) of the heavy-mineral concentrates	75
Figure 55.	Paired-element correlation coefficients for 25 elements observed in samples of the nonmagnetic fraction (C3) of the heavy-mineral concentrates	79
Figure 56.	Frequency and geographic distribution of the high and low factor scores for Factor I of the six-factor model, which represents the multi-element associations among Sn, Y, Sc, and B in samples of the nonmagnetic fraction (C3) of the heavy-mineral concentrates	81
Figure 57.	Frequency and geographic distribution of the high and low factor scores for Factor II of the six-factor model, which represents the multi-element associations among P, Ca, Y, La, and -Fe in samples of the nonmagnetic fraction (C3) of the heavy-mineral concentrates	82
Figure 58.	Frequency and geographic distribution of the high and low factor scores for Factor III of the six-factor model, which represents the multi-element associations among Mg, Mn, B, and Fe in samples of the nonmagnetic fraction (C3) of the heavy-mineral concentrates	83
Figure 59.	Frequency and geographic distribution of the high and low factor scores for Factor IV of the six-factor model, which represents the multi-element associations between Sr and Fe in samples of the nonmagnetic fraction (C3) of the heavy-mineral concentrates	85
Figure 60.	Frequency and geographic distribution of the high and low factor scores for Factor V of the six-factor model, which represents the multi-element associations among Cr, Ga, Sc, and Mn in samples of the nonmagnetic fraction (C3) of the heavy-mineral concentrates	86
Figure 61.	Frequency and geographic distribution of the high and low factor scores for Factor VI of the six-factor model, which represents the multi-element associations between Ga and Cr in samples of the nonmagnetic fraction (C3) of the heavy-mineral concentrates	87
Figure 62.	Geographic distribution of gold particles visually observed in samples of the nonmagnetic fraction (C3) of the heavy-mineral concentrates	89
Figure 63.	Geographic distribution of scheelite and powellite visually observed in samples of the nonmagnetic fraction (C3) of the heavy-mineral concentrates	90

Figure 64.	Geographic distribution of pyrite visually observed in samples of the nonmagnetic fraction (C3) of the heavy-mineral concentrates	91
Figure 65.	Geographic distribution of cassiterite and the extreme values of andalusite and sillimanite visually observed in samples of the nonmagnetic fraction (C3) of the heavy-mineral concentrates	93
Figure 66.	Geographic distribution of apatite visually observed in samples of the nonmagnetic fraction (C3) of the heavy-mineral concentrates	94
Figure 67.	Geographic distribution of tourmaline visually observed in samples of the nonmagnetic fraction (C3) of the heavy-mineral concentrates	95
Figure 68.	Geographic location of the individual sample sites with extreme characteristics	101

TABLES

Table 1.	Summary of frequency distribution data for the 35 elements analyzed in the samples of the paramagnetic fraction (C2) of the heavy-mineral concentrates	50
Table 2.	Summary of elements that show a significant difference in their means between samples from the various glacial lobes in the paramagnetic fraction (C2) of the concentrates	51
Table 3.	Summary of frequency distribution data for 35 elements analyzed in the samples of the nonmagnetic fraction (C3) of the heavy-mineral concentrates	76
Table 4.	Summary of elements that show a significant difference in their means between samples from the various glacial lobes in the nonmagnetic fraction (C3) of the concentrates	77

ACKNOWLEDGEMENTS

Mr. Henk Dahlberg, Minnesota Department of Natural Resources, Division of Minerals, Hibbing, initiated this project and opened the doors that led to the cooperative involvement of the U.S. Geological Survey. His enthusiasm and support for this project has been invaluable.

We are grateful for the support of this project by the U.S. Department of the Interior, Geological Survey, with special thanks to Mr. Glenn H. Allcott, Office of Mineral Resources, Reston, Virginia and Dr. Dave Smith, Branch of Geochemistry, Denver, Colorado.

The geochemical and mineralogical analyses on the heavy-mineral-concentrate samples were performed at the U.S. Geological Survey, Branch of Geochemistry laboratories in Denver, Colorado by Mr. Stephen J. Sutley (semiquantitative emission spectroscopy and x-ray diffraction); Mr. Richard B. Tripp (binocular microscopy); and Mr. Bob Carlson, Ms. Betty Adrian, and Mr. Al Meier (fire assay). These individuals brought expertise in heavy-mineral concentration and analysis to this project, and we have been very fortunate to have them as part of our team.

Many other individuals offered assistance and suggestions throughout the course of this study, and we thank them for their contributions. This includes: Mr. Dale Cartwright, Mr. Dennis Martin, and Mr. Barry Frey, all with the MN DNR, Division of Minerals; and Mr. Ted Botinelli and Mr. Steve Smith, both with the U.S. Geological Survey, Branch of Geochemistry, Denver, Colorado.

We would also like to thank the Minnesota Geological Survey, St. Paul, for providing us with the digital files of their 1994 bedrock geology map (Morey, 1994), which we modified to produce a generalized map version for this report.



INTRODUCTION

This report presents an interpretation of the results of a study that analyzed the heavy-mineral content of samples collected in Minnesota northeastern-provenance glaciofluvial sediments. Since its inception, this study has been a cooperative project between the U.S. Geological Survey, Branch of Geochemistry, Colorado, and the Minnesota Department of Natural Resources, Division of Minerals. The project began with an eight-sample test study to determine whether there was enough geochemical and mineralogical variation in the heavy-mineral content of surficial glaciofluvial sediments to observe differences between samples. Test study results showed substantial variation between samples, which led to an eighty-sample pilot study to evaluate whether this variation would show any anomalous values or geographic distribution patterns that could be related to inferred regional bedrock or glacial geology.

The study area traverses Minnesota from the northeast to the southwest and encompasses an area approximately 60 miles wide by 230 miles long (Fig. 1). This area lies on the southern edge of the Canadian Shield and includes several of Minnesota's Precambrian bedrock terranes. Unique lithologic, tectonic, and structural characteristics of the various terranes create an area with diverse mineral potential. The northeast-southwest orientation of the study area was chosen because it is parallel to the major glacial flow and includes glacial sediments with a variety of genetic origins, glacial transport paths, and glacial and fluvial transport distances.

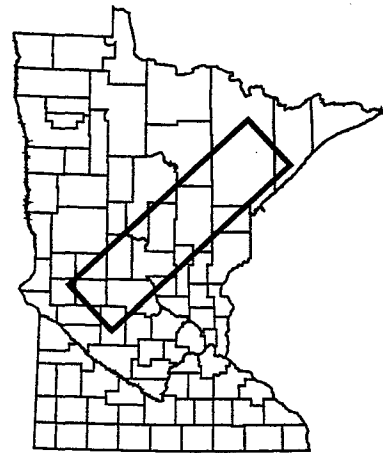


Figure 1. General location of study area in Minnesota.

Within the study area the primary sampling strategy was to collect samples from late Wisconsinan northeastern-provenance glaciofluvial sand and gravel deposits; these deposits have been sorted by currents, which removed most of the silt and clay and produced some concentration of heavy minerals. Preference was given to sites where the depth to bedrock was 100 feet or less, because glacial sediments in these areas are more likely to reflect regional bedrock. Most samples were collected in gravel pits; with sampling preference given to ice-contact stratified sediments over outwash sediments.

Heavy minerals comprise those minerals which have a specific gravity that is usually higher than that of the more common rock-forming minerals and usually includes most of the ore minerals. For this study, approximately 6 liters of minus-10-mesh (2mm) material was collected at each sample site; a heavy-mineral concentrate with a specific gravity of ≥ 2.85 was prepared from the minus-20-mesh (0.83mm) fraction of each sample. Part of each heavy-mineral concentrate was separated by magnetic susceptibility into three heavy-mineral fractions.

Concentrate 1 (C1) or the ferromagnetic fraction consists of the strongly magnetic minerals, such as magnetite and ilmenite. Concentrate 2 (C2) or the paramagnetic fraction consists of most iron and manganese oxides and ferromagnesian silicate minerals. Concentrate 3 (C3) or the nonmagnetic fraction consists of most remaining oxides, sulfides, native metals, and other nonmagnetic ore minerals.

Geochemical analysis was performed on samples of the heavy-mineral concentrates (bulk concentrates) by utilizing fire assay methods to detect low levels of gold and the platinum group elements; and performed on samples of the paramagnetic and nonmagnetic fractions of the bulk concentrates by using semiquantitative emission spectroscopy to determine the concentrations of 37 elements. Mineralogical analysis was performed on samples of the nonmagnetic fraction of the bulk concentrates by utilizing binocular microscopy, shortwave ultraviolet light, and x-ray diffraction techniques.

Open-file Report 284 "Chemical and mineralogical analyses and geological characteristics of heavy minerals from glaciofluvial sediments in Minnesota" (Nelson and others, 1992) contains the geochemical and mineralogical data for the test- and pilot-study samples. The report also includes a discussion of the sampling strategy and collection techniques, the methods of sample preparation and analysis, and a description of the geologic characteristics of each site and sample.

Various interpretative methods were used as tools to look at the geochemical and mineralogical data sets generated in this study. The interpretative methods employed, the interpretative data results, and a discussion of these results is presented in this report. The interpretative data results revealed anomalous values and interesting geographic distribution patterns for many elements and minerals, many of which appear related to regional geologic characteristics. To support the discussion of the results, a geologic picture of the study area is first presented. This includes a summary of the Precambrian geologic setting describing the various geologic terranes and mineral potential, the preglacial setting, and the Quaternary geology describing the pre-late and late Wisconsinan glaciations, within the study area.

[Note: Figure 2 is a reference map which shows the locations of specific geographic and geologic areas in Minnesota that are referred to in this report.]

MINNESOTA LOCATIONS

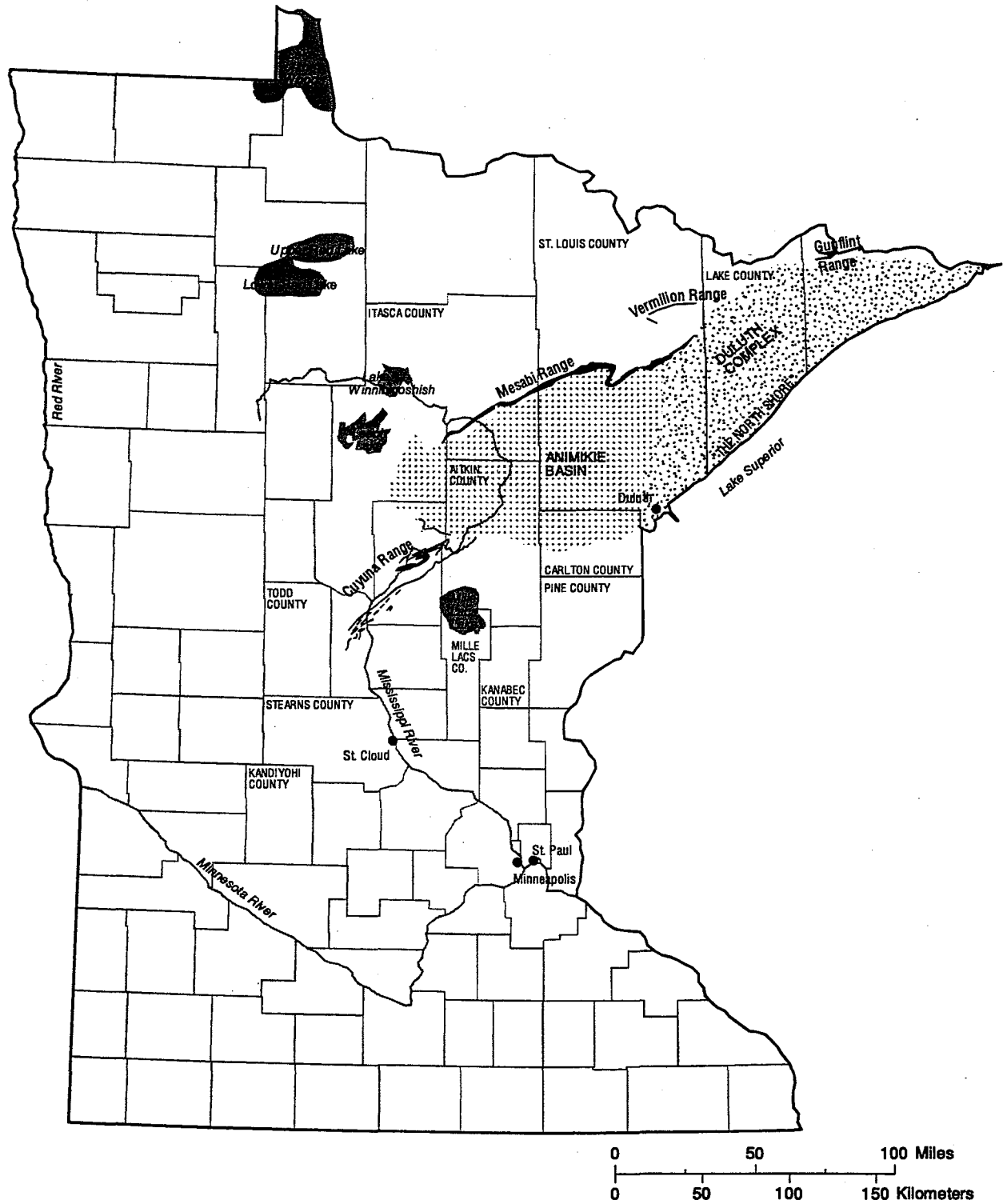


Figure 2. Reference map showing the locations of specific geographic and geologic areas in Minnesota referred to in the text.

GEOLOGIC SETTING

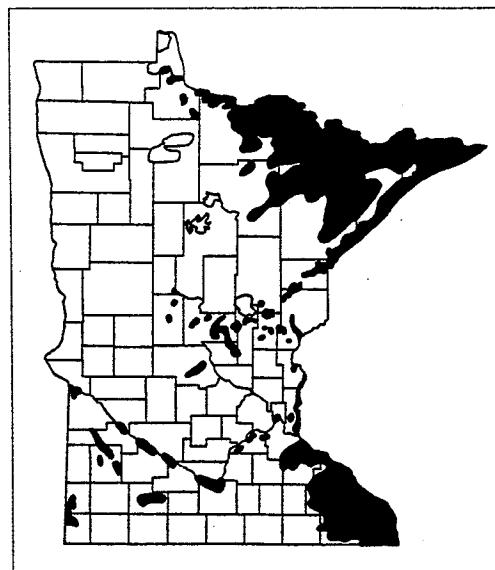
Minnesota sits astride two of North America's largest physiographic provinces—the Laurentian Upland, with its structurally complex Precambrian igneous, metamorphic, and sedimentary rocks and the Interior Lowland with its much younger Phanerozoic sedimentary rocks. The southern boundary of the Laurentian Upland essentially coincides with that of the exposed Canadian Shield of the North American craton (Fig. 3). Precambrian rocks underlie the entire state and are fairly well exposed in northeastern Minnesota. In the southern third of Minnesota, the Precambrian rocks are generally buried by a cover of sedimentary rocks—Paleozoic clastic and carbonate rocks in the southeast and Mesozoic clastic rocks in the southwest. In southwestern Minnesota, Precambrian rocks protrude through these younger sedimentary rocks.



Figure 3. Minnesota's geographic position on the southwestern margin of the exposed Canadian Shield of the North American Craton (modified from Morey, 1976).

Figure 4. Areas (shaded) in Minnesota where bedrock is at the surface or beneath less than 15 meters of glacial sediments (from Ojakangas and Matsch, 1982).

The distribution of bedrock outcrops in Minnesota is sparse, estimated at one percent of the area, and is unequally distributed across the state (Olsen and Mossler, 1982). Figure 4 shows the areas where bedrock is at the surface or beneath less than 15 meters of glacial sediments. Precambrian rock outcrops are most common in the northeastern part of the state and near the Mesabi Iron Range, and next most abundant in some areas of central Minnesota and the Minnesota and Mississippi river valleys. Paleozoic-rock outcrops are common in southeastern Minnesota. Bedrock geology in the study area is





GENERALIZED BEDROCK GEOLOGY

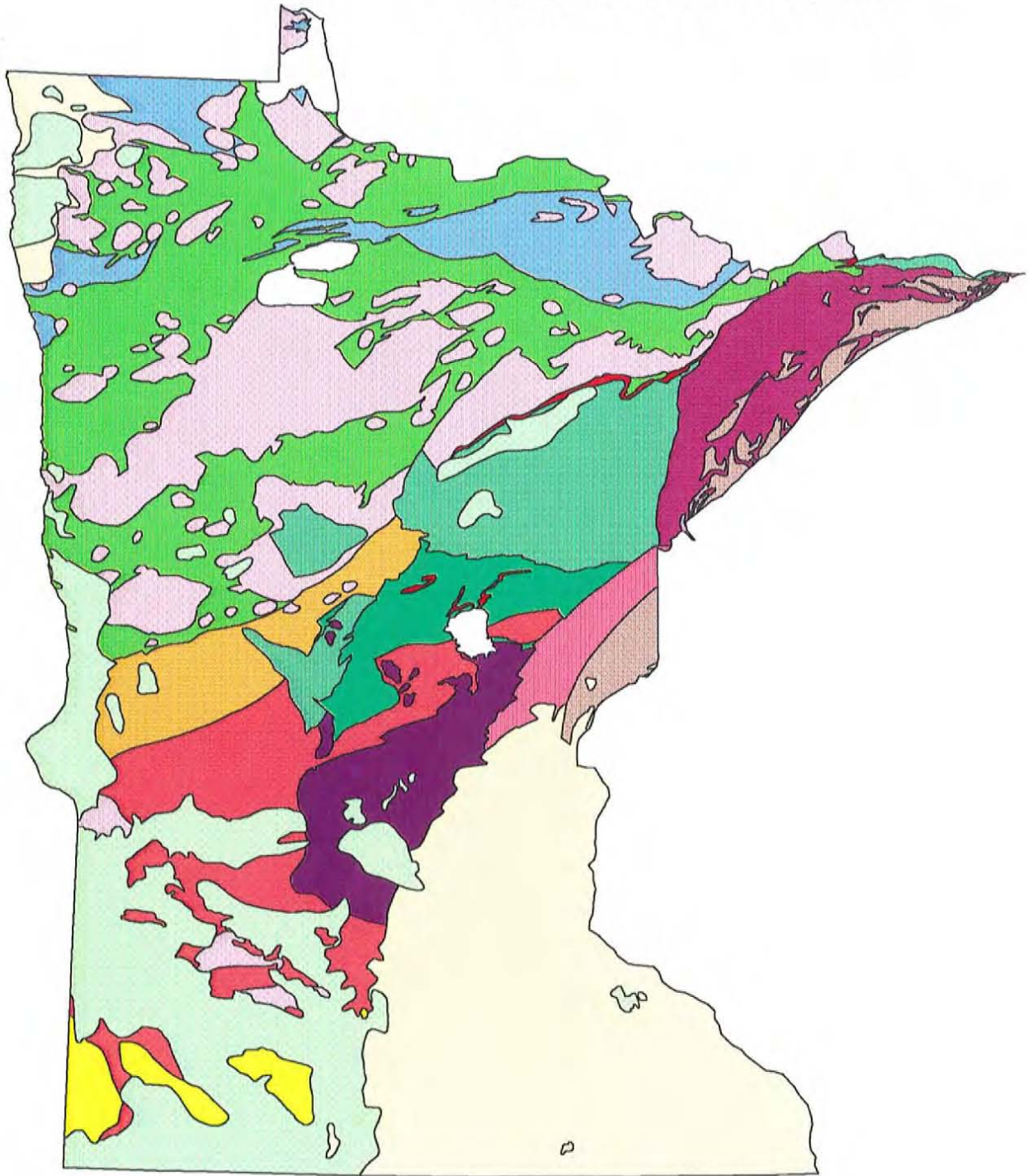



Figure 5. Generalized bedrock geology map of Minnesota. (Modified from Morey, G.B., compiler, 1994, Geologic map of Minnesota: bedrock geology, Minnesota Geologic Survey State Map Series S-20, scale 1:1,000,000.)

DESCRIPTION OF MAP UNITS




MESOZOIC ROCKS, UNDIVIDED (Jurassic to Cretaceous)

-  Dolomitic shale, mudstone, siltstone, sandstone, dolomite and gypsum






PALEOZOIC ROCKS, UNDIVIDED (Cambrian to Devonian)

-  Limestone, dolomite, sandstone and shale





MIDDLE PROTEROZOIC MIDCONTINENT RIFT TERRANE

-  SEDIMENTS -- Shale and arkosic sandstone overlain by quartz arenite
-  EXTRUSIVES -- Basalt, lesser rhyolite, and related volcanogenic & interflow sedimentary rocks
-  INTRUSIVES -- *Duluth Complex and Beaver Bay Complex* Gabbro and anorthositic gabbro and related rocks, troctolitic and gabbroic rocks, granite and granophyric felsic rocks, and subvolcanic mafic rocks

EARLY PROTEROZOIC TERRANE

-  SIOUX QUARTZITE -- Quartzite, lesser quartz-pebble conglomerates and claystone
-  INTRUSIONS OF THE PENOKEAN OROGEN -- Granites, lesser granodiorite, tonalite, and gabbro
-  ANIMIKIE GROUP CLASTIC SEDIMENTS -- Shale, siltstone, graywacke and associated volcanoclastic rocks, and mafic dikes and sills in northeastern Minnesota
-  MAJOR IRON-FORMATIONS
-  FOLD-AND-THRUST BELT METASEDIMENTS, METAVOLCANICS, AND SEDIMENTS -- Slate, metasiltstone, metagraywacke, metabasalt, diabase, lesser schists, shale, siltstone, quartz arenite, dolomite, iron-rich strata, argillite, schist, garnet-staurolite-schist, mudstone, graywacke, claystone, and mafic volcanic and hypabyssal rocks

LATE ARCHEAN GREENSTONE-GRANITE TERRANE

-  GRANITOID ROCKS -- Granite, granodiorite, monzonite, tonalite, diorite and monzodiorite
-  SCHIST- AND GRANITE-RICH MIGMATITE -- Paragneiss and schist-rich migmatite - grades into the metasedimentary rocks; granite-rich migmatite, including granite gneiss, paragneiss, schist, and migmatite - grades into granitoid rocks
-  VOLCANIC, SEDIMENTARY, AND RELATED ROCKS (GREENSTONE BELTS) -- Basalt, mafic to felsic volcanic sequences, iron formation, graywacke, slate, arenite, conglomerate, graphitic slate, felsic volcanogenic and volcanoclastic rocks, gabbro, peridotite, pyroxenite, and their metamorphic equivalents
-  ROCKS OF THE "QUIET ZONE" -- Deformed volcanic & volcanoclastic rocks, mica schist, phyllite, and granitoid rocks; these rocks lack magnetic signature

MIDDLE ARCHEAN GNEISS TERRANE

-  Migmatitic gneiss, amphibolite, granite, and migmatite



based largely on the interpretation of statewide geophysical data, supported by descriptive logs of widely scattered drill core and generally sparse outcrops. However, in some cases, large areas of inferred map units are not confirmed by any bedrock drill samples or outcrops.

A complicated mixture of lithologic units that span geologic time—from the Early Precambrian gneisses to the Cretaceous sediments—underlie the study area. Older units have undergone extensive deformation and have complex metamorphic patterns, while progressively younger rocks are relatively less deformed. Figure 5 (modified from Morey, 1994) shows the various bedrock terranes, which have been generalized, due to map scale, by grouping similar lithologic units or rock ages together. There are four general Precambrian terranes in the study area—the Middle Archean gneiss terrane, the Late Archean greenstone-granite terrane, the Early Proterozoic terrane, and the Middle Proterozoic Midcontinent Rift terrane. Each of these terranes has distinctive lithologic and structural characteristics.

An overview of the major tectonic events in Minnesota includes the following: 1) The growth of very old continental crust in southwestern Minnesota by 3,600 ma. 2) The development of a different continent in northern Minnesota during the Algonian orogenic episode—with its extensive folding, intrusions, and faulting events—produced the greenstone-granite terrane in the Superior Province around 2,700 ma. 3) The collision of these two continents occurred in west-central Minnesota during the late Archean, along a boundary called the Great Lakes Tectonic Zone (GLTZ). The older continent remained tectonically active into the Proterozoic era, while the continent on the north side of the GLTZ was relatively stable. 4) The Penokean orogeny occurred in east-central Minnesota at approximately 1,800 ma, virtually at the boundary of the two former continents. This mountain-forming event caused extensive folding and metamorphism of Early Proterozoic rocks, increasing metamorphic grade from north to south. 5) Major continental rifting occurred along the eastern side of the state at approximately 1,100 ma, and is known as part of the Midcontinental Rift System. Figure 6 is a simplified tectonic map of Minnesota which summarizes the major tectonic elements associated with the Precambrian terranes.

Elsewhere in the world such Precambrian terranes contain many different types of metallic mineral deposits. In Canada the rocks of the Canadian Shield contain significant mineral deposits. In Minnesota, the large areal extent of these geologic terranes strongly supports the idea of undiscovered metallic mineral deposits. Across Minnesota these terranes are largely buried by glacial sediments and in some areas, by Mesozoic and Paleozoic sedimentary rocks.

The present topography of Minnesota largely reflects the effects of the Pleistocene continental glaciation. A variety of landforms were produced as glacial ice eroded the bedrock and deposited materials of diverse lithology and provenance, ranging from 100 to greater than 400 feet thick (Olsen and Mossler, 1982) across much of the state. Samples for this study were collected in glacial sediments of northeastern provenance. At a regional scale, this study looked for relationships between the geochemical and mineralogical sample data and the lithologies of the various bedrock terranes that underlie the glacial sediments.

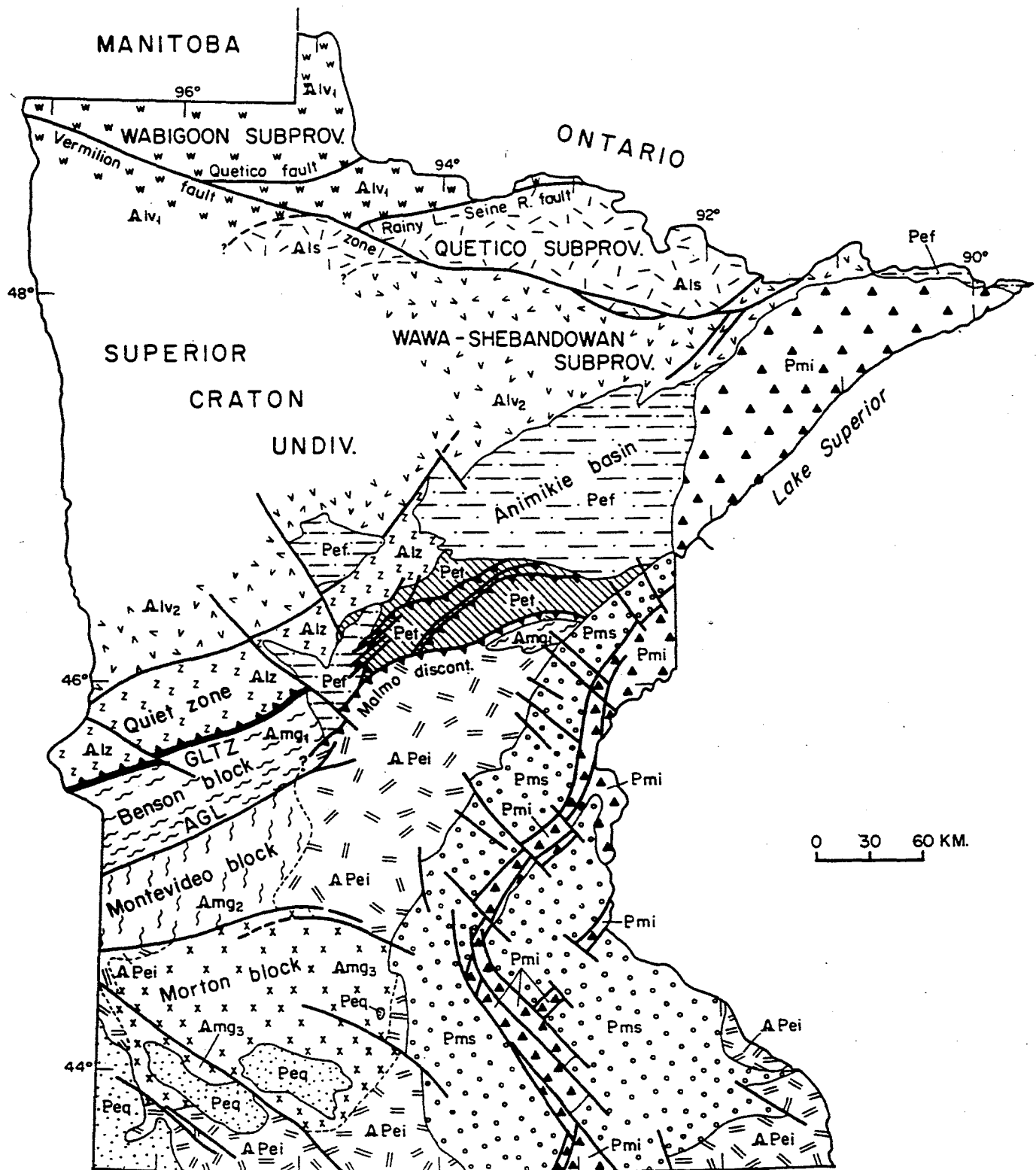


Figure 6. Simplified tectonic map of Minnesota (from Southwick and Morey, 1991)

EXPLANATION

MAJOR PRECAMBRIAN TERRANES OF MINNESOTA

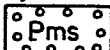


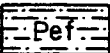


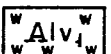
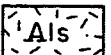
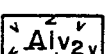
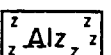
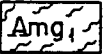
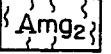

TECTONIC ELEMENT	PRINCIPAL ROCK TYPES	AGE
Midcontinent rift system		
late- and post-rift		Fluvial and lacustrine clastic sedimentary rocks
syn-rift		Basalt, rhyolite, gabbroic intrusions; minor interflow sedimentary deposits
<hr/>		
Sioux Quartzite basins		Fluvial, sand-dominated redbed sequences in basins that may be fault-controlled
<hr/>		
Penokean orogen		
foredeeps		Turbiditic graywacke-shale sequences
fold-and-thrust belt		Passive-margin metavolcanic and meta-sedimentary rocks, tectonically imbricated
intrusion-dominated magmatic terrane		Syn- to post-kinematic intrusions of granitoid rocks into complex metamorphic terrane
<hr/>		
Superior craton		
Greenstone-granite terrane		
Wabigoon subprovince		Arc-like volcanoplutonic sequences; syn- to post-kinematic granitoid intrusions
Quetico subprovince		Turbidite-dominated metasedimentary rocks (accretionary complex?); granitoid intrusions
Wawa-Shebandowan subprovince		Arc-like volcanoplutonic sequences; syn- to post-kinematic granitoid intrusions
"quiet zone"		Poorly known belt of rocks comparable to Wawa-Shebandowan; regionally retrograded
<hr style="border-top: 1px dashed black;"/>		
Gneiss terrane		
Benson block		Poorly known terrane composed of gneiss and abundant granitoid intrusions
Montevideo block		Amphibolite- to granulite-grade gneiss of plutonic and supracrustal derivation; granitoid intrusions
Morton block		
<div style="display: flex; align-items: center; justify-content: center;"> <div style="writing-mode: vertical-rl; transform: rotate(180deg); font-size: small; margin-right: 10px;">inferred sequence of tectonic accretion</div> <div style="font-size: 2em;">}</div> </div>		
Major structural discontinuities		
Malmo discontinuity (Early Proterozoic): Separates supracrustal panels of Penokean fold-and-thrust belt from deeper crustal zone to south		
Vermilion fault zone (late Archean): Obliquely cuts and displaces subprovince boundaries within the Superior craton		
Great Lakes tectonic zone (GLTZ; late Archean with probable Proterozoic reactivation): Separates high-grade gneissic terranes at southern margin of the Superior craton from classic greenstone-granite terranes of lower metamorphic grade on the north		
Appleton geophysical lineament (AGL; late Archean with probable Proterozoic reactivation): Separates Benson and Montevideo blocks in gneiss terranes		

Figure 6 continued. Explanation of units shown on simplified tectonic map (from Southwick and Morey, 1991).

Precambrian Terranes

Middle Archean Gneiss Terrane

The oldest Precambrian terrane (3,600 - 2,750 ma), the Middle Archean gneiss terrane, occurs in south-central to southwestern Minnesota (see Fig. 5). These rocks form an igneous/metamorphic terrane composed predominantly of migmatitic granitic gneisses and amphibolite, with younger intrusive Late Archean and Early Proterozoic granitic rocks (Morey, 1994 and 1993). The younger intrusives include quartz monzonites and tonalites to the southwest and granodiorite on the Mississippi River (Keighin and others, 1972). Within the study area this terrane is inferred to be dominantly of felsic composition. The gneisses generally display characteristics of amphibolite to granulite grade metamorphism (Sims and Morey, 1972).

It appears that this terrane has had a complex tectonic-igneous history and has been intensely metamorphosed at 3,050 and 2,600 ma, and intruded by igneous rocks at 2,600, 1,800, and 1,725 ma—remaining tectonically active into the middle of the Proterozoic era (Boerboom, 1994). The gneiss terrane consists of at least three distinct stratigraphic-tectonic blocks, which are bounded by zones of faulting and regional shear zones that are parallel to the Great Lakes Tectonic Zone in the study area (see Fig. 6) (Southwick and Morey, 1991).

This terrane is best exposed at several locations along the Minnesota River Valley; with a few exposures in Stearns, Mille Lacs, and Pine counties (Morey and Dahlberg, 1995). Little is known about the geology of this terrane beyond these exposures and there is very little hard data for this large area. Still this terrane is of particular interest to the economic geologist because it contains lithologic units, structural features, and metamorphic rank associated with a few world class gold and/or base metal deposits. Based on crude analogies, models for deposits of gold, silver, platinum-group elements, copper, nickel, cobalt, and zinc can be associated with this terrane. Significant laterite-type paleo-weathered deposits blanket part of this terrane, which could be overlying primary gold and base-metal deposits. Other than recent kaolin exploration, very little mineral exploration has occurred in this terrane.

Late Archean Greenstone-Granite Terrane

The next oldest Precambrian terrane, an extension of the Superior Province, occurs in northern to west-central Minnesota. In contrast to the Middle Archean gneiss terrane, a large volume of data is available for the Late Archean greenstone-granite terrane. The rocks in this terrane were involved in or emplaced during a major tectonic-igneous event (2,750 - 2,600 ma) that comprised multiple folding and low grade metamorphism of volcanic and volcanogenic sedimentary rocks, the intrusion of granitic batholiths, and subsequent faulting of these rocks. In northern Minnesota, these rocks are typical of the greenstone-granite complexes of the Canadian Shield.

On Figure 5 the Late Archean rocks are grouped into four simplified units—the rocks of the "quiet zone", the volcanic-sedimentary greenstone belts, the schist- and granite-rich migmatite belts, and the granitoid rocks. In west-central Minnesota, a zone of Late Archean rocks with

a relatively featureless geophysical expression is known as the "quiet zone" (see Fig. 5); these rocks lack magnetic signature because of regional low-grade alteration of oxides and ferromagnesian minerals (Morey, 1993). This zone includes felsic to intermediate volcanic and volcanoclastic rocks, mica schist, and granitoid rocks, all variably deformed cataclastically (Morey, 1994). In the northern half of Minnesota, volcanic and volcanogenic sedimentary complexes occur within northeastward trending belts—referred to as greenstone belts because of their characteristic greenschist facies metamorphism. The generalized greenstone belts shown in Figure 5 (modified from Morey, 1994) include three rock assemblages. 1) Mafic metavolcanic rocks—composed dominantly of basalt, but with thin sedimentary units, including iron-formation and their metamorphic equivalents. 2) Mixed metavolcanic rocks—mafic to felsic volcanic sequences with variable amounts of felsic volcanogenic and volcanoclastic rocks and lean iron-formation. 3) Metasedimentary rocks—dominantly graywacke, also slate, arenite, fine-grained felsic volcanogenic and volcanoclastic rocks and their metamorphic equivalents. Across the extreme northern part of Minnesota, belts typically contain strongly deformed units of migmatite and a large proportion of granite (see Fig. 5). These belts are composed of two units: 1) paragneiss and schist-rich migmatite; and 2) granite-rich migmatite that includes granite gneiss, paragneiss, schist, and migmatite. About 2,650 ma, the greenstone belts were intruded by large batholiths of granite and related coarse-grained granitoids (see Fig. 5). After the solidification of the batholiths, the terrane was subjected to stresses causing movement along numerous faults (see Fig. 6). Within the greenstone belts the metamorphism is generally greenschist facies, but increases to middle-amphibolite facies adjacent to the plutons (Sims and Morey, 1972).

Archean, Algoma-type iron deposits occurring in the Vermilion greenstone belt have been mined on the Vermilion Range of northeastern Minnesota. These deposits contained high grade hematite ores, which occurred on a broad, steep-limbed, southward-overturned anticlinal fold near the northeastern side of the Vermilion greenstone belt.

The Late Archean greenstone belts and the major fault zones within them have attracted exploration interest because of their geologic similarity to gold and base metal mining camps in Canada and elsewhere. Based upon good analogies, there are models for deposits of gold, silver, copper, zinc, lead, molybdenum, nickel, chromium, platinum group elements, and iron in this terrane. In the western half of the state, high grade supergene enrichment zones may occur in preserved weathering profiles.

Considerable exploration has occurred in an area known as the Virginia Horn (near the southeast edge of the greenstone-granite terrane), where visible gold has been found in an outcrop of quartz porphyry, which intrudes faulted metavolcanics/metasediments. A cursory examination of exploration records show drill core assays up to 22.23 ppm gold and outcrop assays up to 740 ppb gold (MN DNR, General Assessment Files).

A recent study found anomalous metal assay values in soil samples overlying this terrane. Just to the west of the Vermilion Range, gold values ranging from <1 ppb to 1,100 ppb and zinc anomalies to 1,000 ppm were found in surface soils (Alminas and others, 1992).

Early Proterozoic Terrane

In Early Proterozoic time (2,200 - 1,770 ma) sediments were deposited in central, east-central, and northeastern Minnesota in basins now partially outlined by the iron-formations of the Mesabi, Gunflint, and Cuyuna ranges. This terrane was deformed during the Penokean orogeny, and can be divided into two distinct tectonic zones in the study area—an older fold-and-thrust belt, which defines the southern area, and a stable foredeep basin, the Animikie Basin, which defines the northern area of this terrane (Southwick and others, 1988).

On Figure 5, the Early Proterozoic rocks are grouped into five generalized map units: 1) the fold-and-thrust belt metasediments/metavolcanics/sediments; 2) the major iron-formations; 3) other Animikie Group clastic sediments; 4) the granitic intrusions of the Penokean Orogen; and 5) the Sioux Quartzite. In the vicinity of the Cuyuna Range and eastward to Carlton County, the fold-and-thrust belt is predominantly composed of a variety of metasedimentary and metavolcanic rocks. These rocks include units of slate, metasilstone, metagraywacke, schist, metabasalt, quartz arenite, argillite, shale, siltstone, dolomite, mudstone, graywacke, and iron-formation—which includes the Cuyuna Range deposits (Morey, 1994). This part of the fold-and-thrust belt is inferred to be dominantly of mafic to intermediate composition. Metamorphic grade is generally greenschist-facies (Morey, 1994). In central Minnesota, the fold-and thrust belt was later permeated by intrusions associated with the Penokean orogeny; these large intrusive bodies are dominantly of felsic composition. To the north of the fold-and-thrust belt, the foredeep basin contains the clastic sedimentary rocks of the Animikie Group, which includes units of graywacke, siltstone, shale, and associated volcanoclastic rocks and the iron-formations and underlying quartzites of the Gunflint and Mesabi ranges (Morey, 1994). The rocks in the fold-and-thrust belt are complexly deformed and metamorphosed, in contrast to the foredeep deposits, which are relatively undeformed, except for regional tilting, local faulting, and minor metamorphism. In southwestern Minnesota, outside the study area, the Sioux Quartzite and related claystone was deposited in a fault-bounded braided stream environment.

The Early Proterozoic iron and manganese iron deposits have been mined on the Mesabi and Cuyuna ranges. The Cuyuna deposits differ from the Mesabi Range deposits in that they contain more manganese, they have undergone more deformation, and their ore was possibly deposited from hydrothermal solutions (Cleland and others, 1996).

The mineral potential of the fold-and-thrust belt is diverse. There are applicable models for deposits of copper, lead, zinc, gold, silver, cobalt, bismuth, platinum group elements, uranium, tin, tungsten, beryl, and rare earth elements.

A study and assay of drill core from Early Proterozoic rocks in central Minnesota has identified a number of gold, gold plus platinum group elements, and base metal anomalies and indicator elements (see Frey and Lawler, 1993 for locations). These anomalous assay results include:

- 1) Gold values of 151 ppb, 112 ppb, 69 ppb, and 61 ppb at four different locations;
- 2) Copper values of 1,622 ppm, 1,468 ppm, 1,328 ppm, 1,084 ppm, and 1,008 ppm at five different locations;
- 3) Barium >2,000 ppm, yttrium 966 ppm, and arsenic 926 ppm values at the same location;

- 4) Gold 1,383 ppb, palladium 1,339 ppb, zinc 1,343 ppm, and fluorine 1,100 ppm values at the same location;
- 5) Zinc values of >20,000 ppm, 4,000 ppm, and 4,000 ppm in three different samples at one location;
- 6) Arsenic 776 ppm at one location; and
- 7) Fluorine 1,639 ppm at one location.

The fold-and-thrust belt sediments have been explored for base metals and uranium. In Aitkin County, a sulfide facies iron-formation with carbonaceous shale and a carbonate facies iron-formation has been investigated as a source of iron and sulfur. Estimated reserves are 39 million tons, which average 13.8 to 13.9 percent sulfur with some base metals (Pennington and Davis, 1953). In a prospect known as the Arrowhead Mine (located near the south edge of the Animikie Basin), pyrite samples contain up to 50 ppm uranium, and 352 ppb gold (Lawler, 1997). This mine is in an area mapped as slate, metasiltsone, and metagraywacke (Mc Swiggen, 1987), and in the late 1970's this area was extensively explored for Athabaska-type uranium deposits (MN DNR, General Assessment Files; Martin, 1985). In Carlton County anomalous values have been reported as high as 7,400 ppm zinc, 1,600 ppm lead, 1,250 ppm copper, 1,000 ppm arsenic, 710 ppm silver, and 3,155 ppb gold (MN DNR, General Assessment Files).

Several inferred geologic maps were recently produced utilizing all available geophysical and geologic data previously collected in the central part of the study area (Spector, 1992, 1993, 1994, and 1995a). These maps identify sixty-one mineral potential areas, mostly gold and base metal, with mention of uranium and cobalt. Ten holes were drilled to substantiate the lithologic interpretations on the maps. Also in the central part of the study area, three existing ground water and lake sediment geochemical data sets were recently reinterpreted using statistical and modeling methods (Shettel and O'Hara, 1992). From these data, geochemical anomaly maps for base and precious metals, iron, and uranium were constructed ; in several places, these geochemical anomalies were coincident with the areas of high mineral potential defined by Spector (1992, 1993, 1994, 1995a).

Middle Proterozoic Midcontinent Rift Terrane

The Midcontinent Rift System (1,100 ma) extends from Lake Superior, through eastern Minnesota, and in the subsurface, southwestward into Kansas. These Middle Proterozoic rocks form a distinct volcanic-sedimentary sequence in northeastern and east-central Minnesota; on Figure 5 they are grouped into extrusive, intrusive, or sedimentary units. The rift-related extrusive rocks, found along the north shore of Lake Superior and in another area extending south of Duluth, are composed primarily of basalt, but include some rhyolites and related volcanogenic and interflow sedimentary rocks of intermediate composition (Morey, 1994). The intrusive rocks of the Midcontinent Rift include the Duluth Complex and the Beaver Bay Complex, which are composed predominantly of gabbro, anorthosite, troctolite, and related rocks—with some granite and granophyric rocks (Morey, 1994). The Duluth Complex crops out in an arcuate pattern extending from Duluth northeastward nearly to the northeastern tip of Minnesota. The Beaver Bay intrusives are on the east side of the Duluth Complex, adjacent to and intruding the extrusive rocks along Lake Superior. Overall, both

the intrusive and the extrusive units are dominantly mafic in composition. In an area southwestward from Duluth, the youngest rocks in this terrane were deposited in rift valleys. These basins are filled with predominantly sandstones—quartz arenite, feldspathic sandstone, arkose— with some shale and a quartz-pebble conglomerate at the base (Morey, 1994).

The regional metamorphism in the Midcontinent Rift rocks is very low grade. Intrusive rocks of the Duluth Complex metamorphosed the Early Proterozoic iron-formations and other rocks along the contact, which produced local high-grade metamorphic zones. Within the Complex, various magmatic units have been defined and several alteration assemblages have been recognized within them.

The Duluth Complex has attracted considerable attention as a potential source of precious and base metals. This terrane has potential to contain the following commodities: copper, nickel, platinum-group elements, gold, silver, titanium, vanadium, cobalt, and chromium. Non-economic occurrences of these metals have been found in several different rock types and structural settings within the Complex. In the Complex, thirteen significant prospects for copper and nickel deposits have been defined, one prospect for platinum-group elements, and ten or more prospects for titanium (Morton and Hauck, 1991). For example, along the northwestern (basal) contact of the Duluth Complex, copper-nickel-precious metals mineralization is found and several deposits with an average grade of 0.66% copper and 0.2% nickel have been defined in St. Louis County (Listerud and Meineke, 1977). In St. Louis County at one of the thirteen defined copper-nickel deposits, the massive sulfide ores also include maximum values of 11,100 ppb palladium, 8,300 ppb platinum, 10,900 ppb gold, and 34 ppm silver (Severson and Barnes, 1991). Within the Complex in adjacent Lake County, precious metal occurrences have also been defined, and one area averages 1.234 ppm silver, 49.0 ppb gold, 94.3 ppb platinum, and 321.2 ppb palladium (Hauck and Barnes, 1989; Geerts and others, 1990). In the same general vicinity, three drill cores contained combined gold plus platinum plus palladium values exceeding 1000 ppb (Dahlberg and others, 1989). In addition, some oxide-bearing ultramafic intrusions in the Complex contain titaniferous magnetite deposits with grades of $\geq 10\%$ titanium dioxide (Severson, 1995).

Along the northwestern contact of the Duluth Complex, six areas were recently mapped by geophysical interpretation that have high mineral potential (Spector, 1995b). Four of these areas are in the footwall Virginia Slate, and have not been explored, and the other two have unexplored features that suggest high potential for copper, nickel, and platinum-group deposits.

Preglacial Setting

Little is known about the geologic history of the study area from the middle Proterozoic to the late Cretaceous, since rocks of this age have not been identified from this part of Minnesota. During this time, the Precambrian rocks of the study area were probably subjected to chemical weathering and erosion. Just south of the central part of the study area, weathering of Early Proterozoic rocks of the Penokean orogen, prior to deposition of the Upper Cambrian Mt. Simon Sandstone, is evidenced by the presence of a saprolite containing kaolinite, and mixed-layer illite/montmorillonite (Morey, 1972). This weathering probably produced a similar saprolite over most of the Precambrian rocks of the study area.

Another episode of deep chemical weathering occurred during the early part of the Late Cretaceous Period. This weathering resulted in a wide-spread saprolite in the western part of the state, composed predominately of kaolinite with lesser amounts of halloysite, gibbsite, and boehmite (Parham, 1972). This saprolite developed in a variety of Precambrian lithologies as well as older saprolite. Total thickness of saprolite in parts of the study area is commonly 50 to 150 feet, and is locally more than three hundred feet thick in the southwestern part of the study area (Southwick, 1989). A similar saprolite probably covered Precambrian rocks in the northeastern part of the study area, but it has been for the most part, eroded from these areas.

During the Late Cretaceous, the eastern margin of the Western Interior Seaway transgressed into Minnesota, depositing primarily shale and sandstone, with minor amounts of marl (Setterholm, 1990), at least as far east as the central Mesabi Range. To the east of the fluctuating strandline of the Western Interior Seaway in Minnesota, a variety of fluvial and deltaic sediments were deposited by westward flowing streams draining the Precambrian uplands of northeastern Minnesota and central and northern Wisconsin (Witzke and others, 1983).

Throughout most of the Tertiary Period, erosion must have been the dominant geologic process in the study area, since no rocks of Paleocene to Miocene age have been identified in Minnesota. Post-Cretaceous erosion has removed most of the Cretaceous sedimentary rocks, including the underlying saprolite, in the central and northeastern parts of the study area. In the southwestern part of the study area, Cretaceous strata range up to a few hundred feet in thickness (Setterholm, 1990), overlying as much as a few hundred feet of saprolite. Outcrops of Precambrian crystalline rock occur in the Minnesota River valley, where late Pleistocene glacial meltwater erosion cut a valley a few hundred feet deep.

Quaternary Geology

Pre-late Wisconsinan Glaciations

Minnesota was glaciated repeatedly during the late Cenozoic ice age, but little is known about these early glaciations, since many of their deposits have been eroded either during interglacial stages or by subsequent glaciations, while most old deposits that remain are deeply buried. However, it is worthwhile briefly mentioning these pre-late Wisconsinan glaciations as a way to emphasize the complexity of glacial dispersal.

The earliest glaciations would have been fairly effective at removing the thick saprolite that at one time must have been present over much of Minnesota (Gravenor, 1975). Evidence from near the glacial limit in North America supports this. In this area, the oldest tills have a low percentage of unstable heavy minerals, such as hornblende and apatite, and high percentages of heavy minerals produced through weathering, such as limonite. In the overlying tills, the percentage of unstable heavy minerals increases, and the percentage of those heavy minerals common in weathering profiles decreases (Gravenor, 1975).

On a continental scale, there is a broad zone of extensive glacial scour near the center of the former North American ice sheets, where outcrops of fairly unweathered bedrock are common. Flanking this scoured area to the south and west is an area of predominantly glacial

deposition, and Minnesota straddles this transitional zone (Sugden, 1978). For example, in the northeastern part of the study area, bedrock outcrops are fairly common and till stratigraphy is typically fairly simple (Lehr and Hobbs, 1992). This contrasts with portions of the central and southwestern parts of the study area, where there are multiple tills overlying Cretaceous rocks, which in turn, overlie thick saprolite developed in Precambrian crystalline rock (Southwick and others, 1986; Southwick and others, 1990). The total depth of glacial erosion in the scoured zone of the Canadian shield consists of what saprolite was present, plus on the order of a few tens of meters of sound rock (Shilts and Kaszycki, 1986).

Till of probable Pliocene age (approximately 2.14 ma) is exposed at the surface in southeastern Minnesota (Matsch and Schneider, 1987) and tills of similar age are undoubtedly present in the subsurface in portions of the study area (Meyer, 1986). A series of interbedded tills of both northeastern and northwestern provenance, speculated to be of pre-late Wisconsinan age, are present in the subsurface of the central part (Todd County) of the study area (Meyer, 1986). Work done in adjacent areas (Gilbertson, 1990; Martin and others, 1988; Martin and others, 1989; Martin and others, 1991; Winter and others, 1973) can be used to speculate on the older till stratigraphy and glacial history of other parts of the study area. Thick sequences of older glacial sediments are present in areas where the depth to bedrock is greatest (Olsen and Mossler, 1982).

Late Wisconsinan Glaciations

The late Wisconsinan glaciation of Minnesota is the best understood because these deposits occur at the surface throughout most of the state. Also, these deposits are young enough not to have been appreciably eroded. Consequently, the interpretation of genesis, including vertical and lateral facies variability, can be accomplished through study of these depositional landforms and their constituent sediments (Eyles, 1983a). The samples collected and studied for this project were, for the most part, late Wisconsinan glaciofluvial deposits. A general description of the different genetic types of glaciofluvial deposits sampled for this study is presented below as background for interpreting sedimentological variability between samples.

Genetic Types of Glaciofluvial Deposits

The glaciofluvial sediments sampled for this study can be broadly grouped into two genetic types, outwash and ice-contact stratified sediments. Outwash is deposited by glacial meltwater streams emanating from the glacier's margin, hence the term *outwash*. Glacial meltwater streams are typically heavily loaded with sediment derived from melting of debris-rich ice, and are therefore braided and generally aggrading streams (Miall, 1983). Diurnal and seasonal changes in the melting rate of the glacier produce widely variable discharge rates in meltwater streams, causing sediments ranging from silt to boulder-gravel to be deposited. Because glacial meltwater streams are highly charged with sediment, and discharge rates are extremely variable, vertical and horizontal facies changes in the outwash environment are abrupt (Smith, 1985). If meltwater streams are restricted to a preexisting valley, the resulting landform is called a valley train. If meltwater streams are not constrained by a valley, they migrate laterally across the proglacial zone depositing an outwash plain (Smith, 1985).

The distance of fluvial transport in outwash systems is generally longer relative to the ice-contact depositional environment (Lilliesköld, 1990). With detailed study of geomorphology, most of the outwash systems sampled can be traced up-stream to an ice margin.

By definition, ice-contact stratified sediments are deposited in contact with either stagnant or active ice. As debris-rich ice near the glacier margin melts, small streams develop either on top of, beneath, or within the disintegrating glacier. These streams deposit sediments ranging from sand to boulder-gravel in channels to silt, clay, and till in small, ephemeral lacustrine basins on the ice (Eyles, 1983b). Eskers are a type of ice-contact landform composed primarily of sand and gravel deposited in ice-walled channels. When the surrounding ice melts, the channel deposits remain as ridges approximately parallel to ice flow. Kames are another type of ice contact landform, deposited by flowing water and gravity processes as sediment is transported into low areas on the glacier or at its margin. Outwash fans are another type of ice-contact landform that is genetically intermediate between ice-marginal kames and outwash plains. The most common ice-contact landform sampled for this study was stagnation moraine. In this depositional environment, sorted sediments ranging from clay and silt to bouldery gravel, in addition to unsorted sediments (till), are deposited in low areas on top of the glacier. Because the substrate is melting ice, this depositional environment is highly dynamic, with inversions of topography and resedimentation occurring until all underlying ice has melted. Stagnation moraine is recognized by its characteristic "knob and kettle" topography and diverse sequence of sediments. Linear zones of stagnation moraine that are inferred to mark former ice margins are called end moraines.

The distance of fluvial transport in the ice-contact depositional environment is generally less than in the outwash environment (Lilliesköld, 1990), but varies considerably. In esker systems, distance of fluvial transport is a function of the length of the fluvial system, the amount of locally derived subglacial debris available and the resistance of the substrate (either bedrock or glacial sediments) to fluvial erosion. In stagnation moraine, end moraines, outwash fans, and kames, the distance of fluvial transport is generally short. Supraglacial streams erode debris and rapidly deposit their load in low areas on, or adjacent to the disintegrating ice (Eyles, 1983b).

Late Wisconsinan Glacial History

An understanding of the sequence of events responsible for deposition of the sediments sampled for this study is useful in interpreting bedrock provenance of mineralogical and geochemical anomalies. Therefore, a brief summary of the late Wisconsinan glacial history of the study area is presented below.

The late Wisconsinan Laurentide Ice Sheet spread out from several accumulation centers in Canada, three of which influenced glaciation in Minnesota: one on land west of Hudson Bay (Keewatin ice), one in the southern part of Hudson Bay (Hudson ice), and one in northern Quebec (Labrador ice) (Dyke and others, 1989). From a perspective in Minnesota, Keewatin ice advanced from the northwest, while Hudson and Labrador ice advanced from the northeast. As the Laurentide Ice Sheet expanded southward, its margin became lobate, following major preexisting lowlands such as the Great Lakes. In Minnesota, late Wisconsinan glacial deposits can be differentiated based on provenance and are mapped

according to the glacial lobe from which they were deposited. The lobe of Keewatin ice that advanced south-southeastward through the Red River valley is referred to as the Des Moines lobe. Two distinct lobes of Hudson ice advanced into Minnesota at different times during the late Wisconsinan, the Wadena lobe and the Rainy lobe. A fourth major lobe, the Superior lobe, advanced into Minnesota from Labrador ice to the northeast, following the axis of the Lake Superior basin. The chronology of these glacial lobes, as well as the overall lithologic character of their deposits, is presented in the following paragraphs.

The first few glacial advances of the late Wisconsinan are not as well understood as the last few, but the first advances were probably of the confluent Superior and Wadena lobes into western and southwestern Minnesota and adjacent parts of the Dakotas (Fig. 7). These northeastern advances were immediately followed by multiple advances of the Des Moines lobe into southwestern Minnesota and northern Iowa (Fig. 8) (Lehr and Hobbs, 1992). Deposits of these early late-Wisconsinan advances are present in the subsurface of the study area, but were not sampled for this study.

As the confluent Wadena and Superior lobes retreated into central Minnesota, the margin of the Wadena lobe stabilized at the Alexandria moraine complex and the Superior lobe at the southern part of the St. Croix moraine (Fig. 9). The Wadena and Superior lobes stood at this position for some time, because both the Alexandria and St. Croix moraines are massive end moraine complexes composed of several individual end moraine ridges and a variety of thick ice-contact stratified deposits. Most of the Wadena lobe samples in the southwestern part of the study area were taken from ice-contact stratified deposits of the Alexandria moraine complex.

As the Wadena lobe retreated from the Alexandria moraine complex, it formed the Wadena drumlin field, stabilizing, at times, long enough to deposit narrow belts of stagnation moraine, small outwash plains, and valley trains (Fig. 10). Concurrent with the retreat of the Wadena lobe, the Superior lobe withdrew from the western part of the St. Croix moraine, also periodically stabilizing long enough to deposit belts of stagnation moraine.

Continued ice recession resulted in a reorientation of ice flow in the Wadena lobe from southwesterly to a more southerly direction and a stabilization of the ice margin at the Itasca moraine (Fig. 11). The Wadena lobe stood at the Itasca moraine for quite some time, as evidenced by the size of the moraine and the extent of outwash deposited south of the moraine. Upon retreat of the Wadena lobe to the Itasca moraine, the Rainy lobe advanced west-southwesterly into an area formerly occupied by the Wadena lobe. At this time, the Superior lobe was confluent on the south flank of the Rainy lobe, forming a lobate ice margin marked by the St. Croix moraine (Fig. 11). The St. Croix moraine within the study area is a fairly narrow ridge of stagnation moraine containing a few glacial thrust systems (Mooers, 1988).

The Wadena lobe remained at the Itasca moraine while the Rainy and Superior lobes retreated from the St. Croix moraine, depositing a series of end moraines and other ice-marginal deposits (Fig. 12). The Rainy and Superior lobes behaved quite differently as they withdrew from the St. Croix moraine. The Rainy lobe, being colder than the Superior lobe, deposited hummocky end moraines containing a wide variety of ice-contact stratified sediments, and large thrust blocks of bedrock and older glacial sediments. There is little evidence for

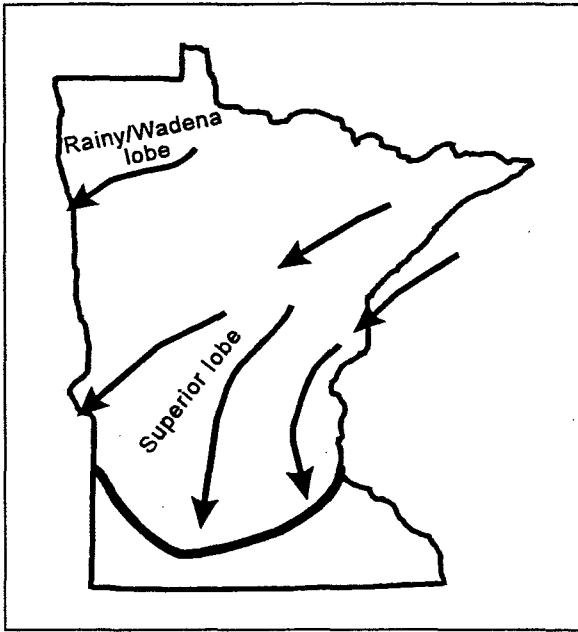


Figure 7. Early late-Wisconsinan advance from the northeast

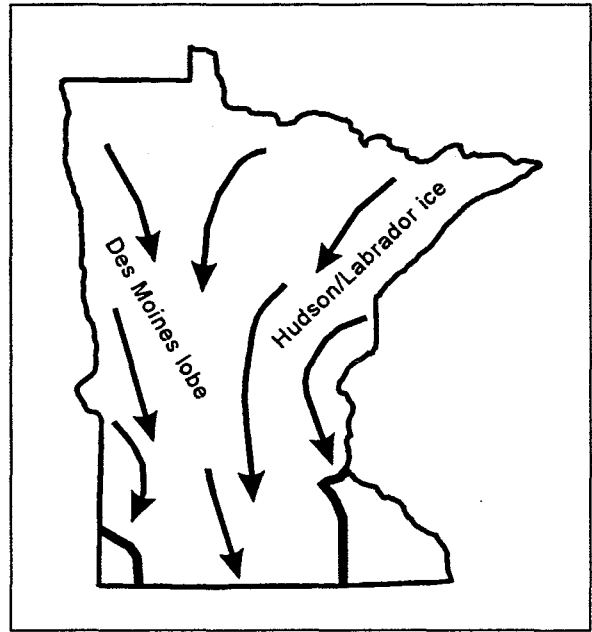


Figure 8. Early late-Wisconsinan advance from the northwest

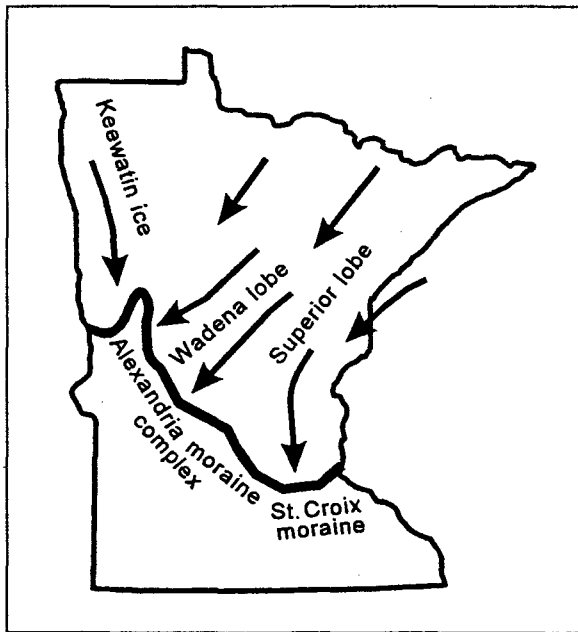


Figure 9. Alexandria phase

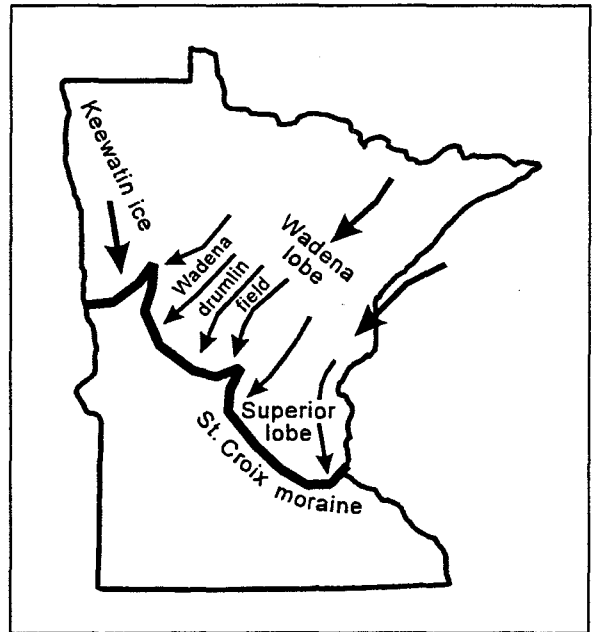


Figure 10. Recession from the Alexandria moraine complex

Ice movements associated with late Wisconsinan glaciation in Minnesota.

channelized subglacial drainage in the Rainy lobe at this time, and the end moraines are fronted by substantial outwash plains. Also, conditions were less favorable for drumlin formation in the Rainy lobe than in the Superior lobe. (Mooers, 1988). This style of deglaciation contrasts with the warmer Superior lobe, which developed extensive subglacial drainage networks, as evidenced by numerous tunnel valleys and eskers. Ice marginal positions are marked by kames, small uncollapsed outwash fans and large hummocky ice-contact fans, many of which represent terminations of tunnel valley systems. Hummocky end moraines and large outwash plains are generally less common, and drumlins are particularly abundant (Mooers, 1988).

Following retreat of the Rainy and Superior lobes from the St. Croix moraine, the Des Moines lobe began a series of rapid advances south down the axis of the lowlands now occupied by the Red and Minnesota Rivers (Figs. 13 and 14). Most of these advances are considered surges and were probably followed by mass stagnation of the entire lobe and another readvance of lesser extent. Some of this northwestern ice spilled into low areas to the east, formerly occupied by either the Wadena, Rainy, or Superior lobes. One of these offshoots, the St. Louis sublobe, advanced through the gap between the Itasca moraine and the Mesabi Range into the lowlands of the Animikie basin (see Fig. 15). This rather weak advance deposited a mantle of fine-grained till over northeastern provenance deposits. In some areas covered by the St. Louis sublobe, Wadena, Rainy, and Superior lobe ice-contact stratified sediments extend upward through the younger northwestern provenance sediments.

A similar situation exists in the Alexandria moraine complex in the southwestern part of the study area, where Wadena lobe ice-contact stratified sediments are thinly mantled by Des Moines lobe till. In the southwesternmost part of the study area, the cover Des Moines lobe till is quite extensive, and surface exposures of northeastern provenance sediments are rare.

The location of sampling sites in this study was influenced by the distribution and thickness of Des Moines lobe tills, since northwestern provenance sediments were intentionally avoided during sampling. The reason for this bias is that Des Moines lobe deposits contain a large component of distally derived material, in particular, a large amount of siliceous shale derived from the Cretaceous Pierre Shale, which is present in eastern North Dakota and southern Manitoba, but not present in Minnesota. Also, the dynamics of the Des Moines lobe were generally not conducive to incorporation of large amounts of local material. A notable exception to this generalization is where the Grantsburg sublobe of the Des Moines lobe overrode the St. Croix moraine between St. Cloud and St. Paul and incorporated large amounts of reddish-colored Superior lobe sediment.

While the Des Moines lobe was active in the western and southern parts of the state, the Rainy and Superior lobes continued to retreat to the northeast. The Superior lobe, being thicker and more dynamic than the Rainy lobe, flowed into an area formerly occupied by the Rainy lobe in the Mille Lacs Lake area and built the Mille Lacs moraine along the west shore of the lake (Wright, 1972). The margin of the Rainy lobe at this time was just north of Mille Lacs Lake (Mooers, 1988) and was probably drained by meltwater streams (Fig. 13). As it retreated into the Animikie basin, the Rainy lobe became bordered by a lake (Lehr and Hobbs, 1992), but interpretation of these Rainy lobe sediments is difficult, as they are now covered by deposits of the St. Louis sublobe.

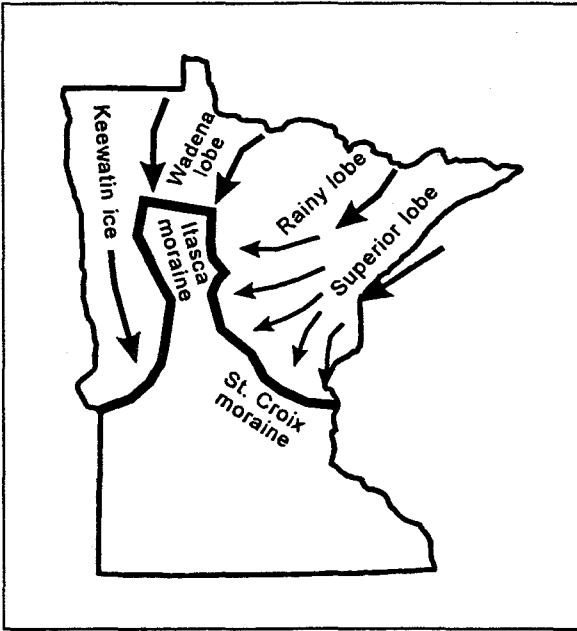


Figure 11 St. Croix phase

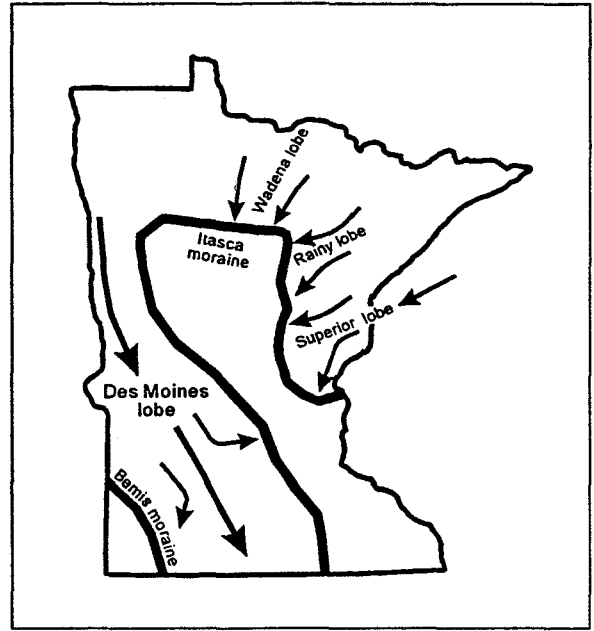


Figure 12. St. Croix phase recession

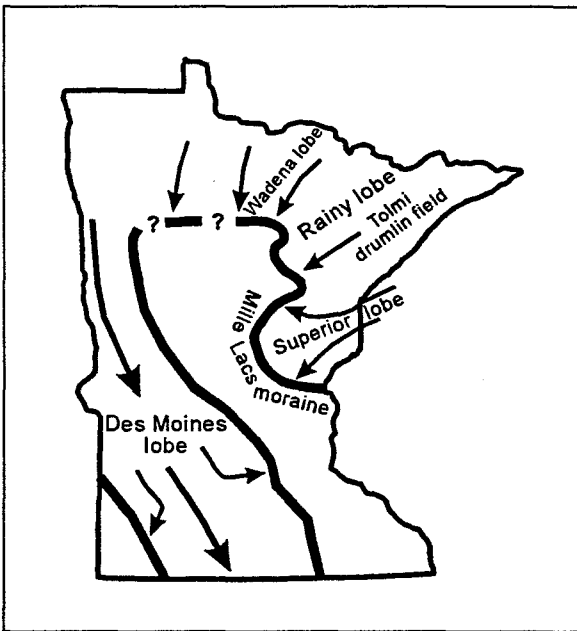


Figure 13. Superior lobe readvance to Mille Lacs moraine, Rainy lobe recession and readvance of Des Moines lobe

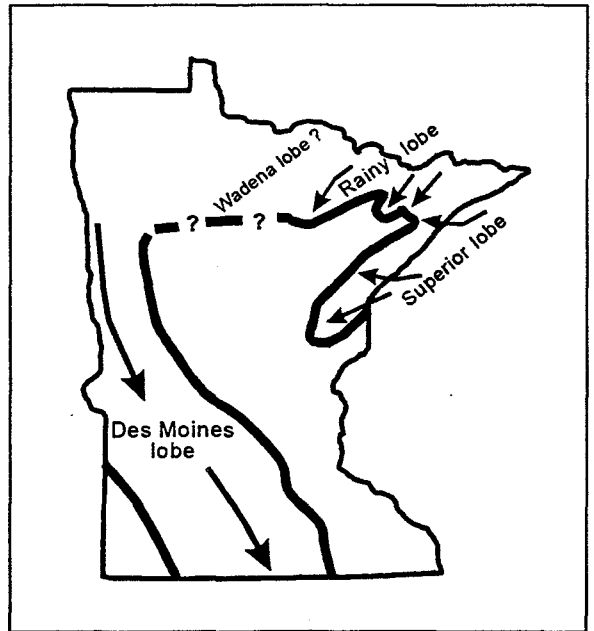


Figure 14. Recession of Rainy and Superior lobes and readvance of the Des Moines lobe

Ice movements associated with late Wisconsinan glaciation in Minnesota.

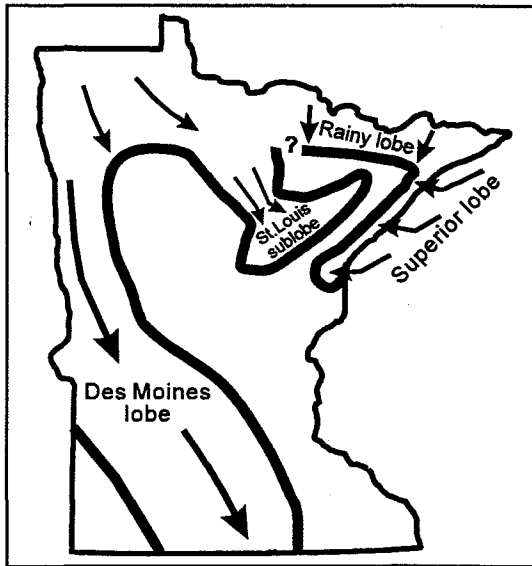


Figure 15. Recession of Rainy and Superior lobes and advance of St. Louis sublobe.

As the Rainy lobe margin continued to recede through the northeastern part of the study area, the topographic high of the Mesabi Range caused the ice margin to split into two smaller lobes (Fig. 14). The lobe north of the Mesabi Range was fronted by a lake in many places (Lehr and Hobbs, 1992). Over the topographically higher Keweenawan rocks in the northeastern part of the study area, the Rainy lobe deposited the Toimi drumlin field (see Fig. 13). Younger outwash valley trains from both the Superior and Rainy lobes, as well as Rainy lobe eskers, occur in low areas between the northeast-southwest oriented drumlins (Lehr and Hobbs, 1992). In the northernmost part of the study area, the Rainy lobe deposited a series of narrow end moraines. Where the Rainy lobe terminated in proglacial lakes, its margin is marked by a series of coalesced ice-contact deltas. Where the ice margin terminated on land, hummocky end moraines with frontal outwash plains were deposited (Lehr and Hobbs, 1992). There are numerous Rainy lobe eskers and bedrock outcrops in the northern part of the study area, indicating a significant amount of subglacial drainage by this stage of deglaciation.

The Superior lobe at this time stood at the Highland moraine, a fairly massive accumulation of ice-contact stratified sediments and till, parallel to the north shore of Lake Superior (Fig. 14). After the Rainy lobe formed the Toimi drumlin field, the Superior lobe advanced northwestward slightly to bury the southeastern part of the drumlin field (Wright, 1972). Since the Superior lobe was thicker, it remained active in Minnesota longer than the Rainy lobe. As the Superior lobe retreated from the Mille Lacs moraine towards the Lake Superior basin, proglacial lakes developed. The last few advances of the Superior lobe were into these proglacial lakes, resulting in clayey tills. The outwash plains and valley trains in Carlton County were deposited from these last Superior lobe advances (Hobbs and Goebel, 1982). It was while the Superior lobe was at these positions near the west end of Lake Superior that the St. Louis sublobe advanced into the Animikie basin (Fig. 15).

General Lithology of Glacial Sediments

Since a comprehensive study of the lithology of glaciofluvial sediments sampled was beyond the scope of this report, the lithologic characteristics of the various glacial lobe deposits must

be summarized from the published literature. However, lithologic studies of glacial sediments typically focus on till, although there is a close relationship between the lithology of tills of a given lobe and their glaciofluvial sediments. For this reason, the following comparison of lithology between the lobe deposits is summarized from lithologic studies of till.

Till deposited by the Wadena lobe in the central part of the study area is calcareous with a yellowish-brown and generally sandy matrix. The magnetic susceptibility of the matrix of Wadena lobe till is quite high, supporting a northeastern provenance for the Wadena lobe (Mooers, 1988). The 1-2 mm sand fraction of Wadena lobe till is chiefly felsic igneous rock types, with mafic igneous and carbonate rock fragments comprising most of the remainder of this fraction (Mooers, 1988). The presence of appreciable amounts of carbonate in both the matrix and pebble fraction of Wadena lobe till suggests that a large component of these deposits was derived from Paleozoic rocks in the Hudson Bay lowland (Lehr and Hobbs, 1992; Gowan, 1993), while the igneous component was derived more locally, from the greenstone-granite terrane of northeastern Minnesota and adjacent Ontario.

Although the Wadena and Rainy lobes had approximately the same flow path during most of the late Wisconsinan, their deposits are quite easily distinguished. Rainy lobe till in the central part of the study area is dark brown and generally noncalcareous and the magnetic susceptibility of the matrix is slightly greater than of Wadena lobe tills (Mooers, 1988). As in Wadena lobe till, the 1-2 mm sand fraction is composed predominantly of felsic igneous rock types, with most of the remainder being mafic igneous and metamorphic rock fragments (Mooers, 1988). In general, Rainy lobe deposits in the northeastern part of the study area contain a greater percentage of locally derived material than Rainy lobe deposits in the central part of the study area. During deglaciation, the pattern of erosion and deposition along the Wadena/Rainy lobe flow path changed. The Wadena lobe deposited a greater percentage of distally derived debris, while as the Rainy lobe retreated from the St. Croix moraine, it became increasingly more effective at eroding local bedrock.

Superior lobe tills in the study area range in color from brown to reddish brown, they are generally noncalcareous, and have magnetic susceptibilities that range from slightly higher to significantly higher than Wadena or Rainy lobe tills (Mooers, 1988). The 1-2 mm sand fraction is composed of approximately equal proportions of mafic and felsic igneous rock types, with lesser amounts of metamorphic rock fragments and reddish-colored shale and sandstone derived from Keweenawan rocks that underlie Lake Superior (Mooers, 1988).

Tills of the Des Moines lobe are easily distinguished from the northeastern provenance tills by their olive-brown color, silt- and clay-rich calcareous matrix, fewer cobbles and boulders, lower magnetic susceptibility, and most prominently, the presence of large amounts of Cretaceous shale and limestone. These lithologic characteristics reflect a source in the Paleozoic and Mesozoic bedrock terranes in northwestern Minnesota and adjacent parts of North Dakota and Manitoba (Mooers, 1988). As previously mentioned, the eastern sublobes of the Des Moines lobe (the St. Louis and Grantsburg sublobes) locally incorporated large amounts of previously deposited northeastern provenance glacial sediments. Therefore, the lithologic character of these deposits is intermediate between those of the main Des Moines lobe and the deposits of the particular northeastern lobe over which the northwestern sublobes advanced.



RESULTS

The results of the interpretative analysis of the heavy-mineral-data sets are summarized below and are illustrated by histogram frequency graphs, geographic distribution maps, and correlation coefficient matrixes. Results are presented for the complete set of 85 samples and also for samples grouped by glacial sediment type—into the 39 samples from the Superior lobe, 29 samples from the Rainy lobe, 16 samples from the Wadena lobe, and 1 sample from the Des Moines lobe. The geographic location of the 85 sample sites, identified by sample number, is shown on Figure 16. Sample localities are also shown on a generalized Quaternary geology map of Minnesota, with each sample site identified by the specific glacial sediment type collected (Fig. 17). Geochemical results are summarized for samples of the bulk heavy-mineral concentrate, the paramagnetic fraction (C2) of the concentrate, the nonmagnetic fraction (C3) of the concentrate, and selected correlations among these three geochemical data sets. The mineralogical results are then summarized for samples of the nonmagnetic fraction (C3) of the heavy-mineral concentrate.

Appendices A and B (located in the back cover pocket) are transparencies that can be overlaid on the geographic distribution maps to provide a geologic dimension. Appendix A is a generalized bedrock geology map of Minnesota that shows the major bedrock types (modified from Morey, 1994). Appendix B is a Quaternary geology map of Minnesota that shows the generalized boundaries of the sediments from the Rainy, Superior, Wadena, and Des Moines lobes (modified from Hobbs and Goebel, 1982).

INTERPRETATIVE METHODS

Various interpretative methods were used to analyze the sets of geochemical and mineralogical data generated in this study. These methods served as tools to statistically look at the data—to provide measures of comparison that would help to identify anomalous values from background values and to highlight any significant relationships in and between the various sets of heavy-mineral data. The sets of geochemical and mineralogical data were converted into a binary form for computerized statistical analysis using STATPAC (VanTrump and Miesch, 1977), a program developed by the United States Geological Survey. A brief explanation of the interpretative methods we utilized follows.

To provide accurate comparisons between samples it was first necessary to start with a set of similar data. All of the samples in this study were collected in glaciofluvial sediments and processed in a similar manner, except three samples. These three non-glaciofluvial samples [23967 (a pre-concentrate), 23969 (a pre-glacial alluvium), and 23971 (an active stream sediment)] were not included in the interpretative data analyses and are not discussed in this report. Nelson and others (1992) contains the descriptive geochemical and mineralogical data for these three samples.

Most of the glaciofluvial-sediment samples were collected in areas underlain by Precambrian bedrock. Four samples (23972, 23973, 23974, and 23975) were collected in east-central Minnesota, outside the main study area, in glaciofluvial sediments underlain by Paleozoic

HEAVY-MINERAL STUDY

LOCATION OF SAMPLE SITES

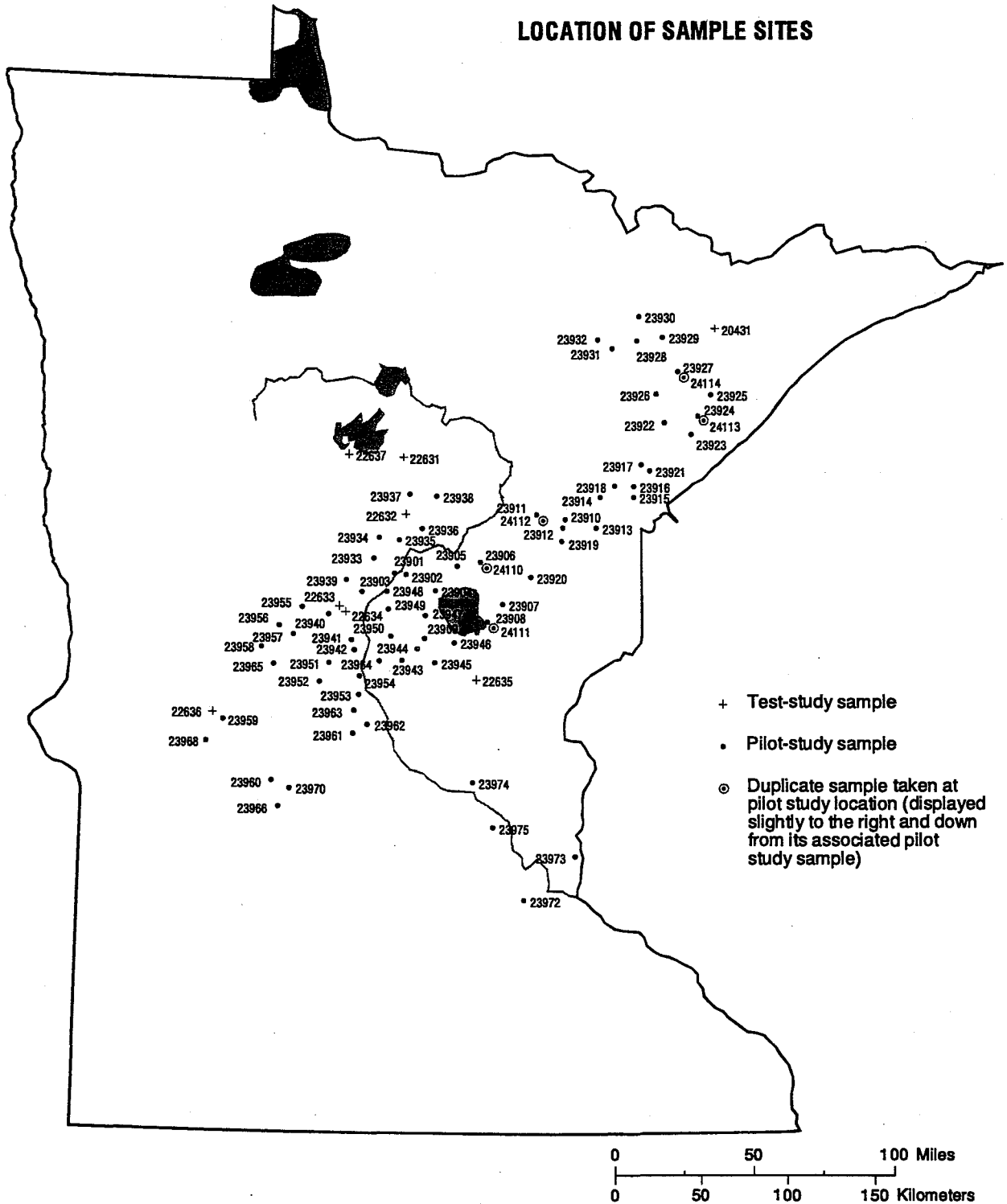


Figure 16. Geographic location of the sample sites for the heavy-mineral study.

GENERALIZED QUATERNARY GEOLOGY

WITH SAMPLE LOCALITIES IDENTIFIED
BY SEDIMENT TYPE COLLECTED

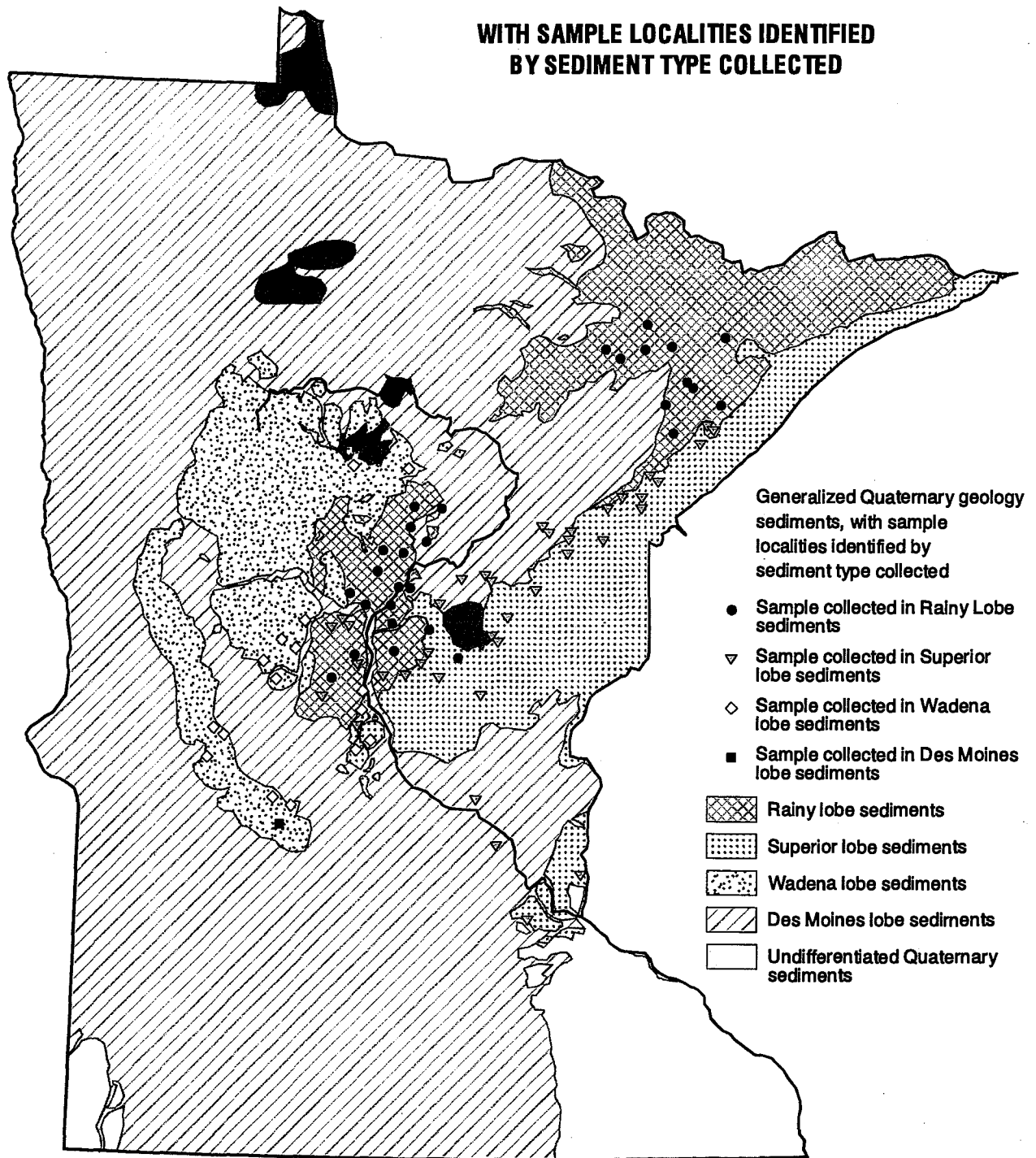


Figure 17. Generalized Quaternary geology in Minnesota, with sample localities identified by the specific glacial sediment type collected. (Modified from Hobbs and Goebel, 1982.)

sedimentary rocks. For completeness, these four samples are included in the interpretative analyses; however, they are not discussed separately by geologic setting because there is not a statistically valid number of samples.

In semi-quantitative spectrographic analysis each element has a lower and upper determination limit based on the sensitivity of the equipment. Indeterminate codes indicate when an element was not (N) detected at the lower determination limit shown, and when an element was observed but was less (L) than the lower determination limit shown or greater (G) than the upper determination limit shown. For interpretative analysis, to determine the maximum possible mean for each element, the "L" data was replaced with a value one reporting step below the lower limit of determination; the "N" data was replaced with a value two reporting steps below the lower determination limit; and the "G" data was replaced with a value one reporting step above the upper limit of determination. These values were used in the STATPAC statistical program for interpretative analysis of the geochemical data.

The element values in the geochemical data sets were converted to logarithm (base 10) normalized data in the STATPAC statistical program. Many geological variables do not follow a normal distribution and will produce a highly skewed frequency distribution curve; converting the variables to logarithmic form provides a geometric scale that approaches a normal distribution for geochemical data values (Davis, 1986).

The presence and abundance of minerals in samples of the nonmagnetic fraction (C3) of the concentrate were described by using binocular microscopy techniques to visually estimate the percentage of each mineral identified in a sample. Because this was a qualitative measurement, for interpretative analysis the relative abundance of a mineral within a sample was converted from the percentage value to a number value between 0 to 5 as follows:

0	Not identified in the sample
1	< 1% of sample or number of grains
2	1 - 10% of sample
3	> 10 - 30% of sample
4	> 30 - 50% of sample
5	> 50% of sample

These number values were used in the STATPAC statistical program for interpretative analysis of the mineralogy data. Because we have a relatively small sample set in this study, this method tended to conceal all but the extreme data results.

Single-element, paired-element, and multi-element statistics were performed on each data set using STATPAC. Univariate or single-element statistics provides descriptive data, including the minimum, maximum, geometric or arithmetic mean, and standard deviation for each variable. Paired-element correlations measures the linear relationship between univariate associations by showing how individual pairs of elements are related to each other. A paired-element correlation coefficient of "+1" indicates a perfect direct relationship between two variables, of "-1" indicates that one variable changes inversely with relation to the other, and of "0" indicates the lack of any sort of linear relationship between variables. Multivariate or multi-element statistics looks for associations between all variables within a data set. We utilized r-mode factor analysis, which uses the correlation matrix as a starting point, and selected an oblique solution with extreme variables as end members in the analysis. Factor analysis provides a technique to represent the many elements in the original data by a smaller

number of "factors", each of which is a linear function of the element concentrations, to provide data compression, which hopefully will also gain something in interpretability (Howarth and Sinding-Larsen, 1983). Factor scores that represented the variables in the factors were calculated; these scores were also used to plot the geographical distribution of the factors.

Histograms were used to visually illustrate the frequency distribution of a variable within a data set. To more accurately display the geologic data sets, the histograms were produced with a geometric scale by using Log 10 normalized data. The lower limit for each variable (minimum value of element in logs minus 0.0834) and a class interval for log scale (0.16666667) was used. (Note: In this report the class boundaries shown on the histograms have been converted to antilogs) The results of the frequency distribution for each variable was used to select the class boundaries of the high and low values to plot on the spatial data maps.

To compare the distribution of the high and low values of one variable to another variable we converted the variable data to a standard form—because the means for these variables were different and therefore, could not be compared directly. We calculated the normalized value (Z) for each variable value and then the normalized sum value (sum of Z) for each variable, which could be used to compared between variables. Z is equal to the variable value minus the variable mean, divided by the variable standard deviation; and the sum of Z is the summation of the Z values.

A t test was used to determine the significance of differences between the variable means in samples from two glacial sediment types (Sinclair, 1983).

BULK CONCENTRATE GEOCHEMICAL RESULTS

The samples of the heavy-mineral concentrates (bulk concentrates) were analyzed by fire assay to determine concentrations in parts per billion (ppb) of gold and the platinum group elements (platinum, palladium, ruthenium, rhodium, osmium, and iridium). The pilot-study samples were analyzed by the nickel-sulfide flux/ acid digestion method (Adrian and Carlson, 1990); and the test-study samples were analyzed by the lead-oxide flux/ silver doré bead method (Meier and others, 1991). These two methods have different element detection levels. Therefore, the data for the test-study samples is not included in the results for the bulk concentrates unless specifically noted.

The gold content of the bulk concentrates ranges from less than 10 to 10,000 ppb (Fig. 18). In over 75 percent of the samples gold was detected but was below the lower determination limit, which varied between 7 to 10 ppb because different sample sizes were assayed (Nelson and others, 1992). We calculated a maximum and a minimum geometric mean for gold because of the varying determination limits and concluded that the mean for gold is less than 10 ppb, but that we do not know the specific value. Positive gold values are distributed throughout the study area and are about equally distributed among samples from the Superior, Rainy, and Wadena lobes (Fig. 18). The positive values for gold from the test-study samples are also shown on Figure 18 because they represent a real occurrence of gold in the sample.

HEAVY-MINERAL CONCENTRATE

GOLD

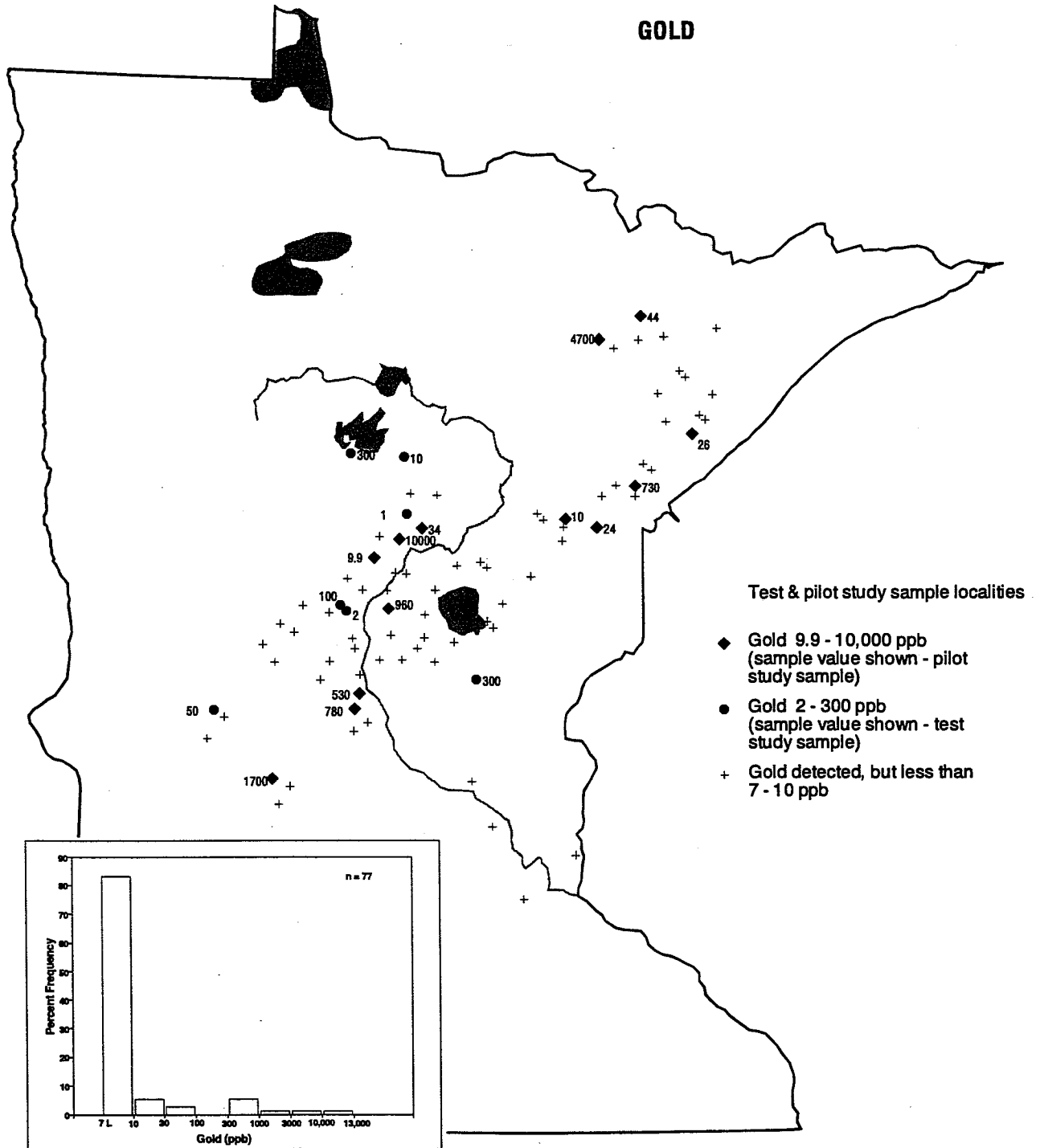


Figure 18. Frequency and geographic distribution of gold in samples of the heavy-mineral concentrates.

The platinum content of the bulk concentrates ranges from 1.2 to 5.3 ppb. The majority of samples contain less than 3 ppb platinum, and the histogram shows a relatively symmetrical distribution of values (Fig. 19). The geographic distribution of samples with platinum concentrations of ≥ 3 ppb are illustrated on Figure 19. The highest values (>4 ppb) cluster on the south edge of the Duluth Complex and scatter down-ice from there, with one isolated value just west of the Mississippi River. Mid-range values (3 to 4 ppb) start in the Duluth Complex and trail down ice to Mille Lacs Lake, with one isolated value further south. Figure 21A-C illustrates the frequency distribution of the platinum values in the bulk concentrates grouped by glacial sediment type. The t-test results confirm that significantly more platinum occurred in samples from 1) the Superior lobe compared with the Wadena lobe ($\alpha < .01$); 2) the Superior lobe compared with the Rainy lobe ($\alpha .01$); and 3) the Rainy lobe compared with the Wadena lobe ($\alpha .01$).

The palladium content of the bulk concentrates ranges from 0.6 to 8 ppb. The histogram shows an analytically-controlled distribution of values, with the majority of samples containing less than 3 ppm palladium (Fig. 20). Figure 20 shows the geographic distribution of samples with palladium concentrations ≥ 3 ppb. The higher values (4 to 5.3 ppb) form a tight cluster along the south edge of the Duluth Complex and trail down ice picking up the mid-range (3 to 4 ppb) values. The highest palladium value of 8 ppb (in sample number 23958) is isolated from the other high values. This value occurs in a sample collected west of the Mississippi River in sediments from the Wadena lobe; in this same area, the lowest palladium values (≤ 1 ppb) cluster (not illustrated). Figure 22A-C shows the frequency distribution of the palladium values in the bulk concentrates grouped by glacial sediment type. As with platinum, the histograms illustrate that palladium values are distinctly high in samples from the Superior lobe and distinctly low in samples from the Wadena lobe. The t-test confirms a distinct difference (significant at $\alpha .01$) in the palladium content of the bulk-concentrate samples between the Superior, Rainy and Wadena lobes.

The ruthenium content of the bulk concentrates ranges from less than 0.6 to 1 ppb. In 85 percent of the samples ruthenium was detected but was below the lower limit of determination, which varied from 0.6 to 1 ppb because different sample sizes were assayed (Nelson and others, 1992). The valid ruthenium values strongly cluster along and just southwest of the south edge of the Duluth Complex in samples from the Superior lobe (Fig. 23) and scatter along the Mississippi River in samples from the Rainy lobe. [Note: analytical interference with the determination of ruthenium is possible.]

Rhodium, osmium, and iridium were detected in the majority of the bulk-concentrate samples, but at concentrations below their lower determination limits. In less than 3 percent of the samples these elements were detected at their lower determination limits. The two valid rhodium values of 0.5 ppb occur in samples from the Superior lobe. The two valid osmium values of 2 ppb occur in samples from the Superior and the Wadena lobes. A single valid iridium value of 0.6 ppb occurs in a sample from the Rainy lobe. These samples are geographically scattered in central Minnesota (Fig. 24).

HEAVY-MINERAL CONCENTRATE PLATINUM

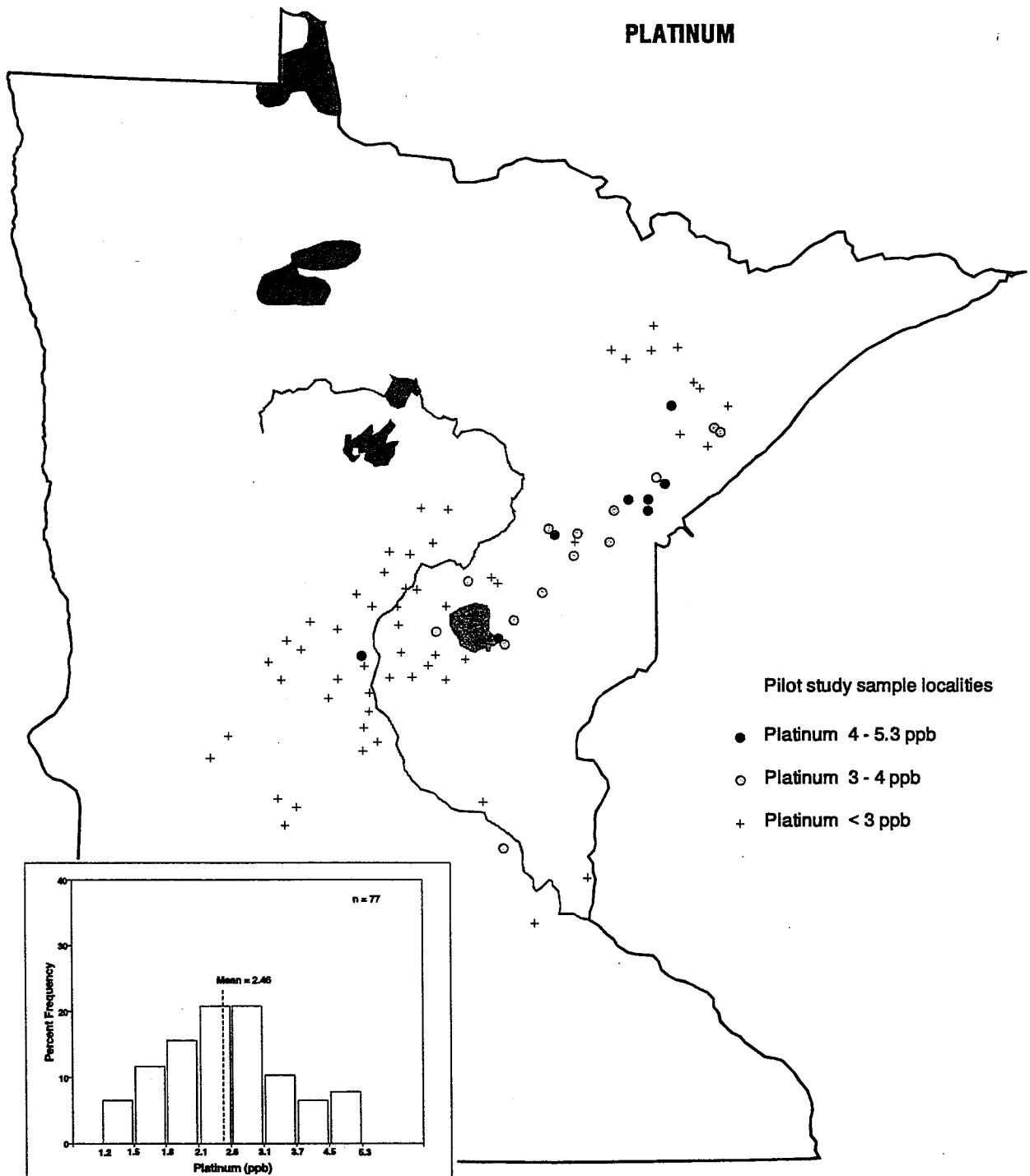


Figure 19. Frequency and geographic distribution of platinum in samples of the heavy-mineral concentrates.

HEAVY-MINERAL CONCENTRATE PALLADIUM

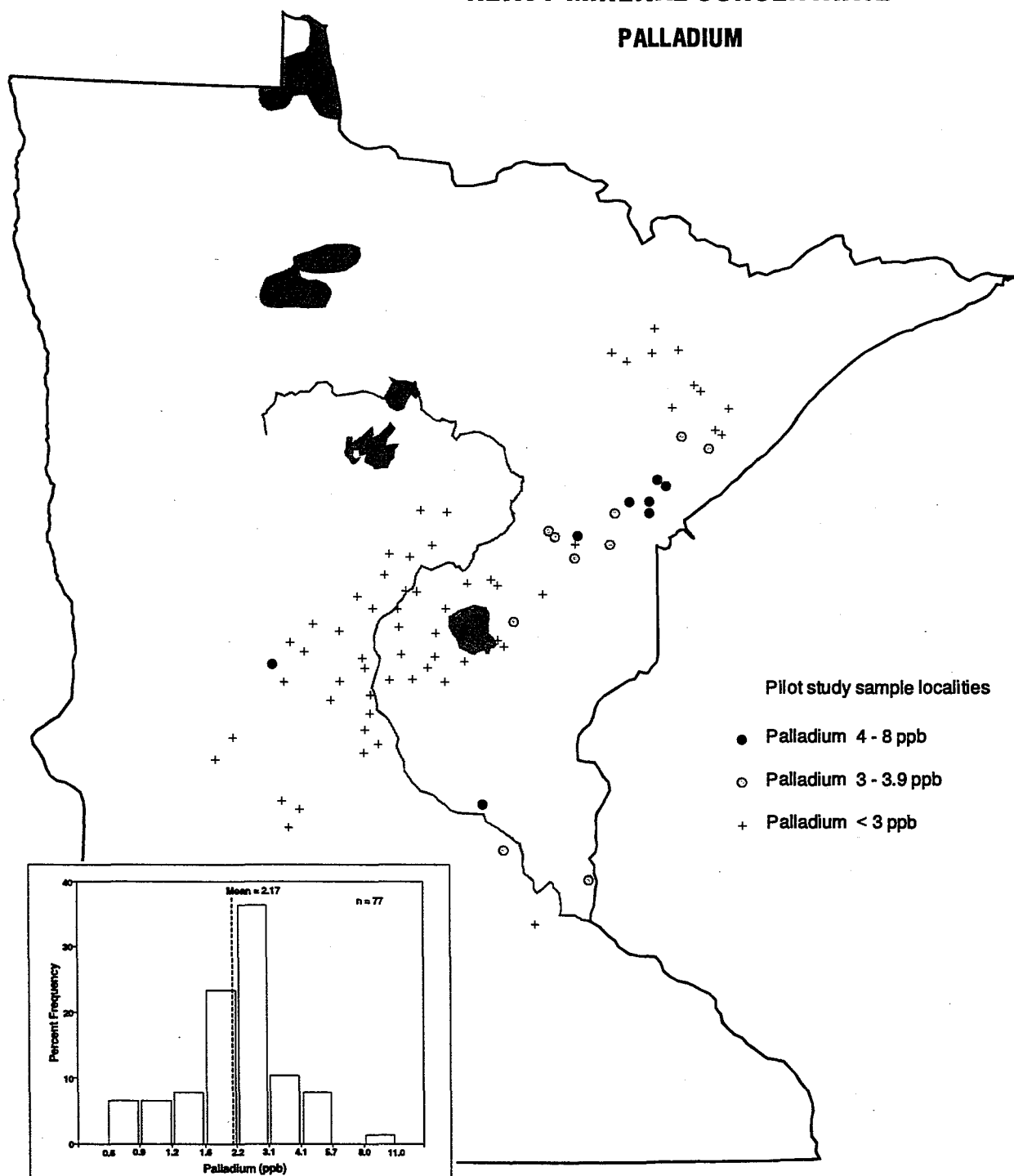


Figure 20. Frequency and geographic distribution of palladium in samples of the heavy-mineral concentrates.

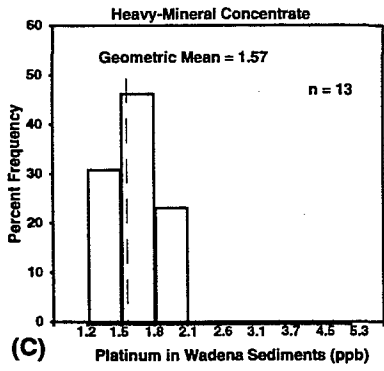
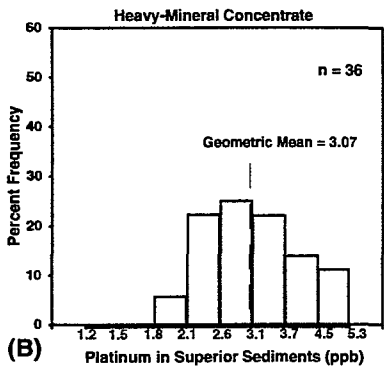
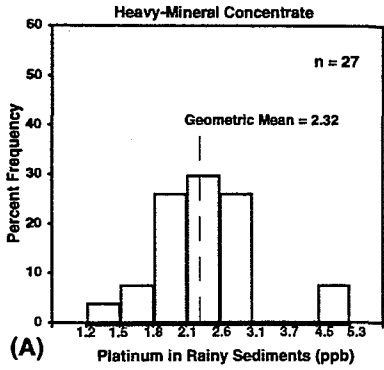


Figure 21A-C. Frequency distribution of platinum in samples of the heavy-mineral concentrates.

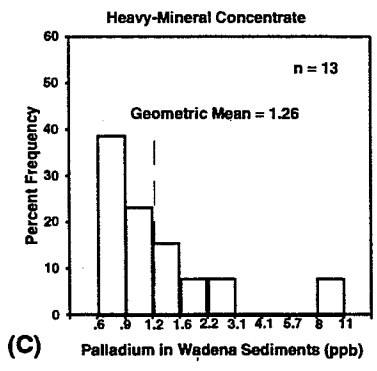
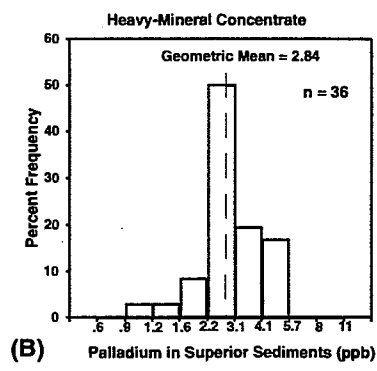
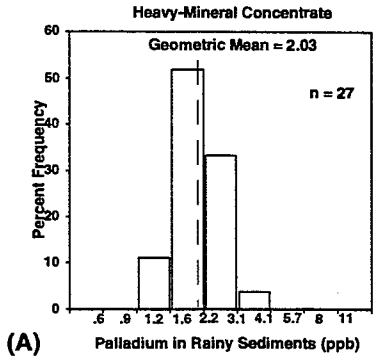


Figure 22A-C. Frequency distribution of palladium in samples of the heavy-mineral concentrates.

HEAVY-MINERAL CONCENTRATE

RUTHENIUM

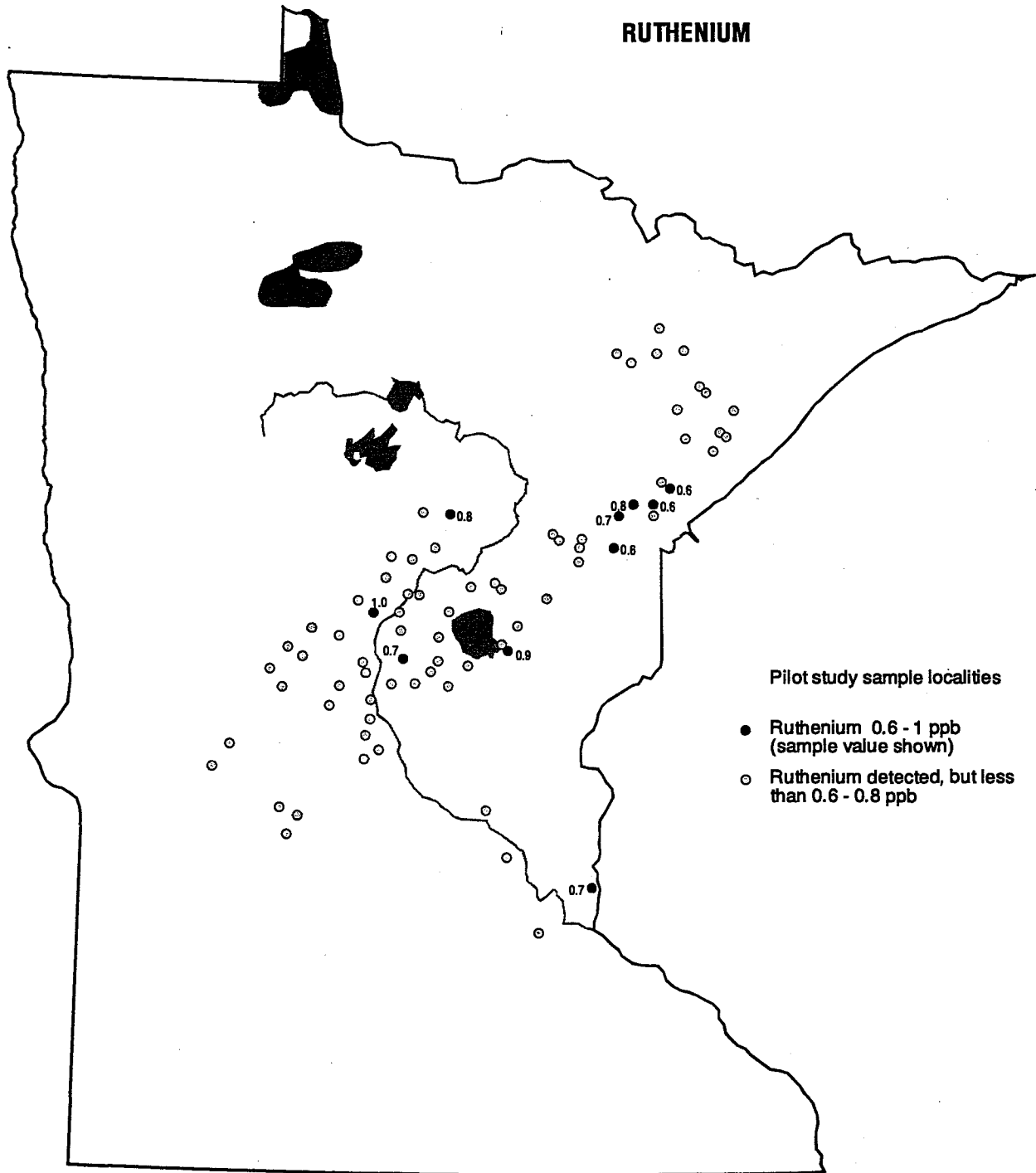


Figure 23. Geographic distribution of ruthenium in samples of the heavy-mineral concentrates.

HEAVY-MINERAL CONCENTRATE IRIDIUM, OSMIUM AND RHODIUM

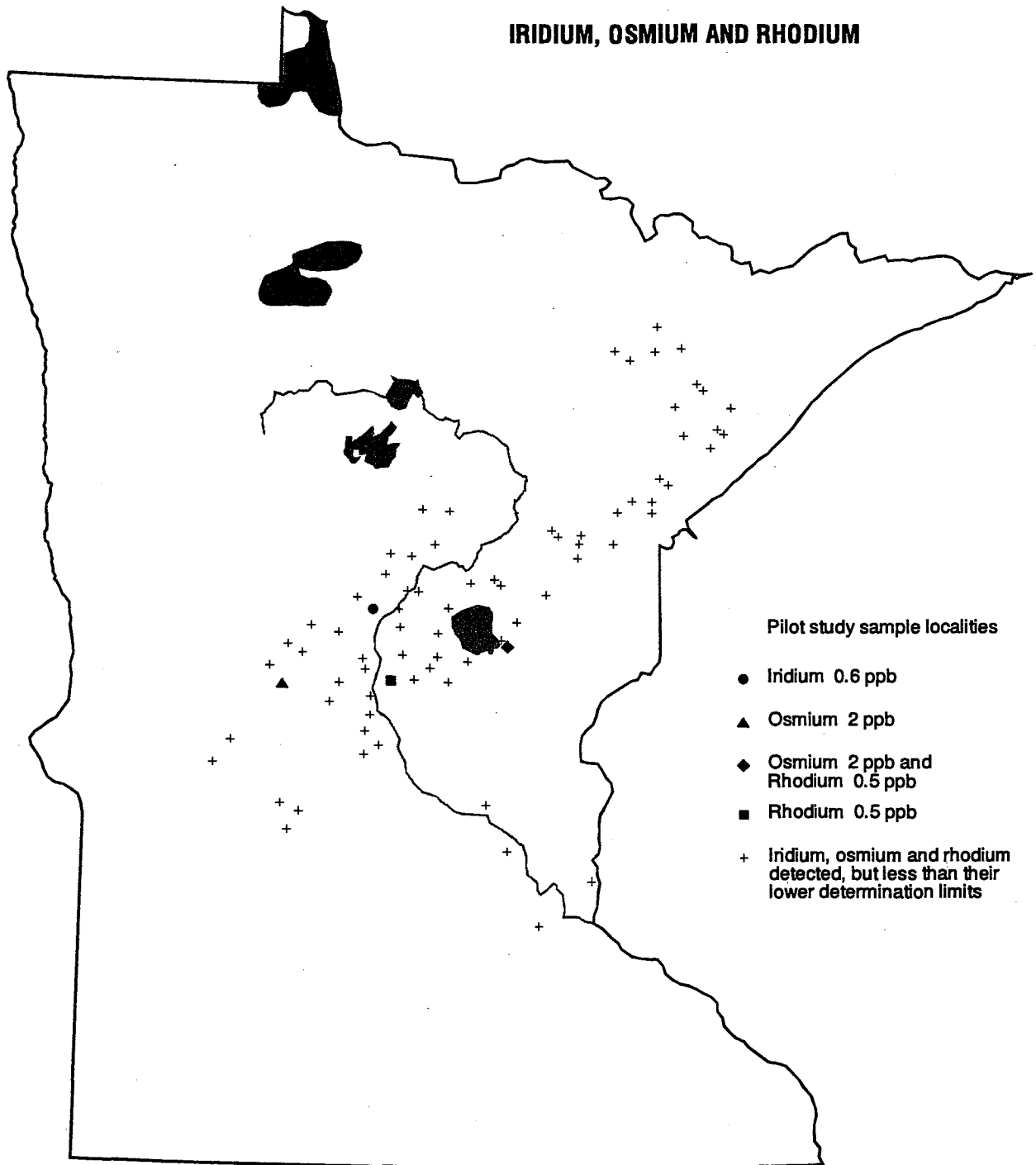


Figure 24. Geographic distribution of iridium, osmium and rhodium in samples of the heavy-mineral concentrates.

PARAMAGNETIC AND NONMAGNETIC FRACTION SAMPLE WEIGHT

To determine any significant variations of sample weight within or between samples from the paramagnetic and nonmagnetic fractions of the heavy-mineral concentrate, we calculated the weight of the samples in each fraction 1) by percent weight (or parts per million) of the minus-20-mesh (<0.83 mm) raw material used, and 2) by percent weight of the heavy-mineral concentrate. The sample weights for the test-study samples are not included because some measurements were not available.

The weights of the samples in the paramagnetic fraction (C2) range from 0.1 to 7.2 percent weight of the minus-20-mesh raw material, and from 61 to 90 percent weight of the heavy-mineral concentrate. These data are shown on figures 25 and 26, respectively, with Figure 25 differentiating the samples with ≥ 2 percent weight from those with < 2 percent weight. The samples with the larger percent weights of the minus-20-mesh raw material strongly cluster in and down ice of the Duluth Complex, with four isolated localities in central Minnesota (illustrated on Fig. 25); over 70 percent of these values are in samples from the Superior lobe, with the remaining from the Rainy lobe. In the vicinity of the Duluth Complex, the quantity of the paramagnetic fraction (C2) is much greater, but the percent weight of the heavy-mineral concentrate is less (see Fig. 26) because the ferromagnetic fraction (C1) is much larger in this same region (see Table 6 in Nelson and others, 1992)

The weights of the samples in the nonmagnetic fraction (C3) range from 20 to 900 parts per million (0.002 to 0.09 percent weight) of the minus-20-mesh raw material, and from 0.03 to 4.8 percent weight of the heavy-mineral concentrate. These data are shown on figures 27 and 28, respectively, with Figure 28 differentiating the samples with > 0.5 percent weight from those with ≤ 0.5 percent weight. The samples with the larger percent weights of the heavy-mineral concentrate strongly cluster throughout the central and southern parts of the study area, with a small tight cluster in the extreme northeastern part of the study area (northwest of the Duluth Complex) (see Fig. 28). These values occur in samples from all four lobes.

Comparing figures 25 and 28, it appears that between the two fractions the larger sample weights have almost an inverse relationship. In and down ice from the Duluth Complex, the weights of the paramagnetic-fraction (C2) samples are larger and the nonmagnetic-fraction (C3) samples are smaller. Throughout the central and southern parts of the study area and in the extreme northeastern part of the area, the weights of the nonmagnetic-fraction (C3) samples are larger and the paramagnetic-fraction (C2) samples are smaller. The sample weights within each fraction also vary substantially.

**PARAMAGNETIC FRACTION
SAMPLE WEIGHT
IN PERCENT WEIGHT
OF MINUS-20-MESH MATERIAL**

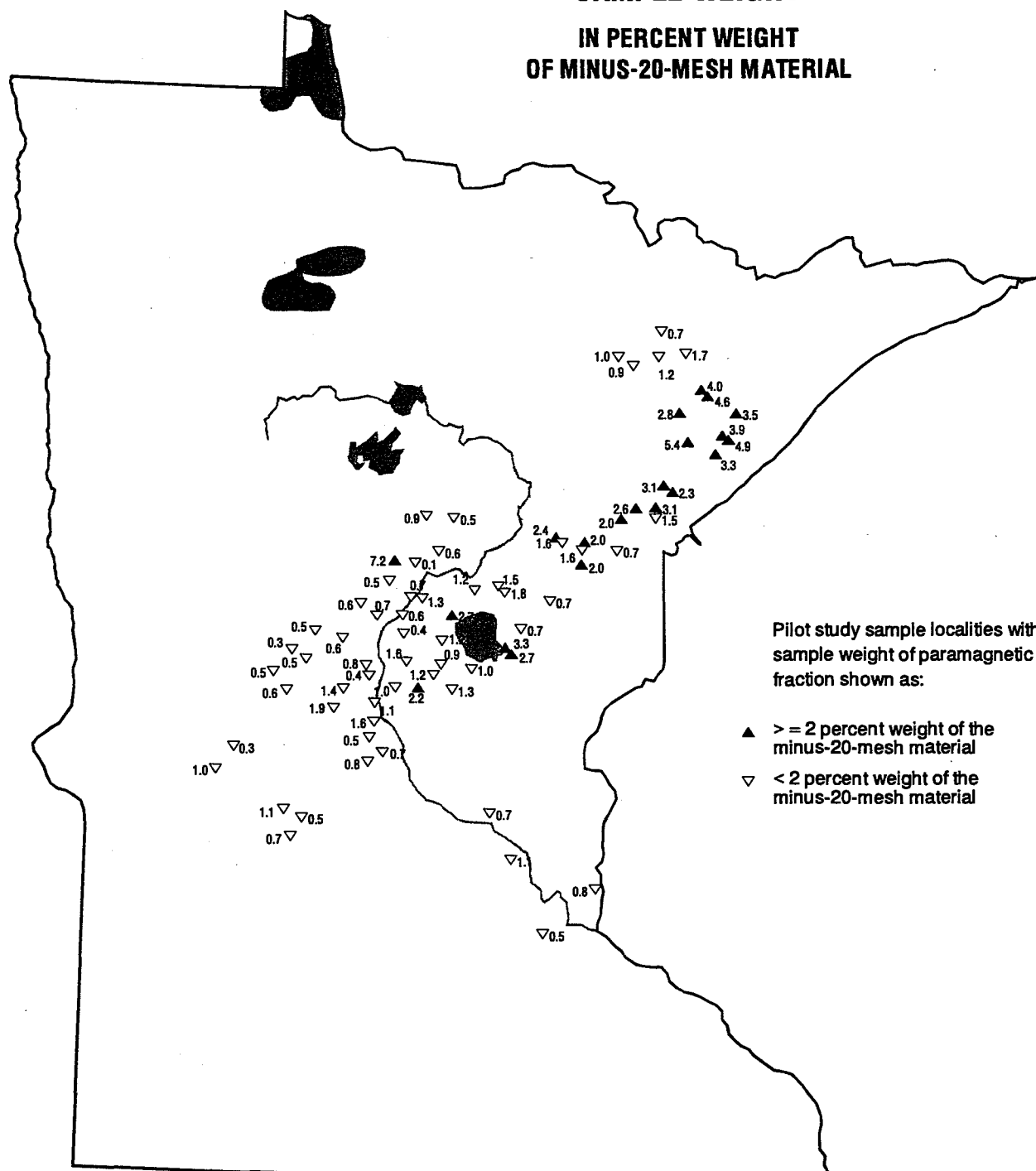


Figure 25. Geographic distribution of the sample weights of the paramagnetic-fraction (C2) samples shown in percent weight of the minus-20-mesh material.

**PARAMAGNETIC FRACTION
SAMPLE WEIGHT
IN PERCENT WEIGHT
OF HEAVY-MINERAL CONCENTRATE**

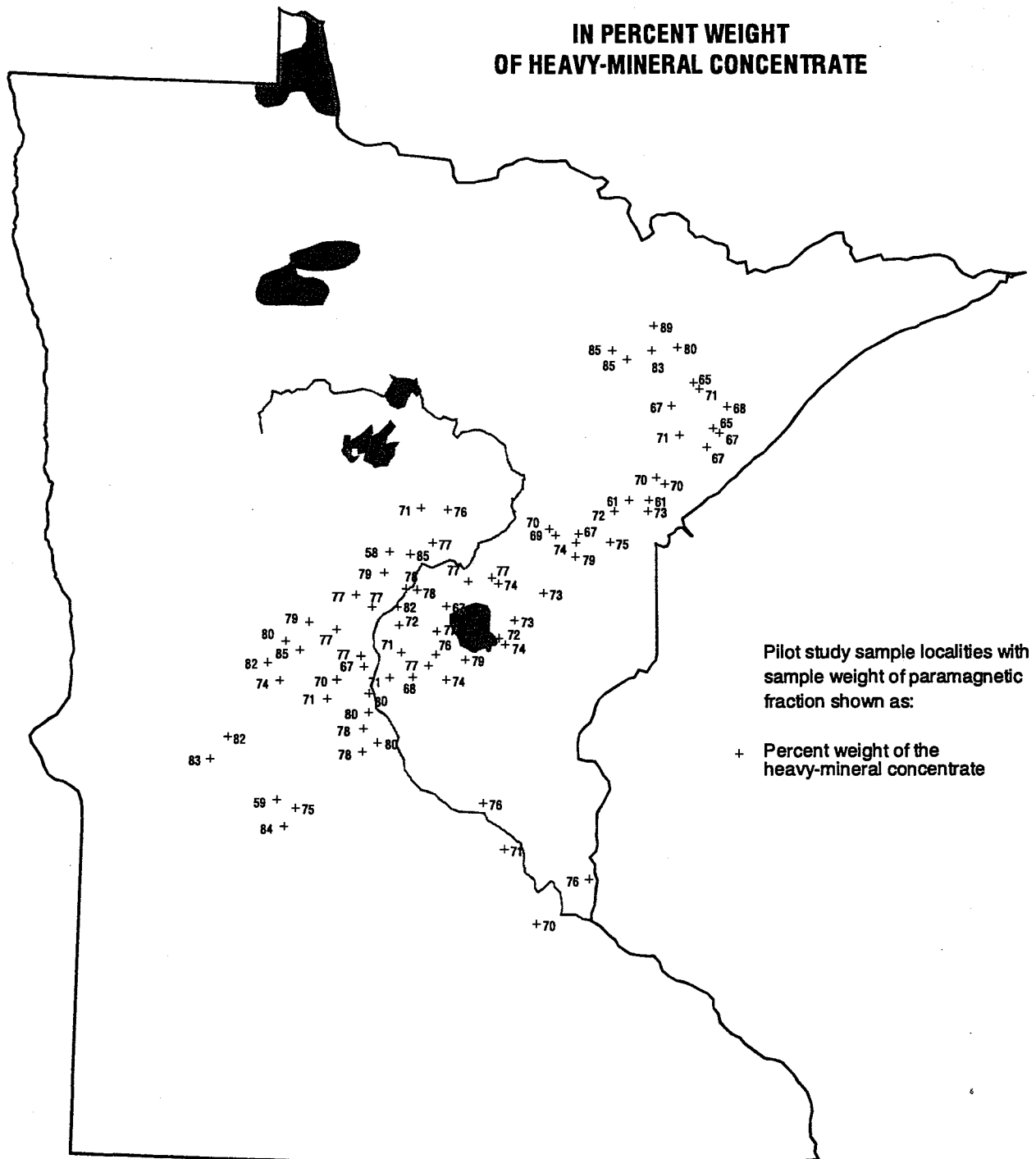


Figure 26. Geographic distribution of the sample weights of the paramagnetic-fraction (C2) samples shown in percent weight of the heavy-mineral concentrate.

**NONMAGNETIC FRACTION
SAMPLE WEIGHT
IN PARTS-PER-MILLION
OF MINUS-20-MESH MATERIAL**

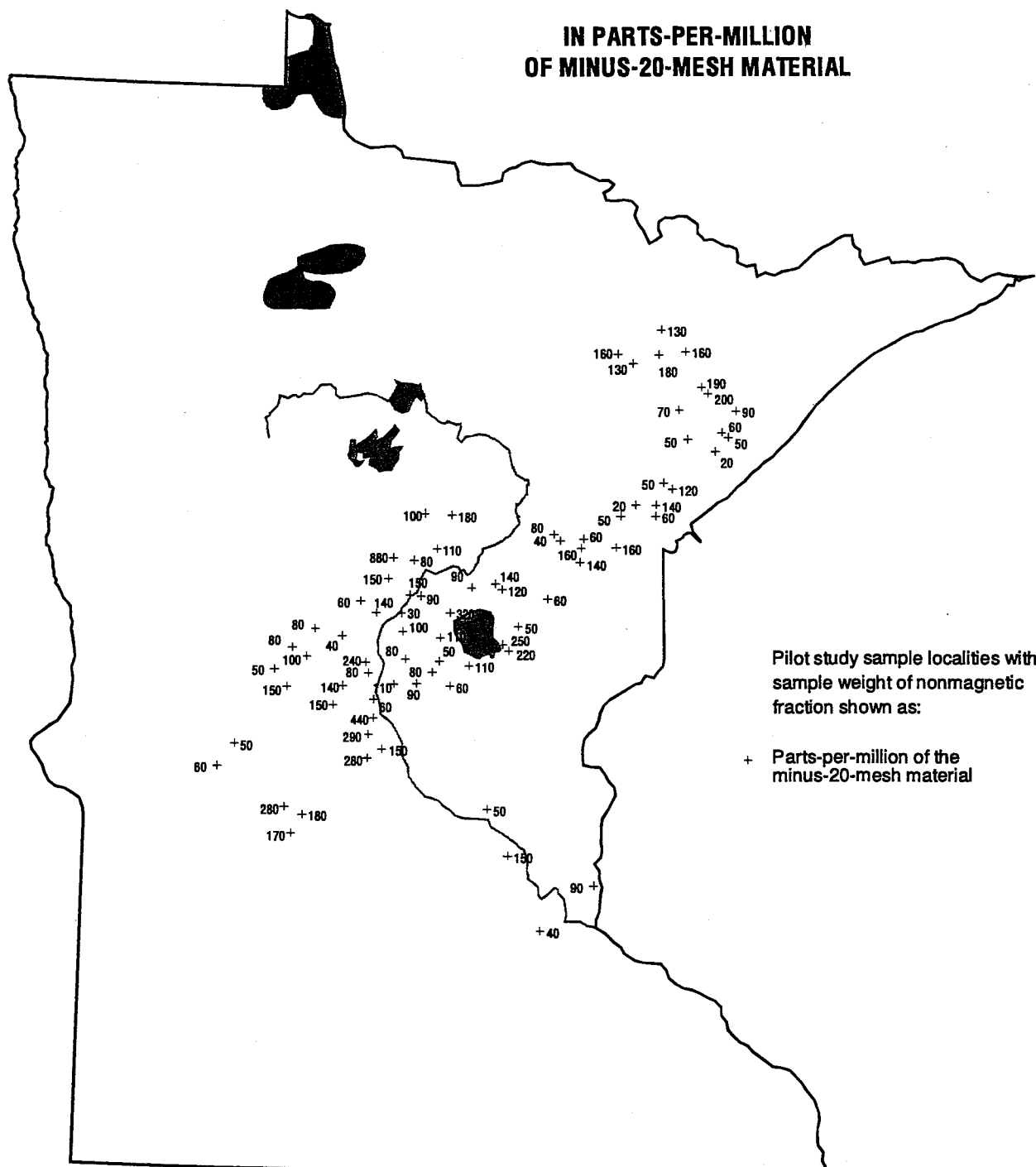


Figure 27. Geographic distribution of the sample weights of the nonmagnetic-fraction (C3) samples shown in parts-per-million of the minus-20-mesh material.

**NONMAGNETIC FRACTION
SAMPLE WEIGHT
IN PERCENT WEIGHT
OF HEAVY-MINERAL CONCENTRATE**

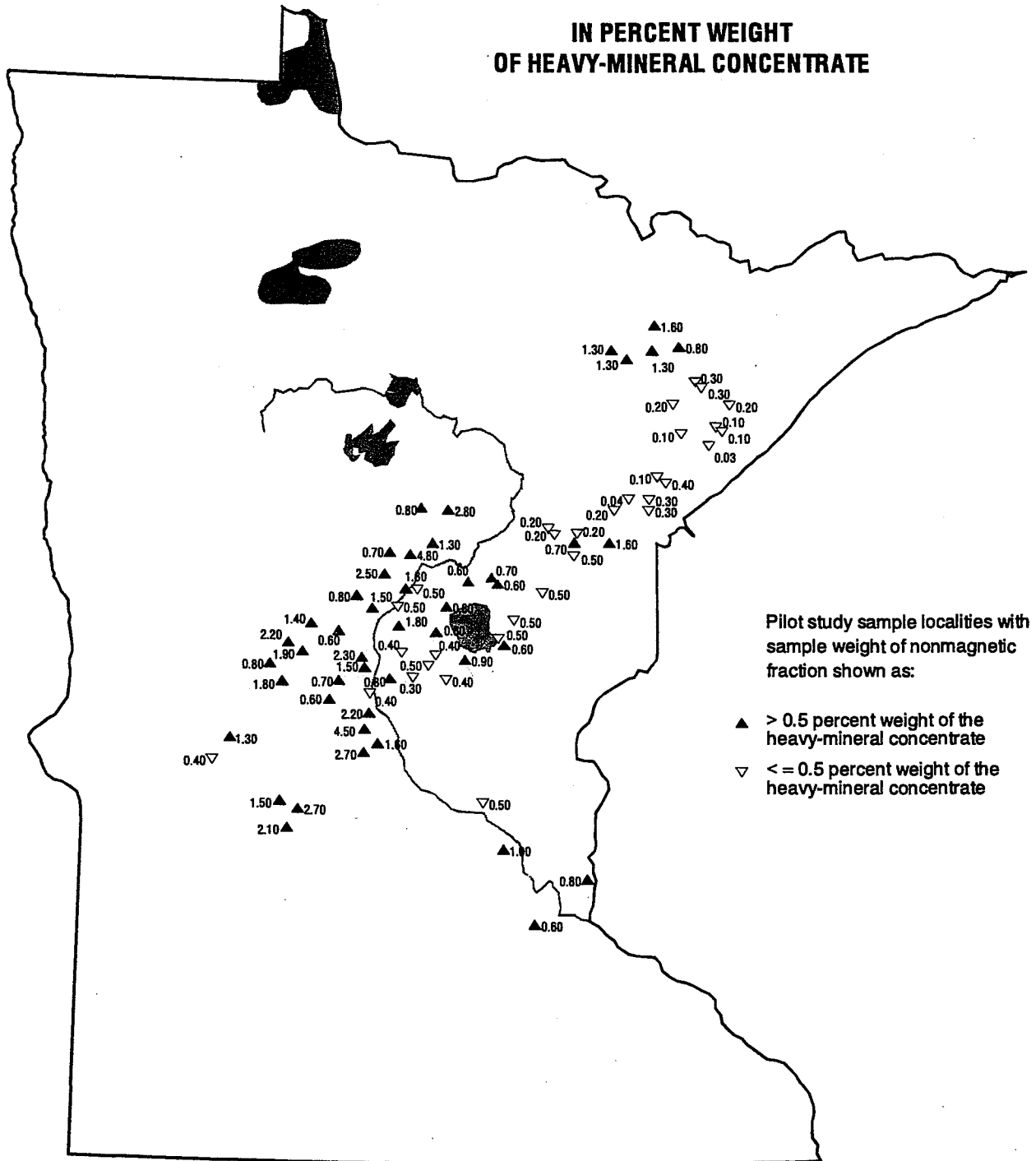


Figure 28. Geographic distribution of the sample weights of the nonmagnetic-fraction (C3) samples shown in percent weight of the heavy-mineral concentrate.

PARAMAGNETIC FRACTION GEOCHEMICAL RESULTS

The paramagnetic fraction (C2) of the heavy-mineral concentrates was analyzed by semiquantitative emission spectroscopy for thirty-five elements. In the eighty-five samples analyzed, nine of these elements were not detected at their lower determination limit: antimony (200 ppm), arsenic (500 ppm), bismuth (20 ppm), cadmium (50 ppm), germanium (20 ppm), gold (20 ppm), phosphorus (0.5 %), tungsten (50 ppm), and zinc (500 ppm). The remaining twenty-six elements with valid observations are summarized below by single-element data, paired-element correlations, and multi-element associations.

Single-element Data in the Paramagnetic Fraction

Six elements have a limited number of valid observations in the samples of the paramagnetic fraction (C2); these elements include sodium, beryllium, silver, molybdenum, tin, and thorium. In the majority of samples these elements, except for sodium, were not detected at their lower determination limits. Sodium was detected in 88 percent of the samples with concentrations at or below the lower determination limit of 0.5 %; only eleven of these samples have valid observations at 0.5 % and these values are in samples from the Rainy and Wadena lobes. Beryllium was detected in 16 percent of the samples with concentrations at or below the lower determination limit of 2 ppm. Most of the samples where beryllium was detected occur along or west of the Mississippi River in sediments from the Wadena and Rainy lobes. The remaining beryllium occurrences, which includes the single valid value of 2 ppm, form a small tight cluster of samples in the northeastern Rainy lobe sediments (Fig. 29). Silver was detected in two samples at the lower determination limit of 1 ppm; one sample is from Rainy lobe sediments that lie over a greenstone belt in the northeast, and the other sample is from Wadena lobe sediments collected southeast of Leech Lake (Fig. 30). Molybdenum was detected in three samples with concentrations at or below the lower determination limit of 10 ppm. A single valid value occurs in the extreme southwestern part of the study area in a sample from the Wadena lobe and two detectable values occur in adjacent sample sites along the Mississippi River in Rainy lobe sediments (Fig. 30). Tin and thorium were detected in a single sample but at concentrations below their lower determination limits of 20 and 200 ppm, respectively; this sample was collected in the extreme southwestern part of the study area in Wadena lobe sediments (Fig. 30). These six elements were excluded from further analysis.

Iron was detected in all paramagnetic-fraction (C2) samples with concentrations ranging from 10 to 30 percent of the sample, but the majority of these values are 20 percent or less. This inadequate variation of values for iron excluded it from further analysis.

The frequency distributions for the remaining nineteen elements observed in the paramagnetic-fraction (C2) samples are shown by groups of elements in figures 31 to 33 and summarized below. Magnesium was detected in all samples in concentrations ranging from 1.5 to 10 percent of the sample (Fig. 31A). Nickel was detected in all samples in concentrations ranging from 50 to 500 ppm, and 65 percent of these values are 100 ppm (Fig. 31B). Cobalt was detected in all samples in concentrations ranging from 50 to 200 ppm (Fig. 31C). Lanthanum was detected in 75 percent of the samples with concentrations ranging from less than 100 to 500 ppm, and over 70 percent of these values are 150 ppm or less (Fig. 31D).

PARAMAGNETIC FRACTION

BERYLLIUM

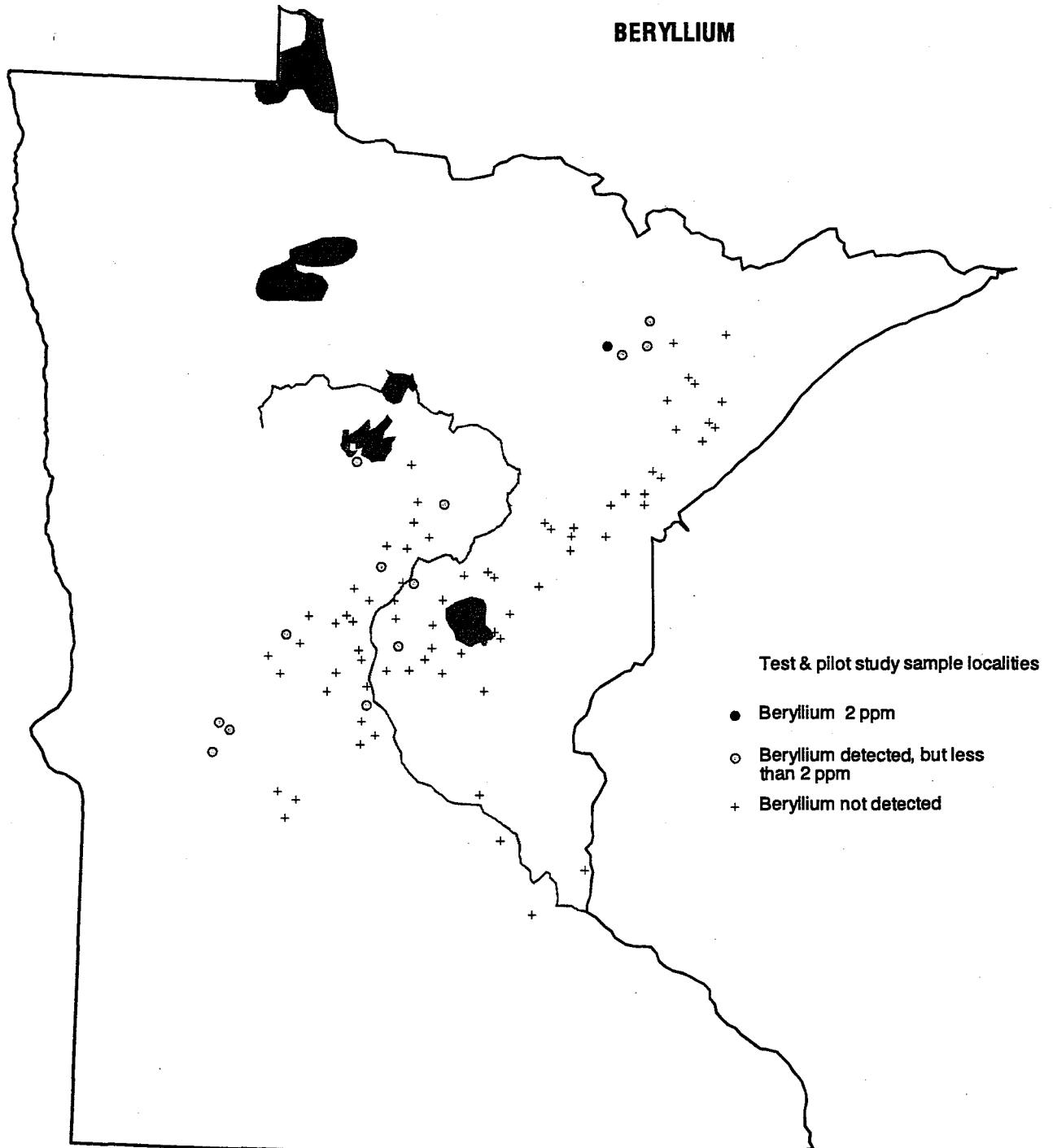


Figure 29. Geographic distribution of beryllium in samples of the paramagnetic fraction (C2) of the heavy-mineral concentrates.

PARAMAGNETIC FRACTION

SILVER, MOLYBDENUM, TIN AND THORIUM

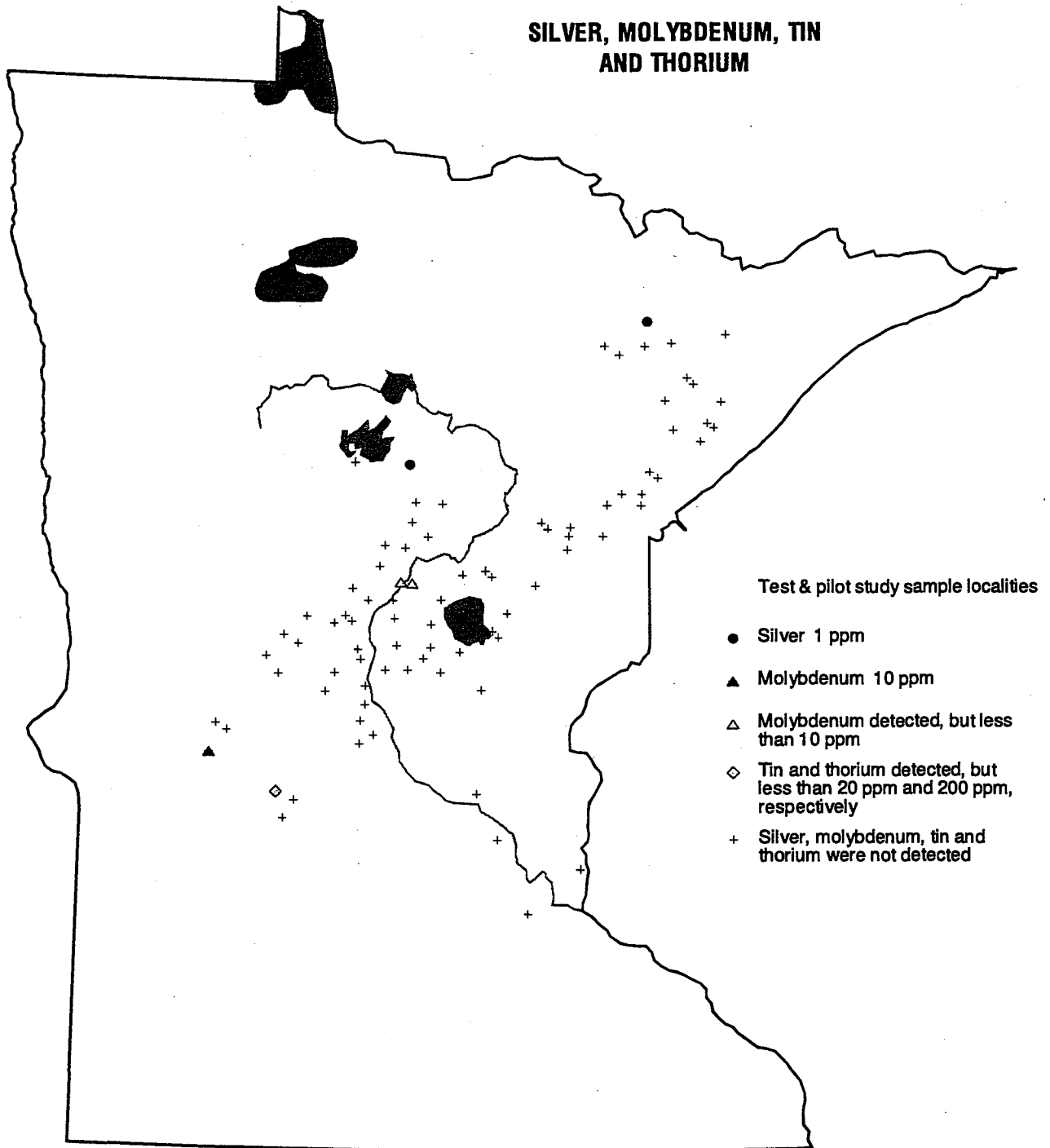


Figure 30. Geographic distribution of silver, molybdenum, tin and thorium in samples of the paramagnetic fraction (C2) of the heavy-mineral concentrates.

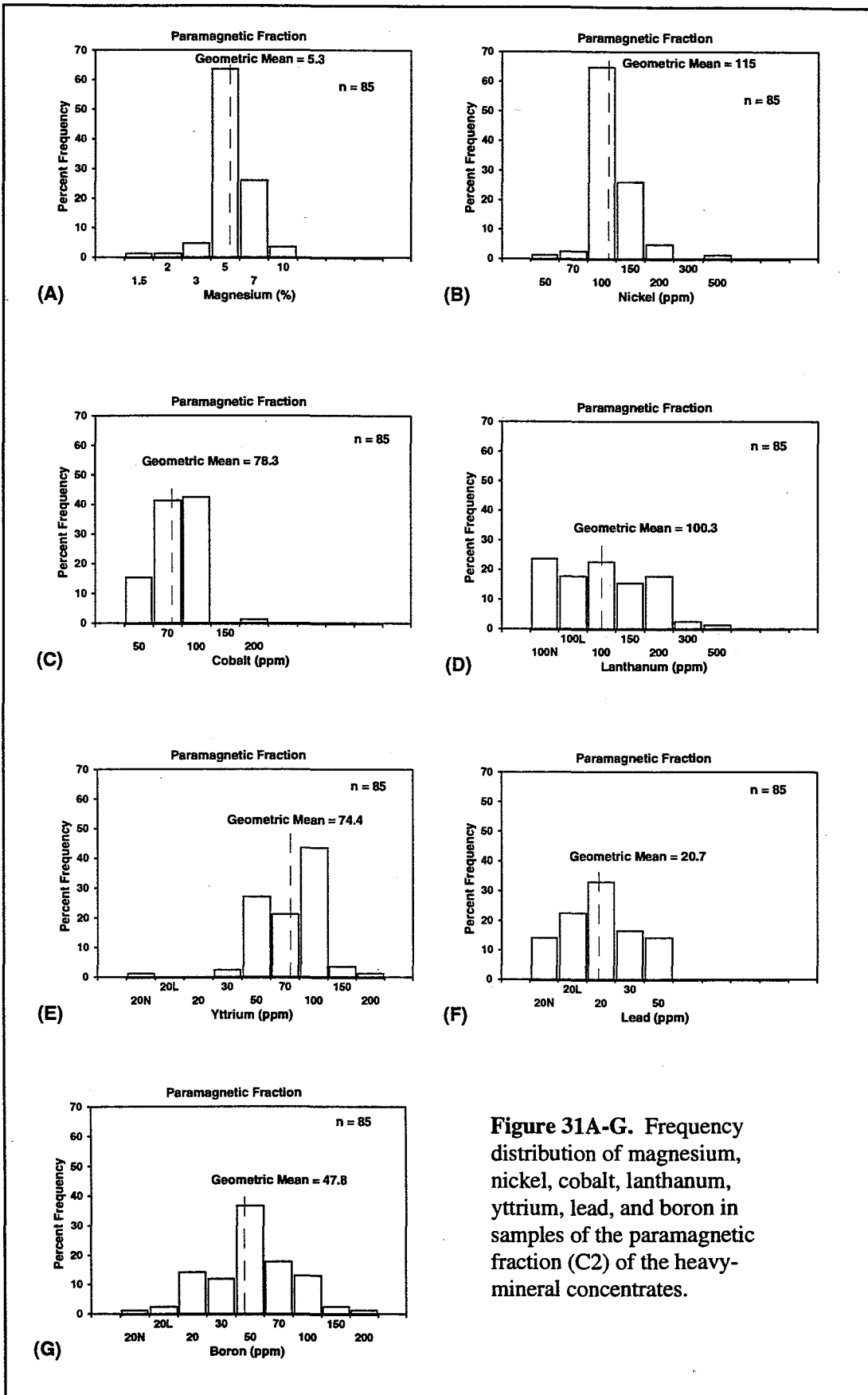


Figure 31A-G. Frequency distribution of magnesium, nickel, cobalt, lanthanum, yttrium, lead, and boron in samples of the paramagnetic fraction (C2) of the heavy-mineral concentrates.

Yttrium was detected in all samples except one, in concentrations ranging from 30 to 200 ppm, and the majority of these values are 100 ppm or less (Fig. 31E). Lead was detected in 85 percent of the samples in concentrations ranging from less than 20 to 50 ppm, and over 60 percent of these values are 20 ppm or less (Fig. 31F). Boron was detected in all samples except one, in concentrations ranging from less than 20 to 200 ppm, and over 80 percent of these values are 70 ppm or less (Fig. 31G). Gallium was detected in over 95 percent of the samples in concentrations ranging from less than 10 to 50 ppm, and the majority of these values are 20 ppm or less (Fig. 32A). Barium was detected in all samples in concentrations ranging from less than 50 to 500 ppm, and the majority of these values are 200 ppm or less (Fig. 32B). Calcium was detected in all samples in concentrations ranging from 0.5 to 10

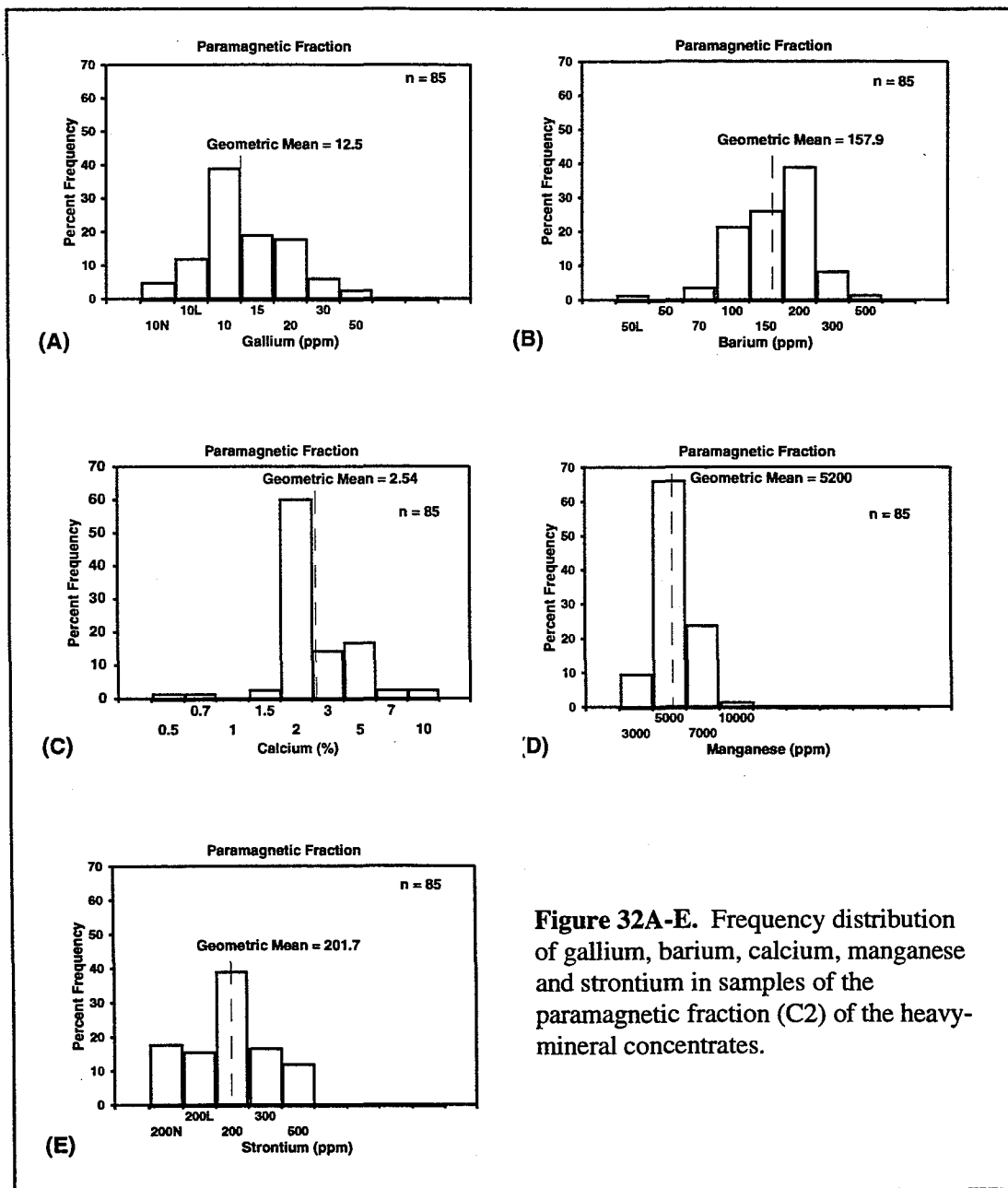


Figure 32A-E. Frequency distribution of gallium, barium, calcium, manganese and strontium in samples of the paramagnetic fraction (C2) of the heavy-mineral concentrates.

percent of the sample, and over 75 percent of these values are 3 percent or less (Fig. 32C). Manganese was detected in all samples in concentrations ranging from 3,000 to 10,000 ppm, and 75 percent of these values are 5,000 ppm or less (Fig. 32D). Strontium was detected in 80 percent of the samples in concentrations ranging from less than 200 to 500 ppm, and 65 percent of these values are 200 ppm or less (Fig. 32E). Chromium was detected in all samples in concentrations ranging from 200 to 700 ppm (Fig. 33A). Scandium was detected in all samples in concentrations ranging from 10 to 50 ppm, and 85 percent of these values are 30 ppm or less (Fig. 33B). Copper was detected in all samples in concentrations ranging from 15 to 150 ppm, and the majority of these values are 70 ppm or less (Fig. 33C). Zirconium was detected in all samples in concentrations ranging from 70 to 300 ppm (Fig. 33D). Niobium was detected in 95 percent of the samples in concentrations of 50 ppm or less. Titanium was detected in all samples in concentrations ranging from 1 percent to greater than 2 percent of the sample, and over one-third of these values are above the upper determination limit. Vanadium was detected in all samples in concentrations ranging from 150 to 300 ppm, and most of these values are 200 ppm.

[See Table 1 for a summary of the frequency distribution data for the 35 elements analyzed in the samples of the paramagnetic fraction (C2) of the concentrate.]

Figure 33A-D. Frequency distribution of chromium, scandium, copper and zirconium in samples of the paramagnetic fraction (C2) of the heavy-mineral concentrates.

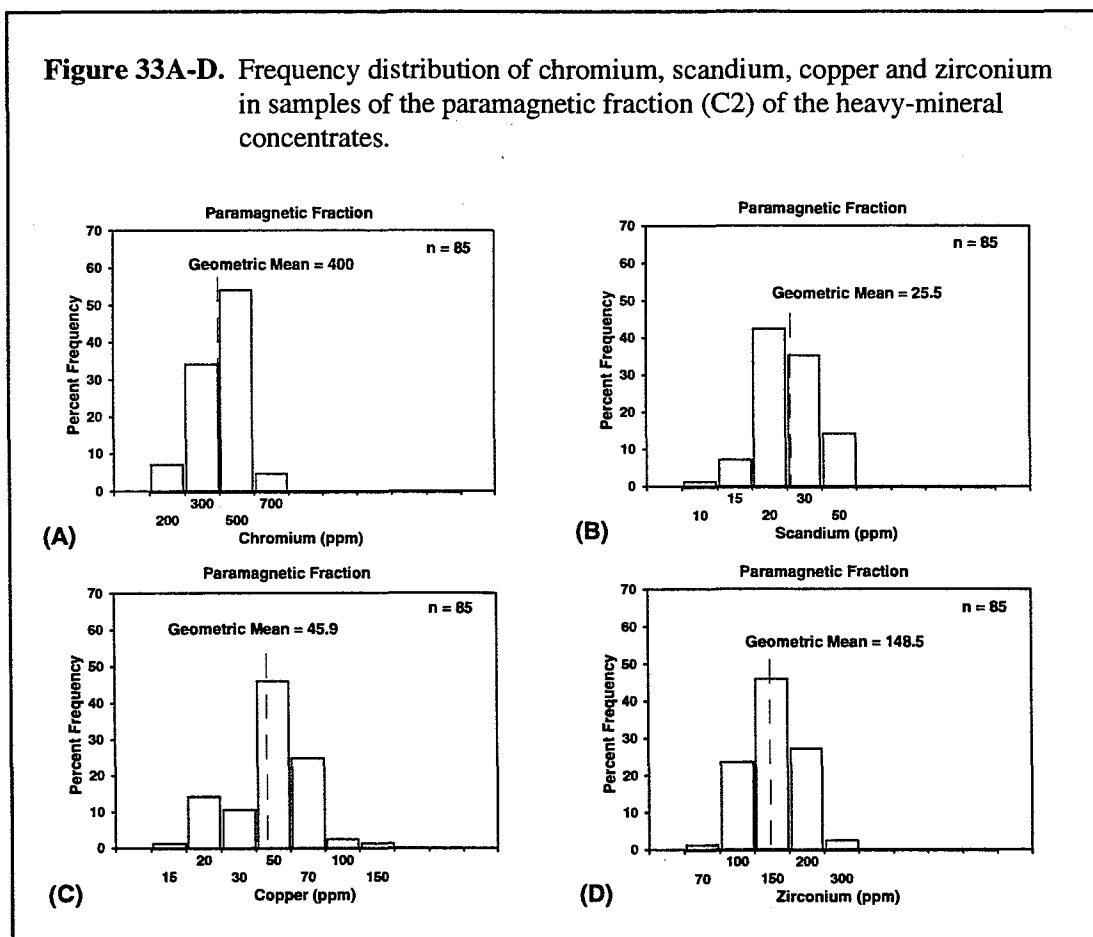


Table 1. Summary of frequency distribution data for the 35 elements analyzed in samples of the paramagnetic fraction (C2) of the heavy-mineral concentrates. [n = 85; elements with many valid observations are in shaded boxes; elements with a limited number of valid observations are in italic type; elements that were not detected are in standard type]

Element	See Histogram	Lower Limit of Determination 5mg sub-sample	% of Samples Element was Detected In	Range of Values Reported	Comments
Antimony (Sb)		200 ppm	0 %		Not detected at 200 ppm
Arsenic (As)		500 ppm	0 %		Not detected at 500 ppm
Barium (Ba)	Fig. 32B	50 ppm	100 %	< 50 - 500 ppm	Majority of values \leq 200 ppm
Beryllium (Be)		2 ppm	16 %	\leq 2 ppm	Only 1 valid value at 2 ppm
Bismuth (Bi)		20 ppm	0 %		Not detected at 20 ppm
Boron (B)	Fig. 31G	20 ppm	99 %	< 20 - 200 ppm	> 80 % of values are \leq 70 ppm
Cadmium (Cd)		50 ppm	0 %		Not detected at 50 ppm
Calcium (Ca)	Fig. 32C	0.1 %	100 %	0.5 - 10 %	> 75 % of values are \leq 3 %
Chromium (Cr)	Fig. 33A	20 ppm	100 %	200 - 700 ppm	
Cobalt (Co)	Fig. 31C	20 ppm	100 %	50 - 200 ppm	
Copper (Cu)	Fig. 33C	10 ppm	100 %	15 - 150 ppm	Majority of values are \leq 70 ppm
Gallium (Ga)	Fig. 32A	10 ppm	96 %	< 10 - 50 ppm	Majority of values are \leq 20 ppm
Germanium (Ge)		20 ppm	0 %		Not detected at 20 ppm
Gold (Au)		20 ppm	0 %		Not detected at 20 ppm
Iron (Fe)		0.1 %	100 %	10 - 30 %	Majority of values \leq 20 %
Lanthanum (La)	Fig. 31D	100 ppm	75 %	< 100 - 500 ppm	> 70 % of values at \leq 150 ppm
Lead (Pb)	Fig. 31F	20 ppm	85 %	< 20 - 50 ppm	> 60 % of values at \leq 20 ppm
Magnesium (Mg)	Fig. 31A	0.05 %	100 %	1.5 - 10 %	
Manganese (Mn)	Fig. 32D	20 ppm	100 %	3000 - 10,000 ppm	75 % of values are \leq 5000 ppm
Molybdenum (Mo)		10 ppm	4 %	\leq 10 ppm	1 valid value at 10 ppm
Nickel (Ni)	Fig. 31B	10 ppm	100 %	50 - 500 ppm	65 % of values at 100 ppm
Niobium (Nb)		50 ppm	95 %	\leq 50	
Phosphorus (P)		0.5 %	0 %		Not detected at 0.5 %
Scandium (Sc)	Fig. 33B	10 ppm	100 %	10 - 50 ppm	85 % of values are \leq 30 ppm
Silver (Ag)		1 ppm	2 %	1 ppm	2 valid values at 1 ppm
Sodium (Na)		0.5 %	88 %	\leq 0.5 %	Only 11 valid values at 0.5 %
Strontium (Sr)	Fig. 32E	200 ppm	80 %	< 200 - 500 ppm	65 % of values are \leq 200 ppm
Thorium (Th)		200 ppm	1 %	< 200 ppm	Detected in 1 sample, no valid values
Tin (Sn)		20 ppm	1 %	< 20 ppm	Detected in 1 sample, no valid values
Titanium (Ti)		0.005 %	100 %	1 - > 2 %	> 33 % above 2 % upper determination limit
Tungsten (W)		50 ppm	0 %		Not detected at 50 ppm
Vanadium (V)		20 ppm	100 %	150 - 300 ppm	Majority of values are 200 ppm
Yttrium (Y)	Fig. 31E	20 ppm	99 %	30 - 200 ppm	Majority of values \leq 100 ppm
Zinc (Zn)		500 ppm	0 %		Not detected at 500 ppm
Zirconium (Zr)	Fig. 33D	20 ppm	100 %	70 - 300 ppm	

The histograms illustrate that Mg, Co, La, Y, B, Ga, Ba, Ca, and Cu have a distribution of values exceeding analytical variation. Lead values show a good frequency distribution, but the valid values have a small range. The frequency distributions for Cr, Mn, Ni, Sc, Sr, and Zr barely exceed analytical variation. Niobium, titanium, and vanadium have inadequate variation in their values.

For these same nineteen elements, we looked at the frequency distribution of the single-element data in samples of the paramagnetic fraction (C2) grouped by glacial sediment type. T-tests measured the significance of any differences in the element means between lobes. Results showed significantly more ($\alpha < .01$) lanthanum, strontium, lead, yttrium, boron, chromium, ($\alpha .01$) manganese, gallium, ($\alpha .05$) barium, niobium, and magnesium in samples from the Wadena lobe compared with the Superior lobe; and significantly more ($\alpha < .01$) lanthanum, boron, ($\alpha .01$) chromium, niobium, lead, yttrium, ($\alpha .05$) strontium, and zirconium in samples from the Wadena lobe compared with the Rainy lobe. Differences in the element means between the sediment types also showed significantly more ($\alpha .01$) nickel, ($\alpha .05$) cobalt and copper in samples from the Superior lobe compared with the Wadena lobe; and significantly more ($\alpha .01$) zirconium in samples from the Superior lobe compared with the Rainy lobe. The t-test results also showed significantly more ($\alpha < .01$) strontium, gallium, lanthanum, and ($\alpha .05$) manganese in samples from the Rainy lobe compared with the Superior lobe; and significantly more ($\alpha .01$) nickel in samples from the Rainy lobe compared with the Wadena lobe. See Table 2 for a summary of the elements in the paramagnetic fraction that show a significant difference in their means between samples from the various glacial lobes.

Table 2. Summary of elements that show a significant difference in their means between the samples from the various glacial lobes in the paramagnetic fraction (C2) of the concentrates. [19 elements compared; element listed below the significance level measured]

Significantly more of the element listed is found in samples in the:	Higher Significance.....Lower Significance		
	$\alpha < .01$	$\alpha = .01$	$\alpha = .05$
Wadena lobe sediments compared w/ Superior	La, Sr, Pb, Y, B, Cr	Mn, Ga	Ba, Nb, Mg
Wadena lobe sediments compared w/ Rainy	La, B	Cr, Nb, Pb, Y	Sr, Zr
Superior lobe sediments compared w/ Wadena		Ni	Co, Cu
Superior lobe sediments compared w/ Rainy		Zr	
Rainy lobe sediments compared w/ Superior	Sr, Ga, La		Mn
Rainy lobe sediments compared w/ Wadena		Ni	

Paired-element Correlations in the Paramagnetic Fraction

Paired-element correlation coefficients that represent the correlations between nineteen elements observed in samples from the paramagnetic fractions (C2) are shown in Figure 34. The three elements with inadequate data variation are separated on the correlation matrix from the other elements. Although the correlation coefficients are significant at 0.2 when $\alpha = .05$ and at 0.28 when $\alpha = .01$, only the stronger paired-element correlation coefficients of $\geq +0.4$ and ≤ -0.4 are highlighted on the matrix.

The positive correlation between chromium and lanthanum of .55 and the negative correlation between chromium and nickel of -.41 (see Fig. 34) is just the opposite of what would be expected between these element pairs. The samples with a high chromium content also contain a high lanthanum content, and the low values for each element also occur together; this is not a case of just one element with a particularly high or low value in the sample. We calculated the normalized sum of chromium and lanthanum values and then plotted the high (>2) and low (<-2) sum values (Fig. 35). All samples with a high chromium-lanthanum correlation occur west of the Mississippi River in Wadena lobe sediments (see Fig. 35). The samples with a low chromium-lanthanum correlation strongly cluster in and down ice of the Duluth Complex in Rainy and Superior lobe sediments (see Fig. 35). Histograms of the sum values grouped by glacial sediment type (not illustrated) show that in the paramagnetic fraction (C2) of the concentrate there is significantly more ($\alpha < .01$) chromium and lanthanum in samples from the Wadena lobe than in samples from either the Superior or Rainy lobes. In the samples west of the Mississippi River, a scanning electron microscope identified chromium in an amphibole, hornblende; and lanthanum in the rare-earth minerals monazite, florencite [$\text{CeAl}_3(\text{PO}_4)_2(\text{OH})_6$], and cheralite [$(\text{Ca,Ce,Th})(\text{P,Si})\text{O}_4$]. These results represent the analysis of the paramagnetic fraction (C2), not the whole heavy-mineral concentrate, which could be a partial explanation of the results.

Other positive correlations highlighted on Figure 34 include the association of: (1) lanthanum with: lead, yttrium, strontium, boron, and manganese; (2) nickel with magnesium and cobalt; (3) chromium with: boron, yttrium, strontium, and lead; (4) manganese with: barium, gallium, lead, strontium, yttrium, and boron; (5) barium with: gallium, boron, calcium, and yttrium; (6) yttrium with boron and strontium; (7) lead with boron and gallium; and (8) gallium with calcium. The negative correlations highlighted on the matrix indicate an inverse relationship between the occurrence of: (1) nickel with: yttrium, boron and lanthanum; (2) magnesium with: lanthanum, yttrium and lead; (3) gallium with scandium; and (4) magnesium with vanadium (Note: vanadium is an element with inadequate data variation). Overall, the matrix shows a significant degree of correlation between many of the elements observed in the paramagnetic-fraction (C2) samples.

We also looked for paired-element correlations in the paramagnetic-fraction (C2) samples grouped by glacial sediment type. These results show many paired-element correlations within samples from the Rainy lobe, less within samples from the Wadena lobe, and very few paired-element correlations within samples from the Superior lobe.

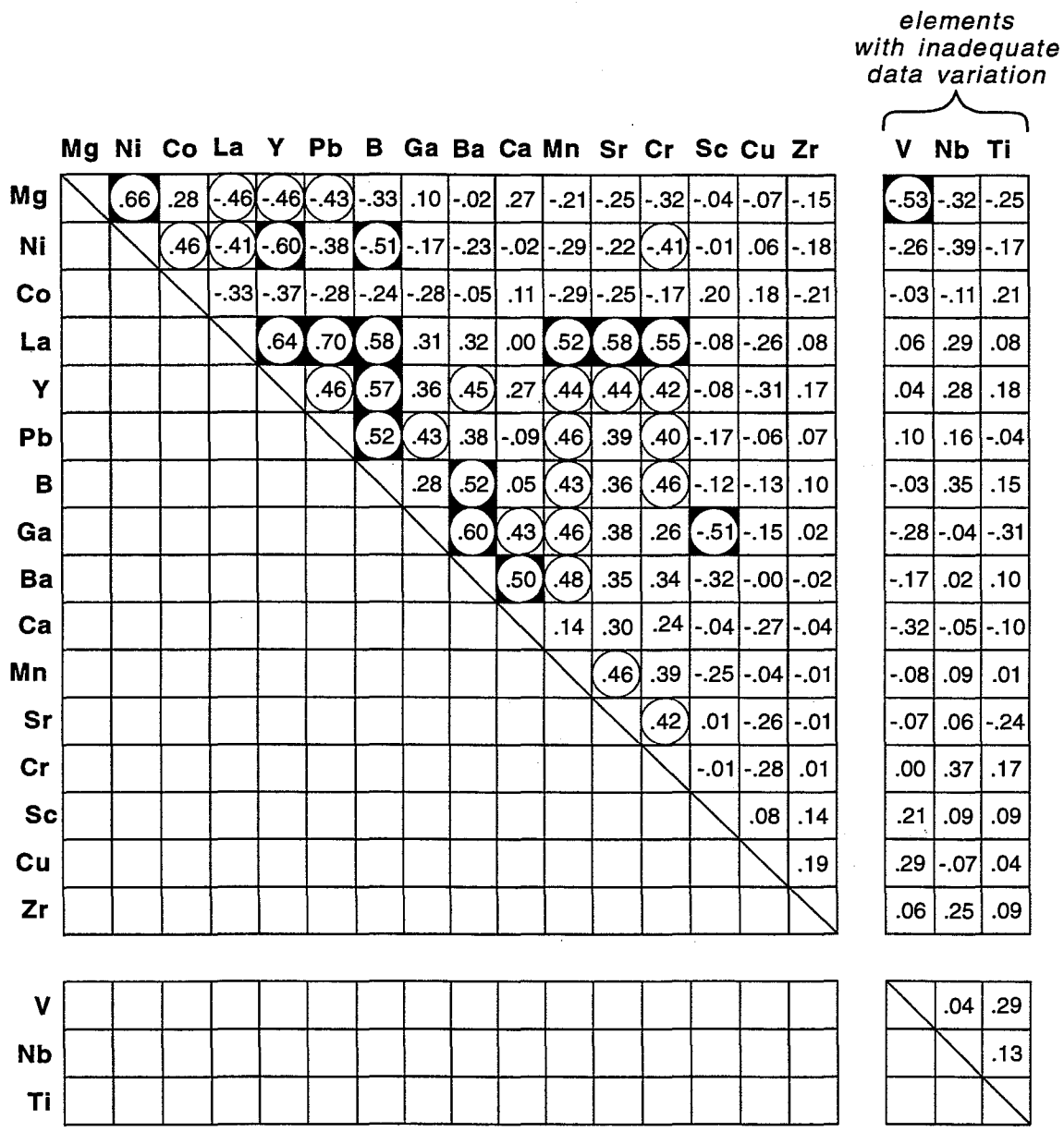


Figure 34. Paired-element correlation coefficients for 19 elements in samples of the paramagnetic fraction (C2) of the heavy-mineral concentrates.

PARAMAGNETIC FRACTION

NORMALIZED SUM VALUES OF CHROMIUM AND LANTHANUM

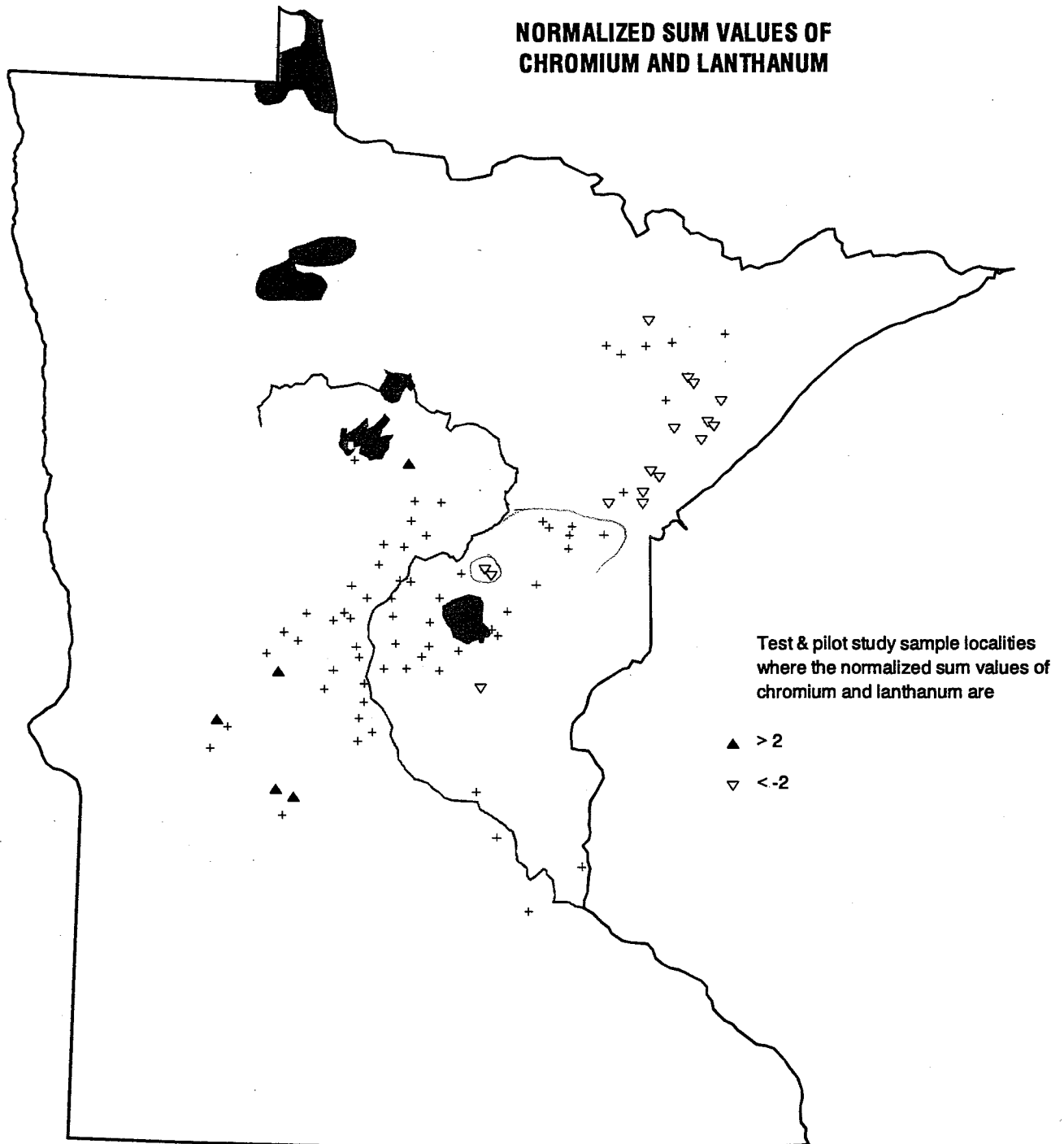


Figure 35. Geographic distribution of the high and low normalized sum values of chromium and lanthanum in samples of the paramagnetic fraction (C2) of the heavy-mineral concentrates.

Multi-element Associations in the Paramagnetic Fraction

R-mode factor analysis, using two- to ten-factor models, examined the multi-element associations among sixteen elements observed (Ba, B, Ca, Co, Cu, Cr, Ga, La, Pb, Mg, Mn, Ni, Sc, Sr, Y, and Zr) in samples of the paramagnetic fraction (C2). The six elements with few valid observations (Na, Be, Ag, Mo, Sn, Th) and the four elements with inadequate data variation (Fe, Nb, Ti, V) were excluded from this analysis. The two-factor model was selected as the most solid factor because it contains both dominant factors, a strong felsic group and a strong mafic group, together in factor I and contains most of the other elements in factor II.

Elements most strongly correlated with factor I of the two-factor model are the positive correlations of magnesium, nickel, and cobalt—elements commonly associated with mafic rocks; and their inverse (negative) correlation with the occurrence of lanthanum, yttrium, lead, and boron—elements commonly associated with felsic rocks. Samples that show the strongest association between magnesium, nickel, and cobalt (factor scores >1) strongly cluster in the northeastern Duluth Complex area (see Fig. 36), which reflects the predominantly mafic character of that terrane. The samples that show the strongest association between lanthanum, yttrium, lead, and boron (factor scores <-1) occur west of the Mississippi River in areas where felsic terrane commonly occurs. Histograms of the factor I scores grouped by glacial sediment type (not illustrated) show that there is significantly more magnesium, nickel, and cobalt in samples from the Superior ($\alpha .01$) and Rainy ($\alpha .05$) lobes compared with samples from the Wadena lobe, which reflects the geographic distribution shown in Figure 36.

Elements most strongly correlated with factor II of the two-factor model are the positive correlations of Ga, Ba, Ca, Mn, Sr, Y, Cr, B, La, and Pb—elements commonly associated with felsic and chemical sedimentary rock constituents; and their inverse correlation with the occurrence of scandium—a common mafic rock constituent. Samples that show the strongest positive element associations (factor scores >1) cluster west of the Mississippi River in areas commonly underlain by felsic or sedimentary rock terrane; two additional samples occur in the northeast in areas underlain by felsic terrane (Fig. 37). The samples that show the strongest concentrations of scandium (factor scores <-1) and the absence of any strong felsic element associations, scatter from the northeastern-most sample to west of the Mississippi River (see Fig. 37) and include areas underlain by mafic or felsic terrane. Histograms of the factor II scores grouped by glacial sediment type (not illustrated) show that there is significantly more Ga, Ba, Ca, Mn, Sr, Y, Cr, B, La, and Pb in samples from the Wadena ($\alpha <.01$) and Rainy ($\alpha .05$) lobes compared with samples from the Superior lobe, which generally reflects the geographic distribution shown in Figure 37.

In the three- to ten-factor models the felsic and mafic components are not as strong as in factor I of the two-factor model, often including elements not usually associated with them. A chromium-lanthanum association shows up in these models, which is absent in the two-factor model.

In the six- to ten-factor models copper and zirconium fall out as single elements, suggesting a weak association with the other elements. Figure 38 illustrates the distribution of the high (≥ 100 ppm) and low (≤ 30 ppm) copper values in samples of the paramagnetic fraction (C2). The three high copper values are widely dispersed across the study area in samples from the Superior or Rainy lobe and are underlain by different bedrock terranes. Two-thirds of the

**PARAMAGNETIC FRACTION
FACTOR SCORES FOR
FACTOR I OF TWO-FACTOR MODEL**

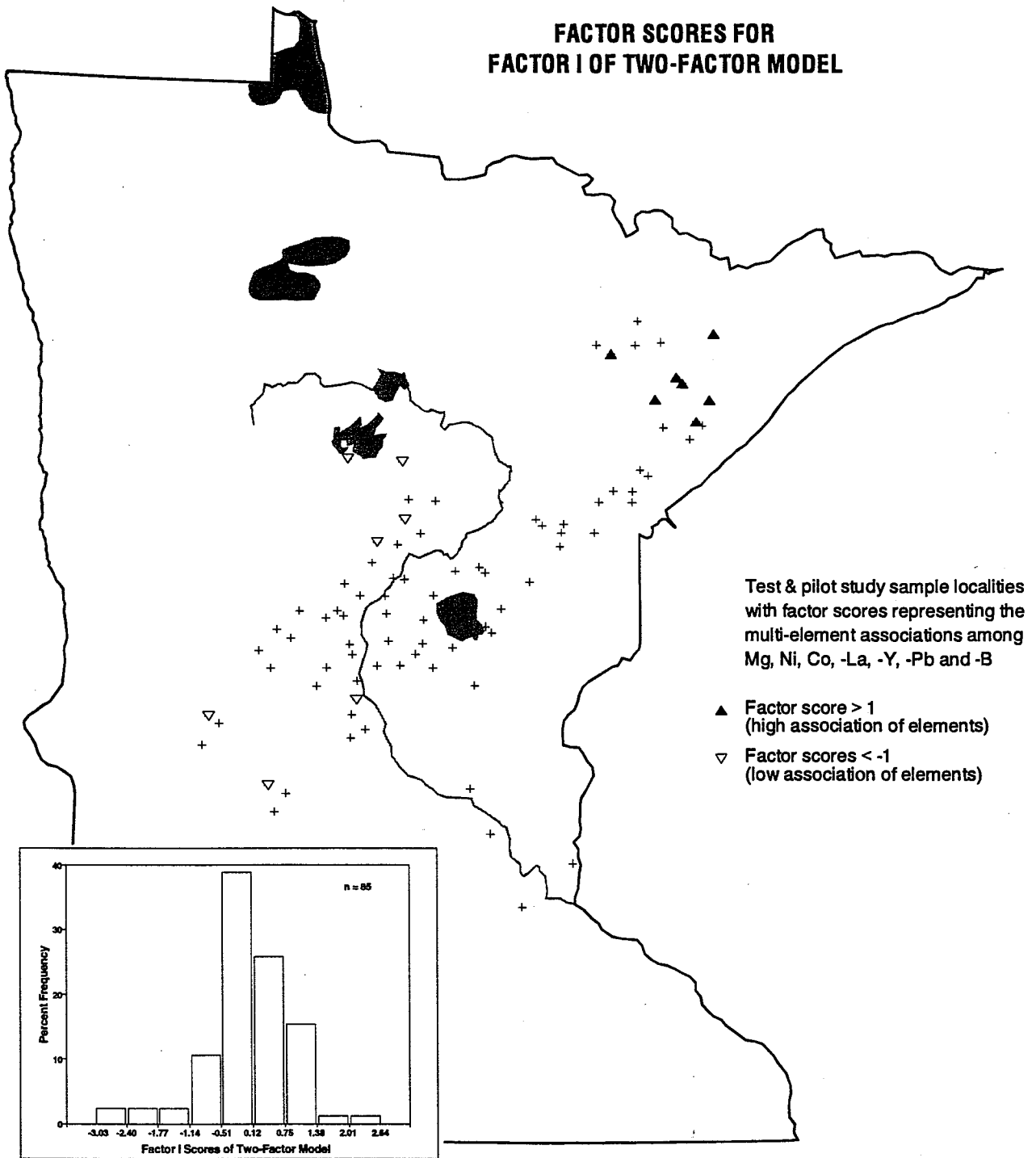


Figure 36. Frequency and geographic distribution of the high and low factor scores for Factor I of the two-factor model, which represents the multi-element associations among Mg, Ni, Co, -La, -Y, -Pb and -B in samples of the paramagnetic fraction (C2) of the concentrates.

PARAMAGNETIC FRACTION
FACTOR SCORES FOR
FACTOR II OF TWO-FACTOR MODEL

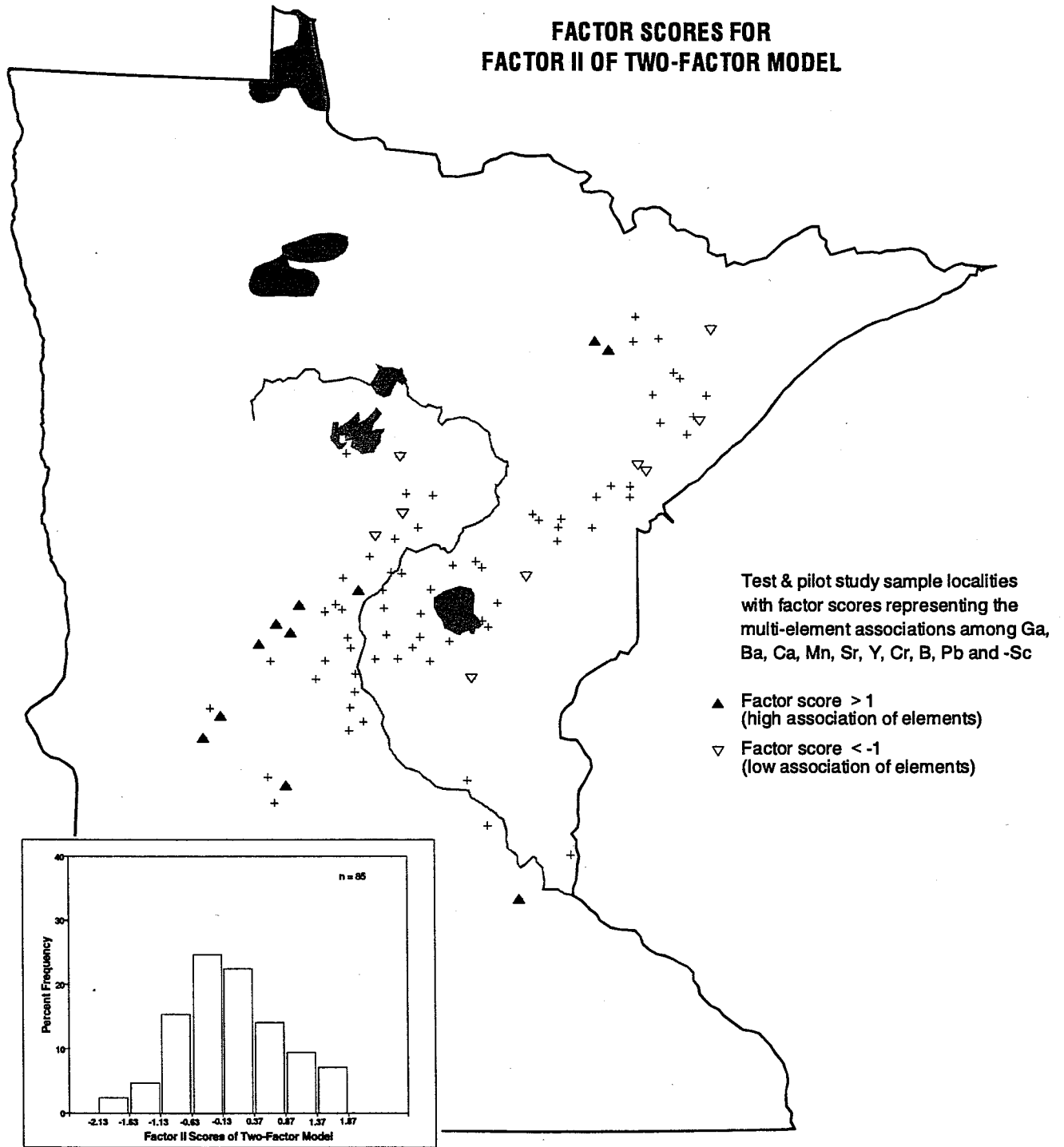


Figure 37. Frequency and geographic distribution of the high and low factor scores for Factor II of the two-factor model, which represents the multi-element associations among Ga, Ba, Ca, Mn, Sr, Y, Cr, B, Pb and -Sc in samples of the paramagnetic fraction (C2) of the concentrate.

PARAMAGNETIC FRACTION COPPER

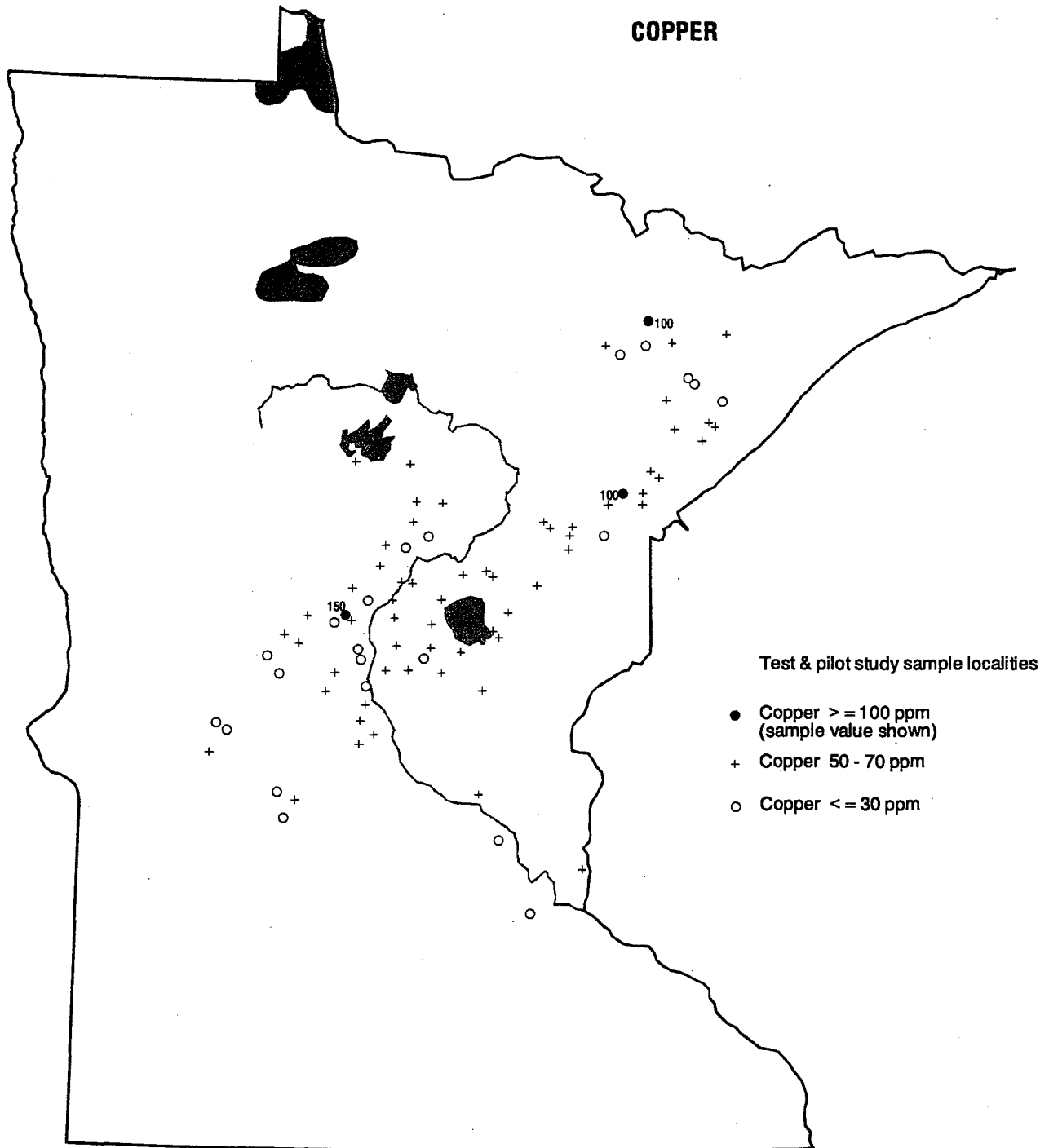


Figure 38. Geographic distribution of copper in samples of the paramagnetic fraction (C2) of the heavy-mineral concentrates.

samples with low copper concentrations occur west of the Mississippi River and occur in all glacial lobes; another small cluster occurs in the northeast, in sediments from the Rainy lobe. The geographic distribution of the zirconium data values (not illustrated) forms a random distribution of concentrations without a strong pattern; the two high (300 ppm) zirconium values occur in samples from the Wadena lobe. Factor analysis was rerun without copper and zirconium; this did not change the overall factor results significantly, therefore, we went back to the results of the sixteen element analysis.

NONMAGNETIC FRACTION GEOCHEMICAL RESULTS

Samples from the nonmagnetic fraction (C3) of the heavy-mineral concentrates were analyzed by semiquantitative emission spectroscopy for thirty-five elements. In the eighty-five samples analyzed, three elements were not detected at their lower determination limit: arsenic (500 ppm), cadmium (50 ppm), and germanium (20 ppm); and two elements were detected at levels above their upper determination limit: titanium (2 percent) and zirconium (2000 ppm). The thirty elements with valid observations are summarized below by single-element data, paired-element correlations, and multi-element associations.

Single-element Data in the Nonmagnetic Fraction

Of the thirty elements with valid observations in the nonmagnetic-fraction (C3) samples, eight of these elements have a limited number of valid observations; these elements include nickel, cobalt, gold, silver, molybdenum, tungsten, bismuth, and thorium. In the majority of samples these elements were not detected at their lower determination limits. Nickel was detected in 16 percent of the samples with concentrations ranging from less than 10 to 100 ppm. Cobalt was detected in 14 percent of the samples with concentrations ranging from less than 20 to 30 ppm. The geographic distribution of the samples with valid nickel (≥ 10 ppm) (Fig. 39) and cobalt (≥ 20 ppm) (Fig. 40) values are quite similar, with over half of these samples containing both elements. These samples are scattered across the study area with a small cluster occurring just west of the Mississippi River; they occur in sediments from the Superior, Rainy, and Des Moines lobes. [If we compare the geographic distribution of cobalt and nickel values in the nonmagnetic-fraction (C3) samples (see Figs. 39 and 40) with the cobalt/nickel factor association in the paramagnetic-fraction (C2) samples (see Fig. 36) we see a different distribution pattern—which probably reflects the different mineralogy of the two fractions.] Gold was detected in 8 percent of the samples with concentrations ranging from less than 20 to 300 ppm; these samples strongly cluster along the Mississippi River and occur primarily in sediments from the Rainy lobe (Fig. 41). Silver was detected in 7 percent of the samples with concentrations ranging from less than 1 to 7 ppm; these values are scattered in the central and northeastern parts of the study area in samples from the Rainy and Superior lobes (Fig. 42). Molybdenum was detected in 5 percent of the samples with concentrations ranging from less than 10 to 15 ppm. The valid molybdenum values occur in the southwestern part of the study area in samples from the Wadena and Superior lobes. The samples where molybdenum was detected at levels below the sensitivity level (10 ppm) occur in the northeastern part of the study area in Rainy lobe sediments (Fig. 43). Tungsten was detected in 4 percent of the

NONMAGNETIC FRACTION

NICKEL

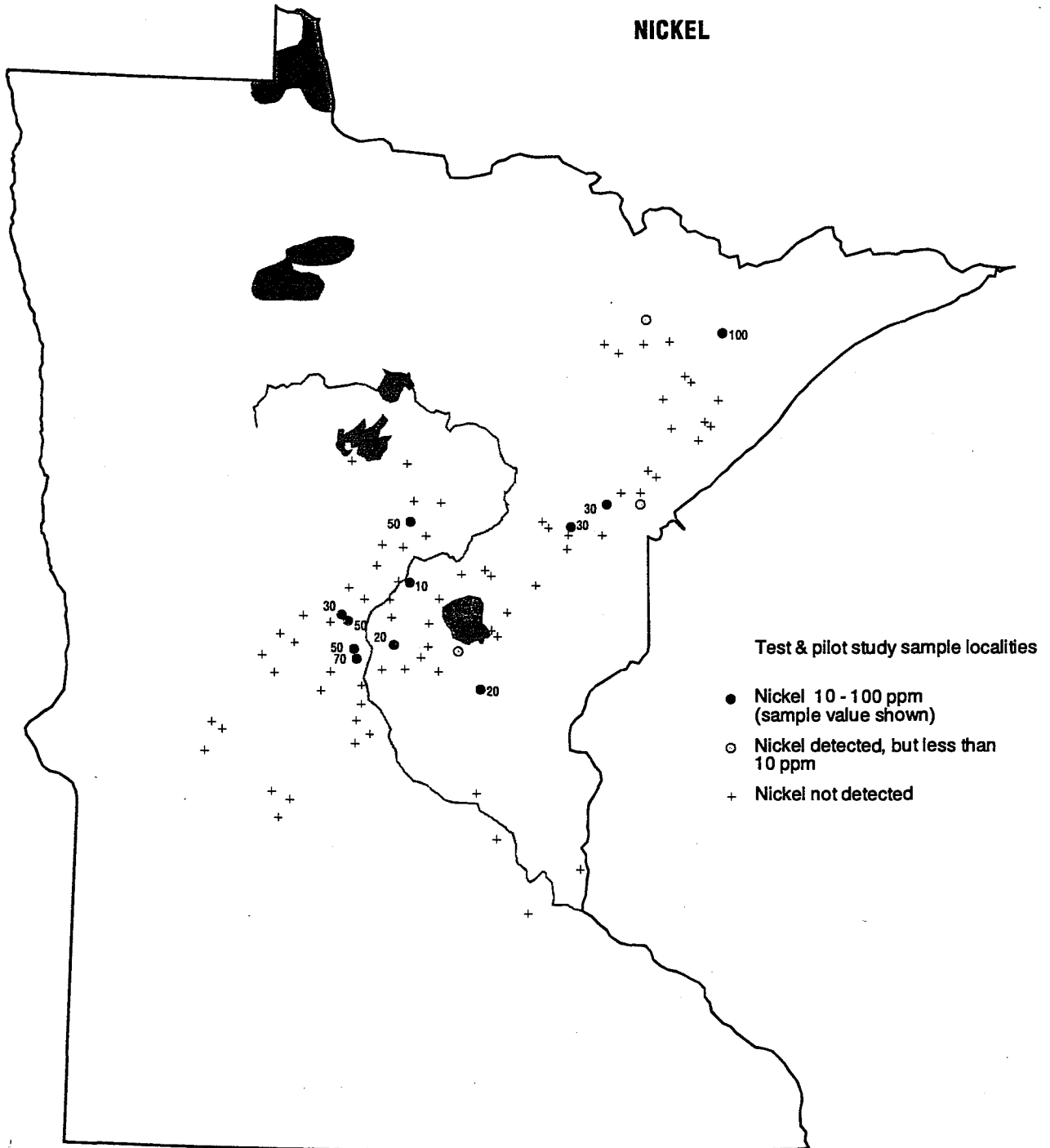


Figure 39. Geographic distribution of nickel in samples of the nonmagnetic fraction (C3) of the heavy-mineral concentrates.

**NONMAGNETIC FRACTION
COBALT**

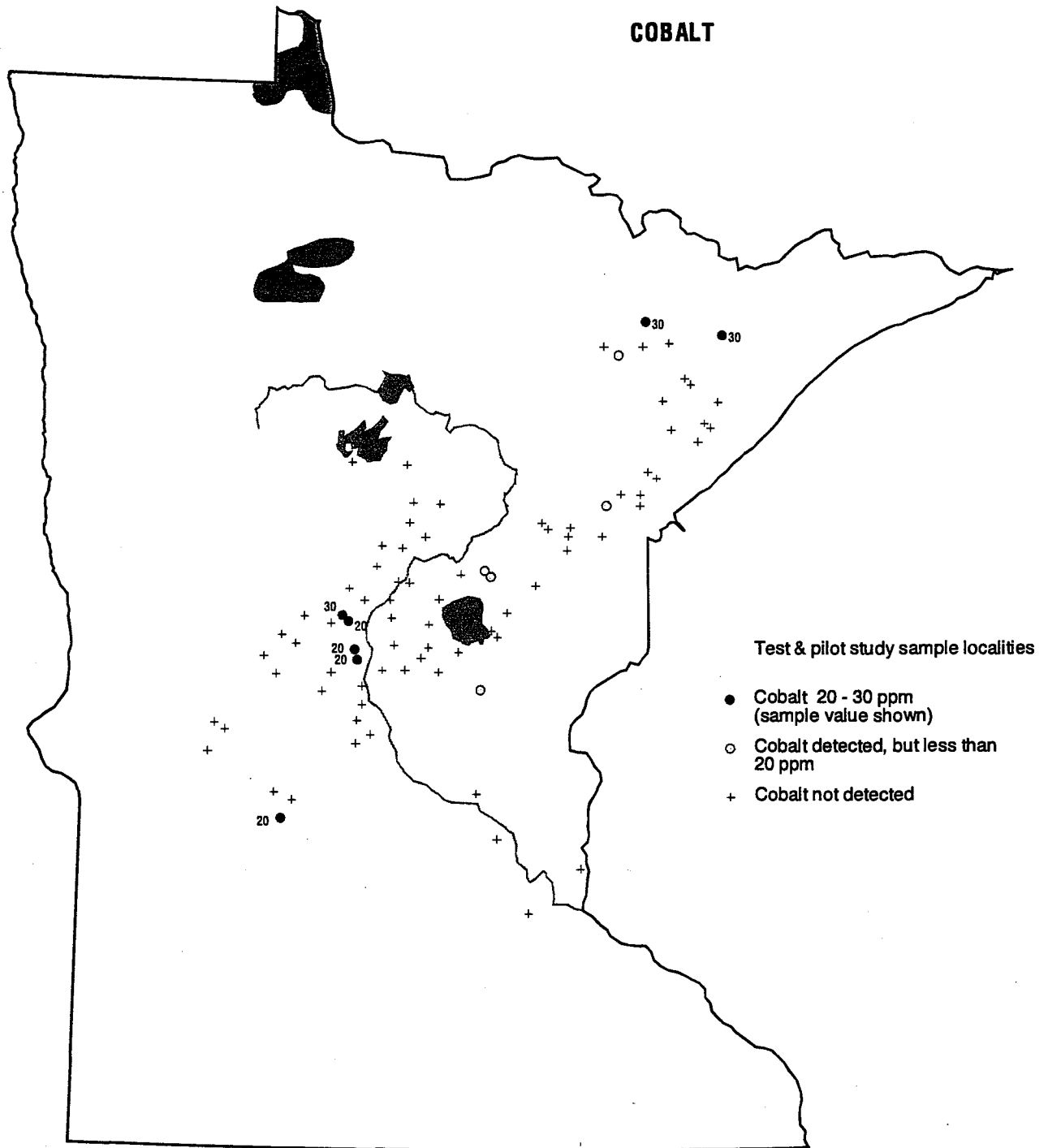


Figure 40. Geographic distribution of cobalt in samples of the nonmagnetic fraction (C3) of the heavy-mineral concentrates.

**NONMAGNETIC FRACTION
GOLD**

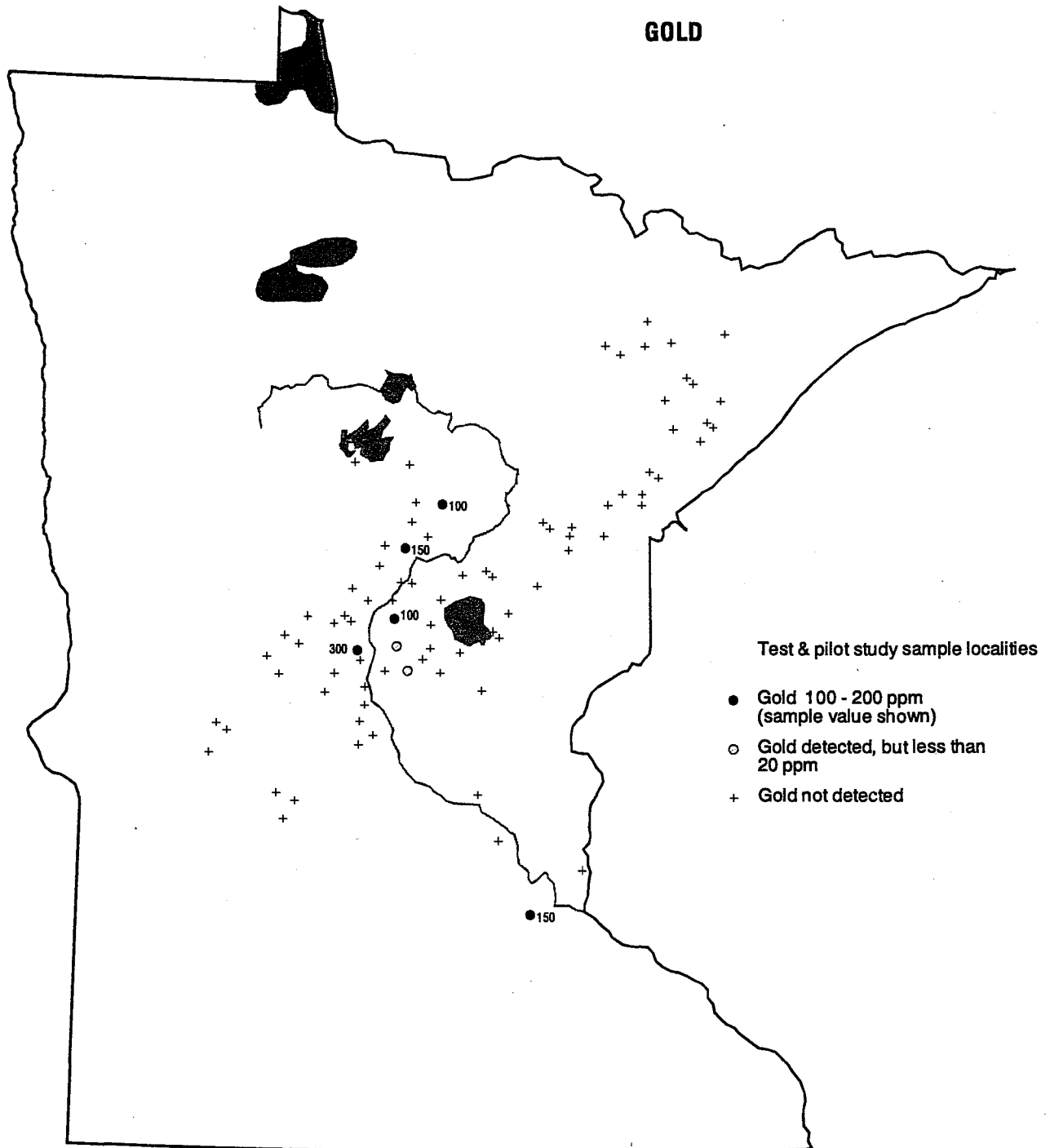


Figure 41. Geographic distribution of gold in samples of the nonmagnetic fraction (C3) of the heavy-mineral concentrates.

NONMAGNETIC FRACTION SILVER

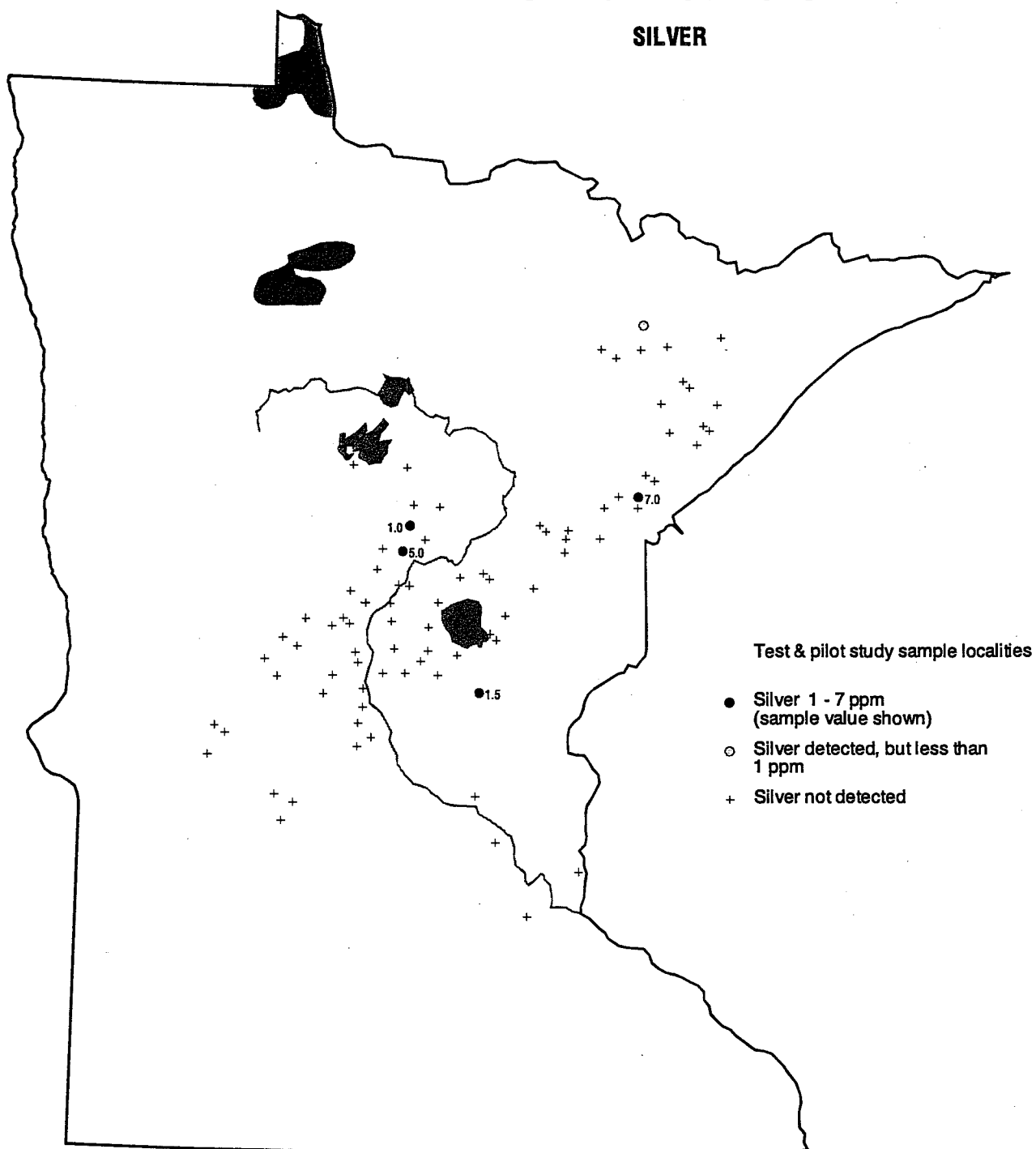


Figure 42. Geographic distribution of silver in samples of the nonmagnetic fraction (C3) of the heavy-mineral concentrates.

samples with concentrations ranging from less than 50 to 100 ppm; these values occur in isolated samples from the southwestern to the northeastern parts of the study area in samples from the Wadena and Rainy lobes (Fig. 44). The geographic distribution of tungsten and molybdenum is very similar, with most samples containing both elements (see Figs. 43 and 44). Bismuth was detected in 5 percent of the samples with concentrations ranging from less than 20 to 100 ppm; these values occur in a small tight cluster of samples from the Rainy and Wadena lobes in the north-central part of the study area, and in two isolated samples from the Superior lobe in the vicinity of Mille Lacs Lake (Fig.45). Thorium was detected below the 200 ppm lower determination limit in a single sample; this sample was collected just west of the Mississippi River in Superior lobe sediments (Fig. 46).

Four elements (Sb, Zn, Cu, Pb) have a limited data set because some samples are contaminated with slivers of lead shot or brass or copper shell casings (Nelson and others, 1992). These samples appear to reflect inflated geochemical values for antimony in sample 22635 and 23951, for zinc in sample 22632, for copper in samples 22632 and 23918, and for lead in samples 22635, 23922, 23943, 23945, 23950, and 23951. These contaminated samples were not included in the data set of the associated element in the following analysis. Lead was detected in all samples with concentrations ranging from 20 to 2000 ppm, with the majority of samples containing less than 100 ppm lead (see histogram Fig. 47). The thirteen samples with lead values greater than 100 ppm are scattered throughout the study area (Fig. 47) in all glacial sediment types. Copper was detected in the majority of samples with concentrations ranging from less than 10 to 300 ppm, and most values are at or near the lower level of determination (10 ppm) (see histogram Fig. 46). The samples with copper values of 70 ppm or greater are distributed from southwest of the Duluth Complex to south of Mille Lacs Lake (Fig. 46) in Superior lobe sediments. [The geographic distribution of copper values between the nonmagnetic- and paramagnetic-fraction samples is very different (see figs. 46 and 38); this is probably related to the difference in mineralogy of the two fractions.] Zinc was detected at the lower level of determination (500 ppm) in a single sample from the Superior lobe collected southwest of the Duluth Complex. This sample (number 23913) also contains the highest copper value in the nonmagnetic fraction and contains high lead and gold values (Fig. 46). Antimony was detected at the lower limit of determination (200 ppm) in a single sample from the Superior lobe collected in the central part of the study area, just west of the Mississippi River. This sample (number 23935) also contains the highest lead concentration in the nonmagnetic fraction and contains high gold and silver values (Fig. 46).

NONMAGNETIC FRACTION MOLYBDENUM

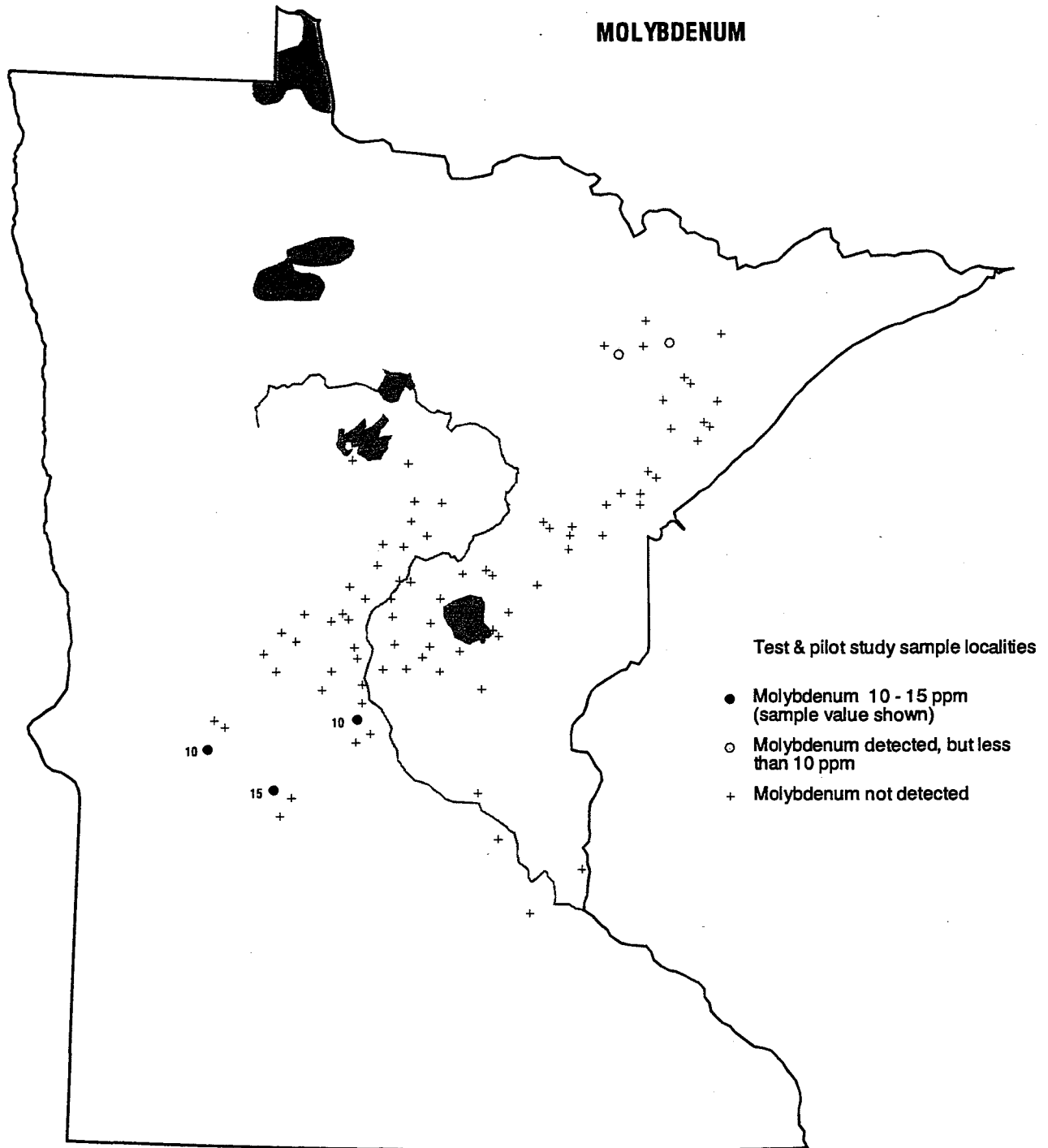


Figure 43. Geographic distribution of molybdenum in samples of the nonmagnetic fraction (C3) of the heavy-mineral concentrates.

**NONMAGNETIC FRACTION
TUNGSTEN**

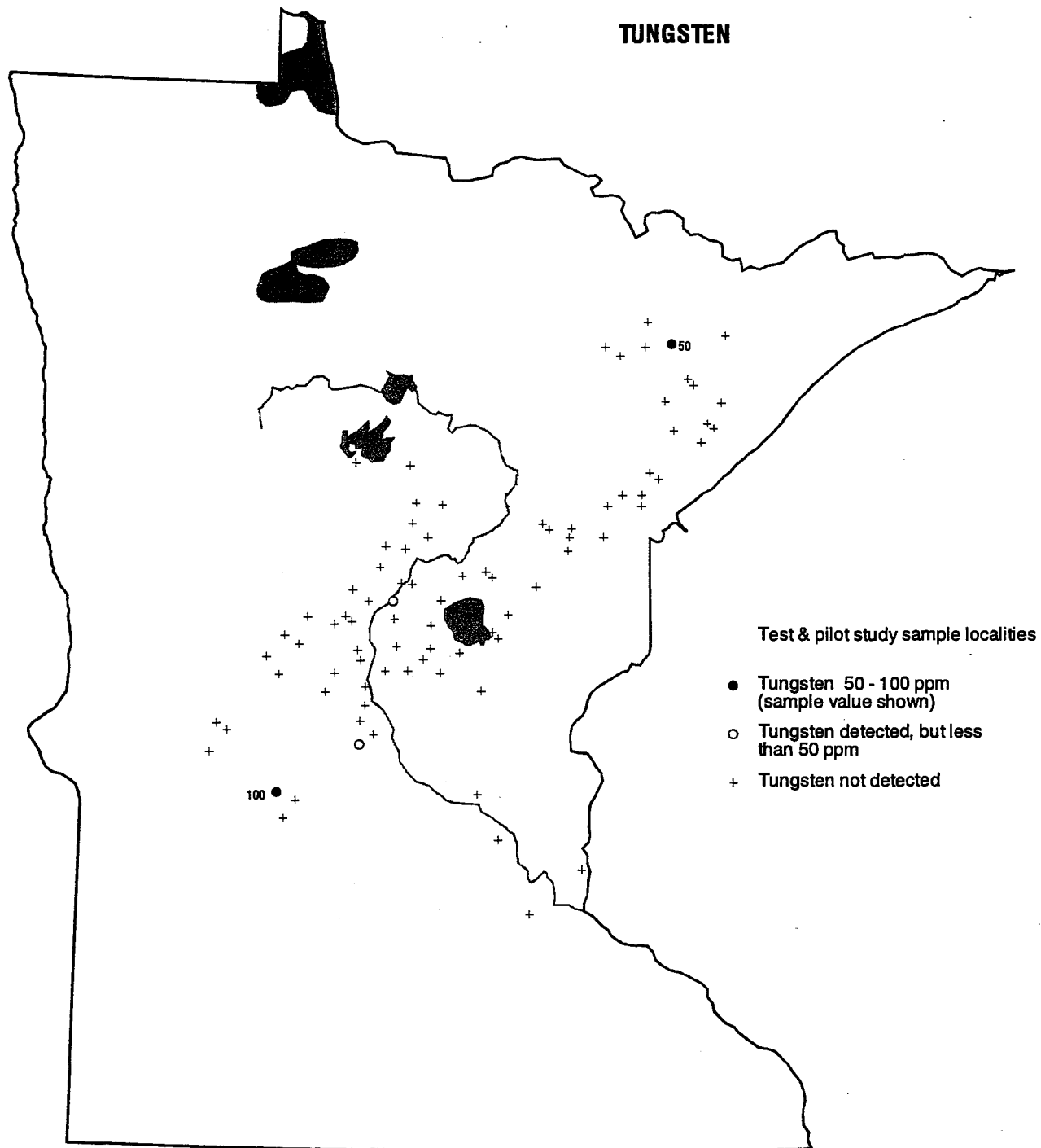


Figure 44. Geographic distribution of tungsten in samples of the nonmagnetic fraction (C3) of the heavy-mineral concentrates.

NONMAGNETIC FRACTION

BISMUTH

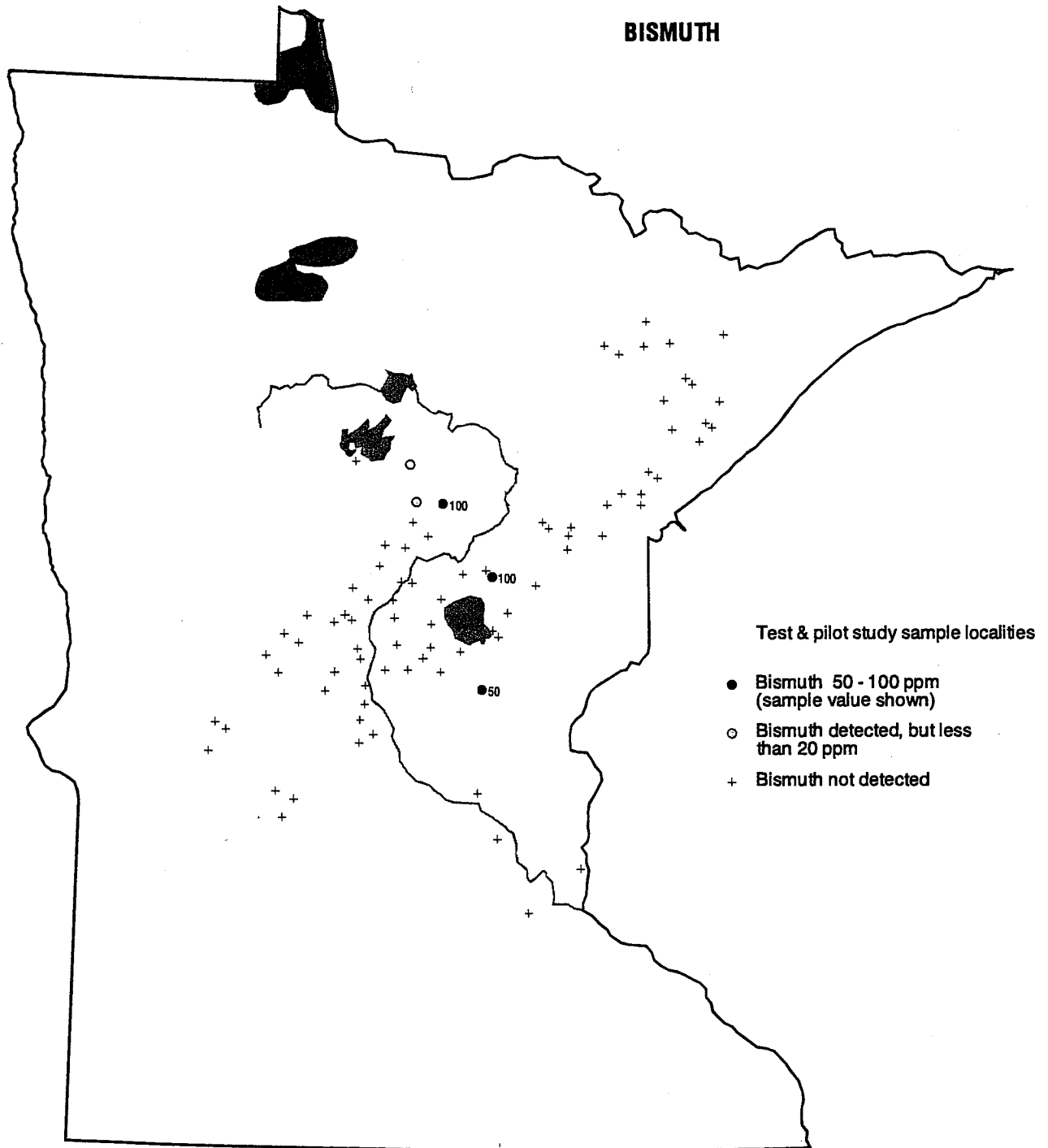


Figure 45. Geographic distribution of bismuth in samples of the nonmagnetic fraction (C3) of the heavy-mineral concentrates.

NONMAGNETIC FRACTION

ZINC, COPPER, ANTIMONY AND THORIUM, WITH ASSOCIATED ELEMENT VALUES

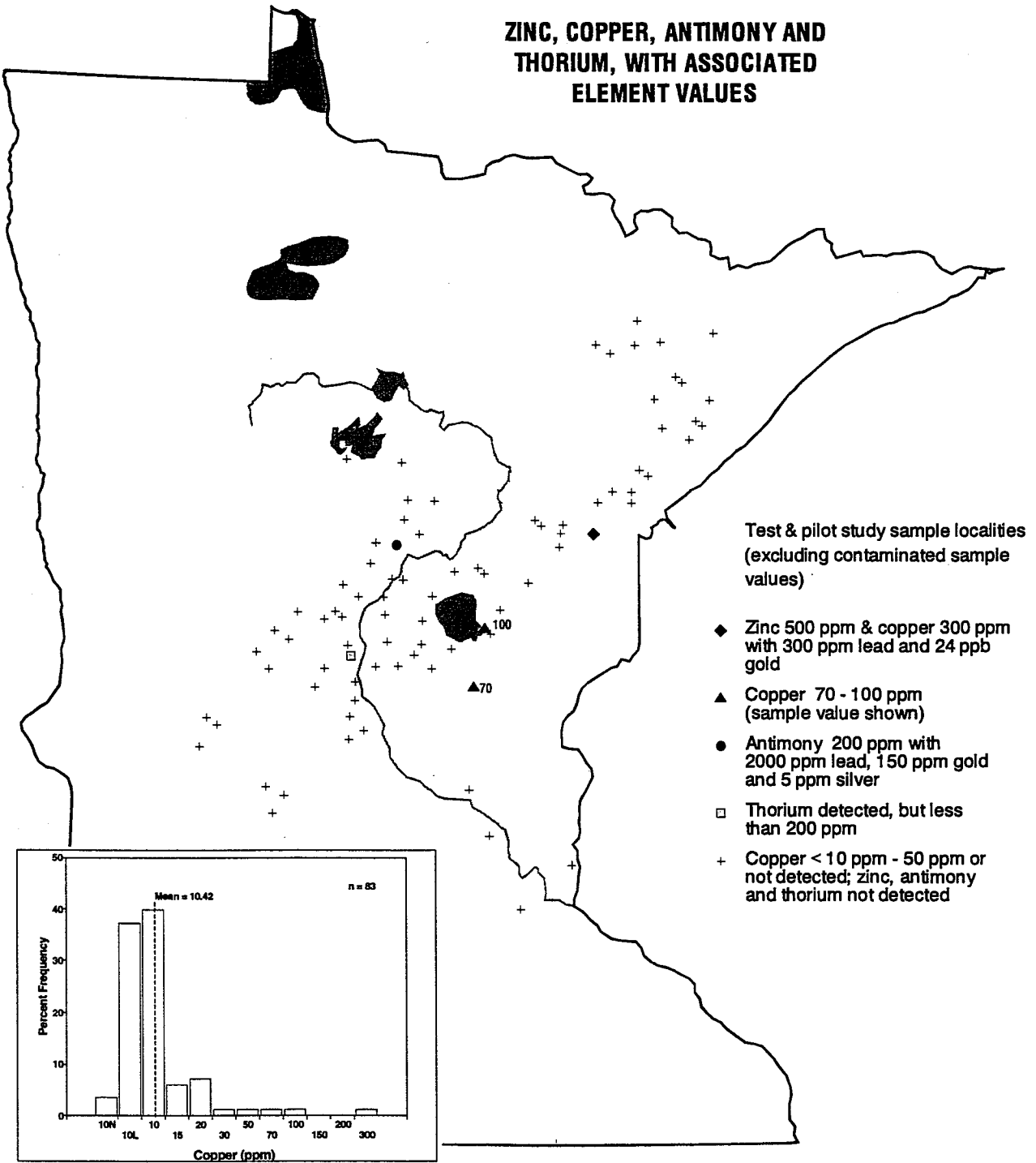


Figure 46. Geographic distribution of zinc, copper, antimony, thorium, and associated element values in samples of the nonmagnetic fraction (C3) of the heavy-mineral concentrates.

NONMAGNETIC FRACTION

LEAD

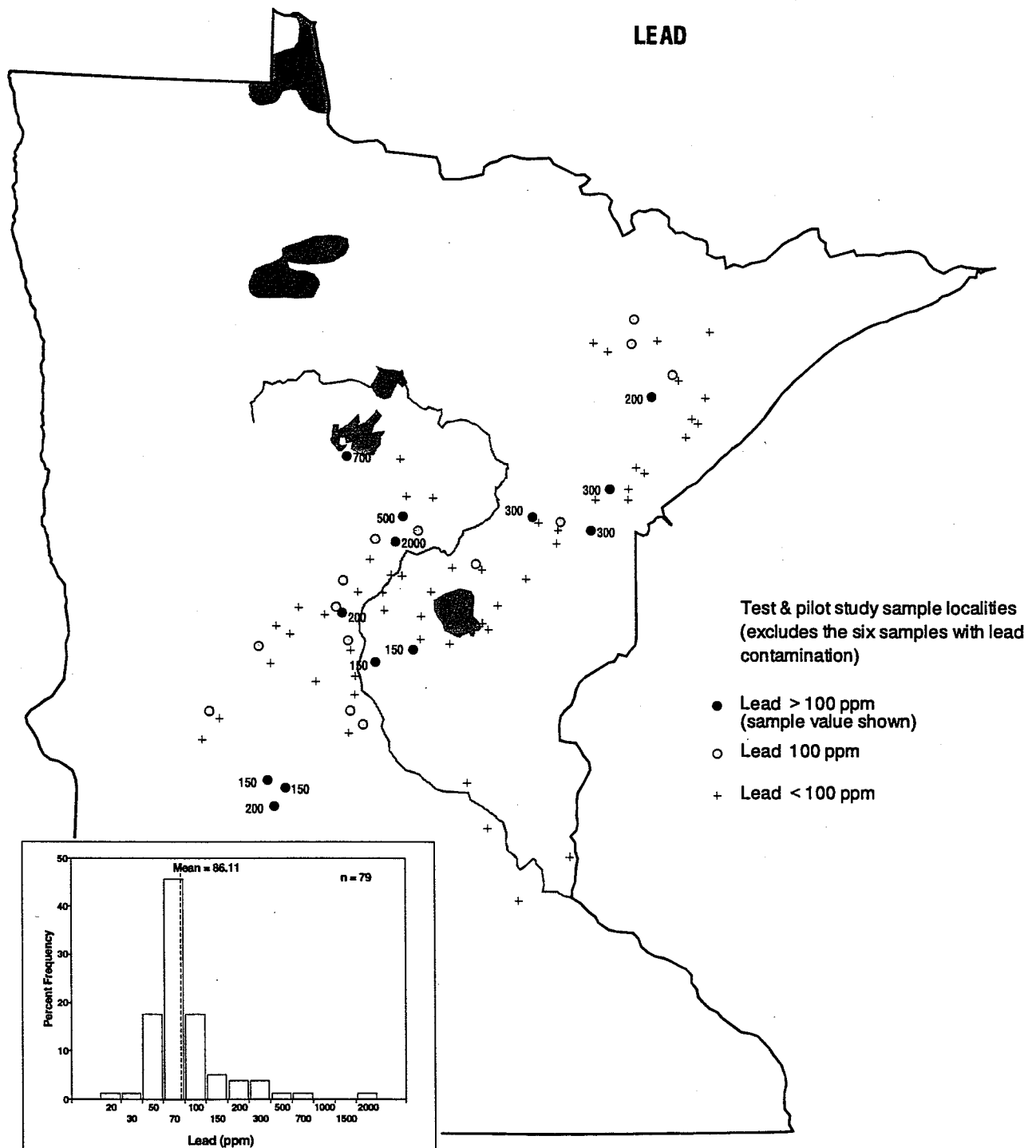
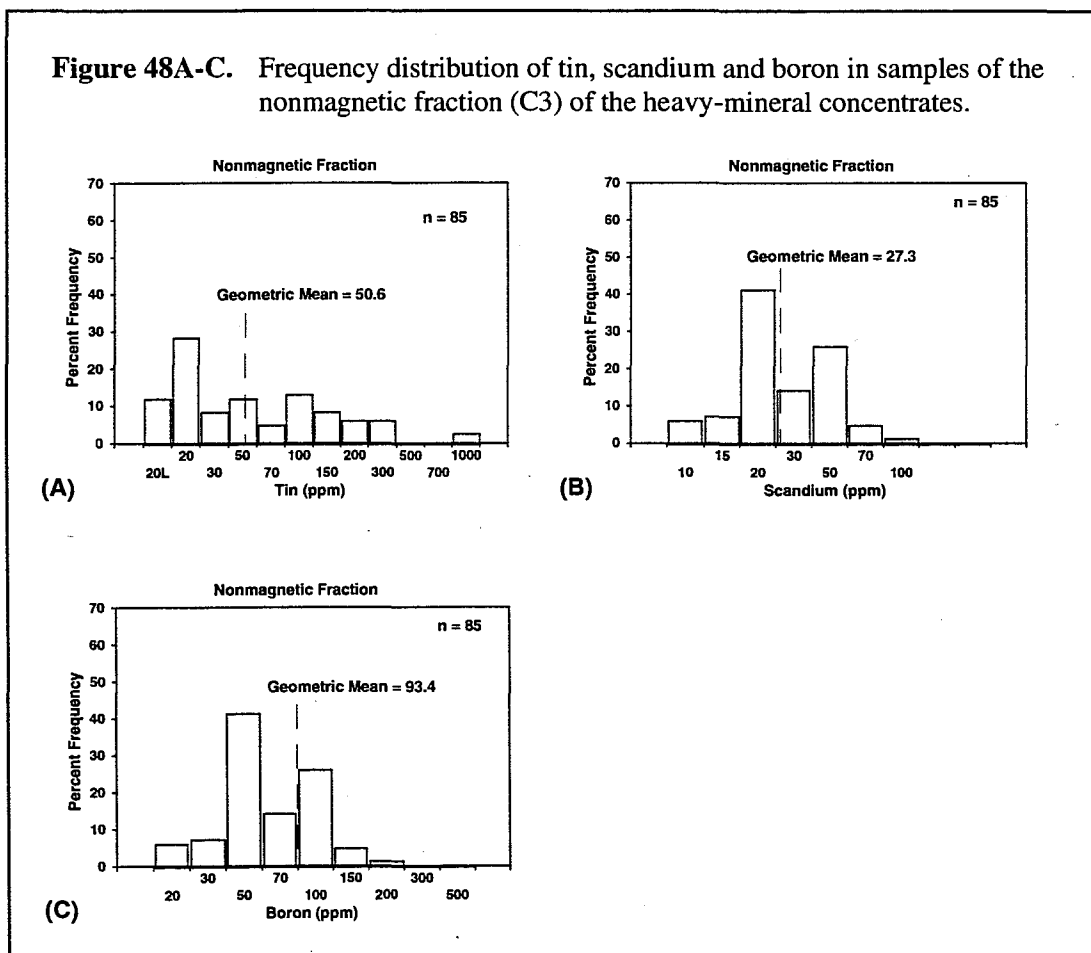


Figure 47. Frequency and geographic distribution of lead in samples of the nonmagnetic fraction (C3) of the heavy-mineral concentrates.

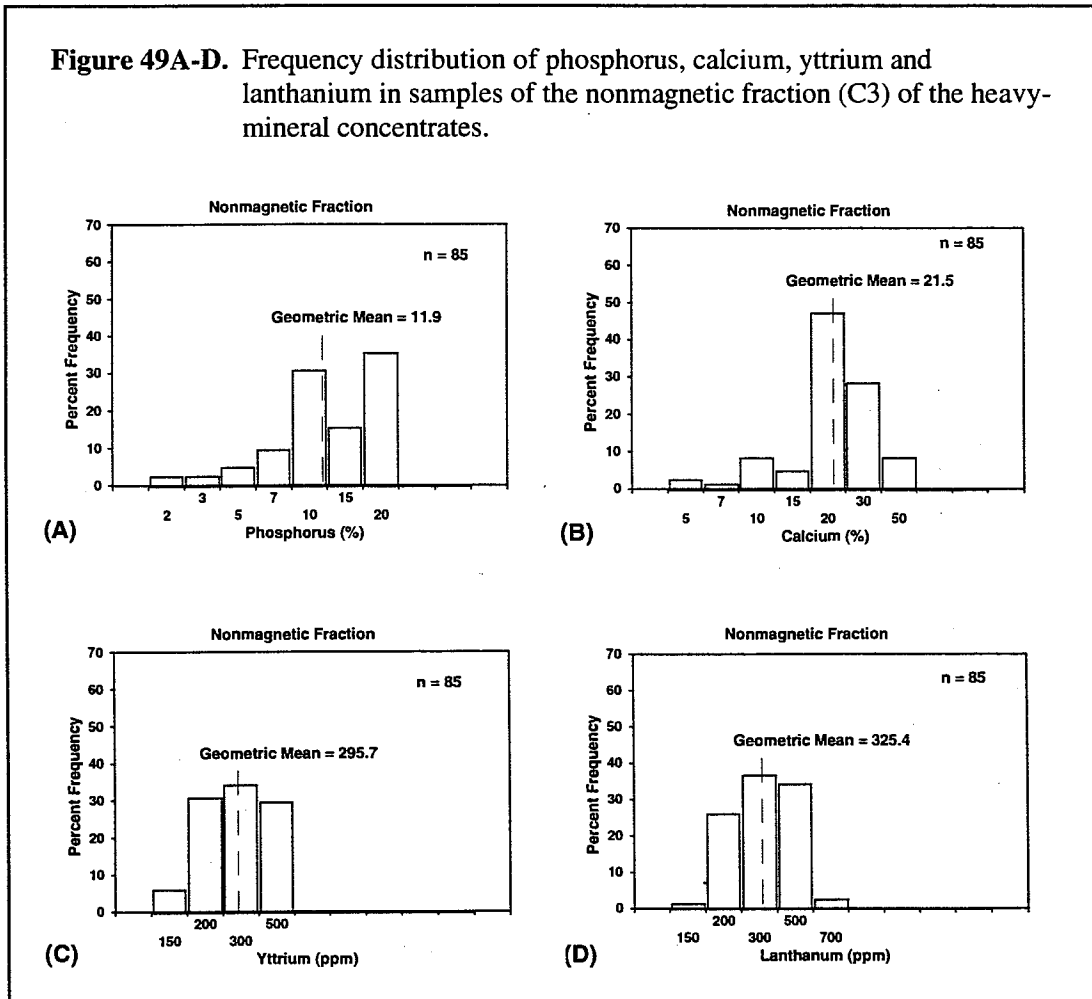
Frequency distributions for the remaining eighteen elements observed in the nonmagnetic-fraction (C3) samples are shown in groups in figures 48 to 52 and summarized below. Tin was detected in all samples with concentrations ranging from less than 20 to 1000 ppm, and nearly half of these values are 30 ppm or less (Fig. 48A). Scandium was detected in all samples with concentrations ranging from 10 to 100 ppm, and over half of these values are 20 ppm or less (Fig. 48B). Boron was detected in all samples with concentrations ranging from 20 to 500 ppm, and over 70 percent of these values are 100 ppm or less (Fig. 48C). Phosphorus was detected in all samples with concentrations ranging from 2 to 20 percent, and nearly half of these values are 10 percent or less (Fig. 49A). Calcium was detected in all samples with concentrations ranging from 5 to 50 percent, and over half of these values are 20 percent or less (Fig. 49B). Yttrium was detected in all samples with concentrations ranging from 150 to 500 ppm, and over 70 percent of these values are 300 ppm or less (Fig. 49C). Lanthanum was detected in all samples with concentrations ranging from 150 to 700 ppm, and over 60 percent of these values are 300 ppm or less (Fig. 49D). Magnesium was detected in all samples with concentrations ranging from 0.2 to 3 %, and over 60 percent of these values are 0.7 % or less (Fig. 50A). Manganese was detected in all samples with concentrations ranging from 200 to 1500 ppm, and over 65 percent of these values are 500 ppm or less (Fig. 50B). Iron was detected in all samples with concentrations ranging from 0.2 to 2 %, and over 70 percent of these values are 0.5 % or less (Fig. 50C).

Figure 48A-C. Frequency distribution of tin, scandium and boron in samples of the nonmagnetic fraction (C3) of the heavy-mineral concentrates.



Strontium was detected in all samples except one, with concentrations ranging from 200 to 3000 ppm, and 60 percent of these values are 500 ppm or less (Fig. 51A). Chromium was detected in all samples with concentrations ranging from 100 to 500 ppm, and over 80 percent of these values are 200 ppm or less (Fig. 51B). Gallium was detected in all samples with concentrations ranging from less than 10 to 50 ppm, and over 80 percent of these values are 20 ppm or less (Fig. 51C). Barium was detected in all samples with concentrations ranging from 70 to 3000 ppm, and the majority of values are 500 ppm or less (Fig. 52A). Sodium was detected in over 80 percent of the samples; most of these values are below the 0.5 % determination limit and the remaining values are at this limit (Fig. 52B). Niobium was detected in almost all samples; most of these values are below the 50 ppm determination limit and the remaining values are at this limit (Fig. 52C). Vanadium was detected in all samples with concentrations ranging from 100 to 200 ppm, and the majority of these values are 100 ppm (Fig. 52D). Beryllium was detected in less than 33 percent of the samples with concentrations ranging from less than 2 to 100 ppm, and over half of these values are less than 2 ppm (Fig. 52E). The histograms show that Sn, Sc, B, P, Ca, Mg, Mn, Fe, Sr, Ga, and Ba have more than analytical variation. The data values for chromium, yttrium, and lanthanum show a small range. Histograms for sodium, niobium, vanadium, and beryllium show inadequate variation for interpretation.

Figure 49A-D. Frequency distribution of phosphorus, calcium, yttrium and lanthanum in samples of the nonmagnetic fraction (C3) of the heavy-mineral concentrates.



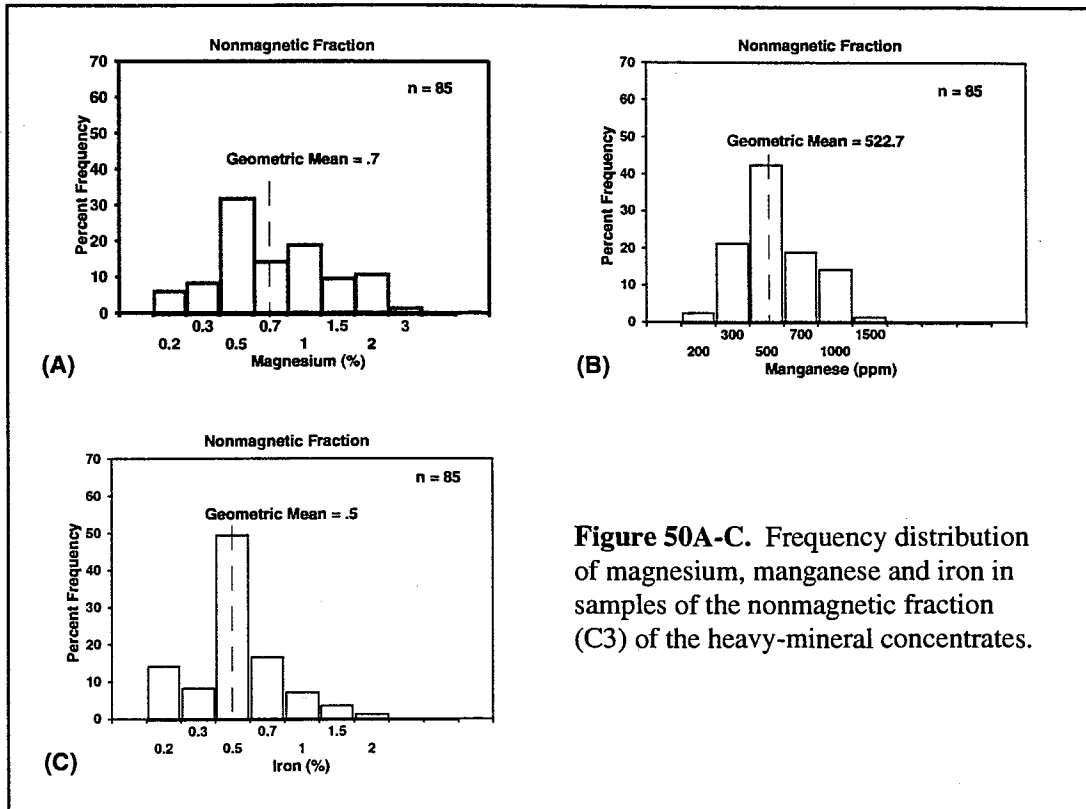


Figure 50A-C. Frequency distribution of magnesium, manganese and iron in samples of the nonmagnetic fraction (C3) of the heavy-mineral concentrates.

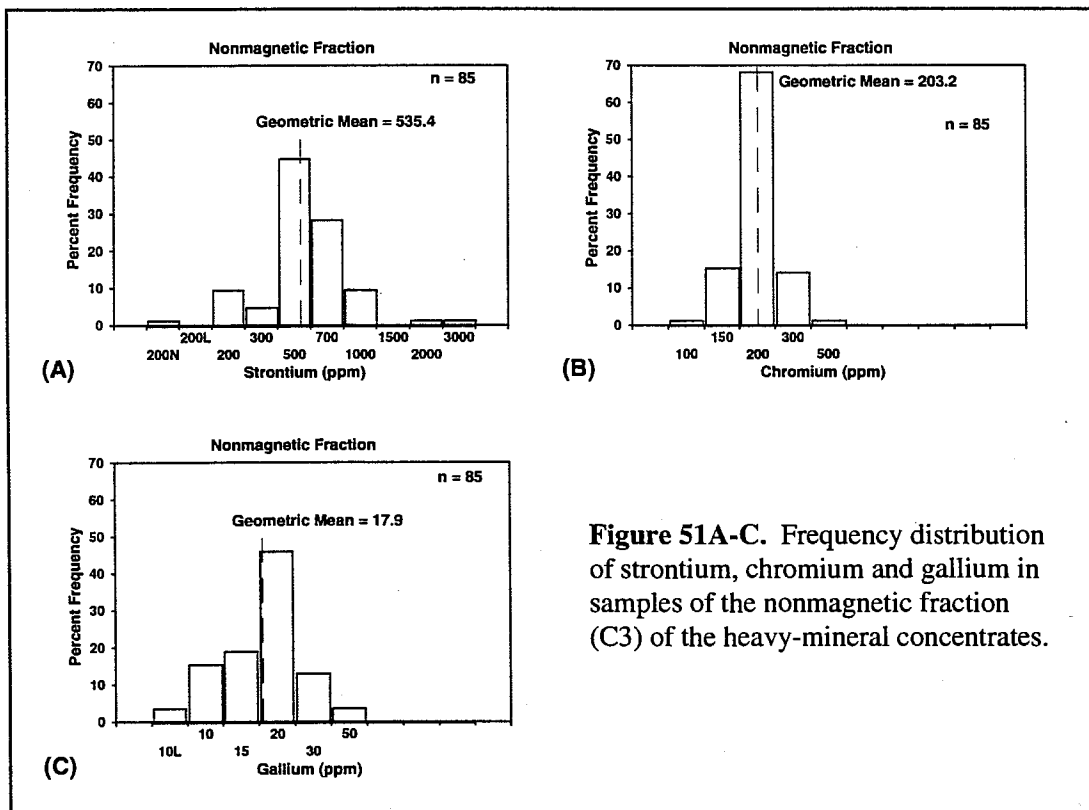


Figure 51A-C. Frequency distribution of strontium, chromium and gallium in samples of the nonmagnetic fraction (C3) of the heavy-mineral concentrates.

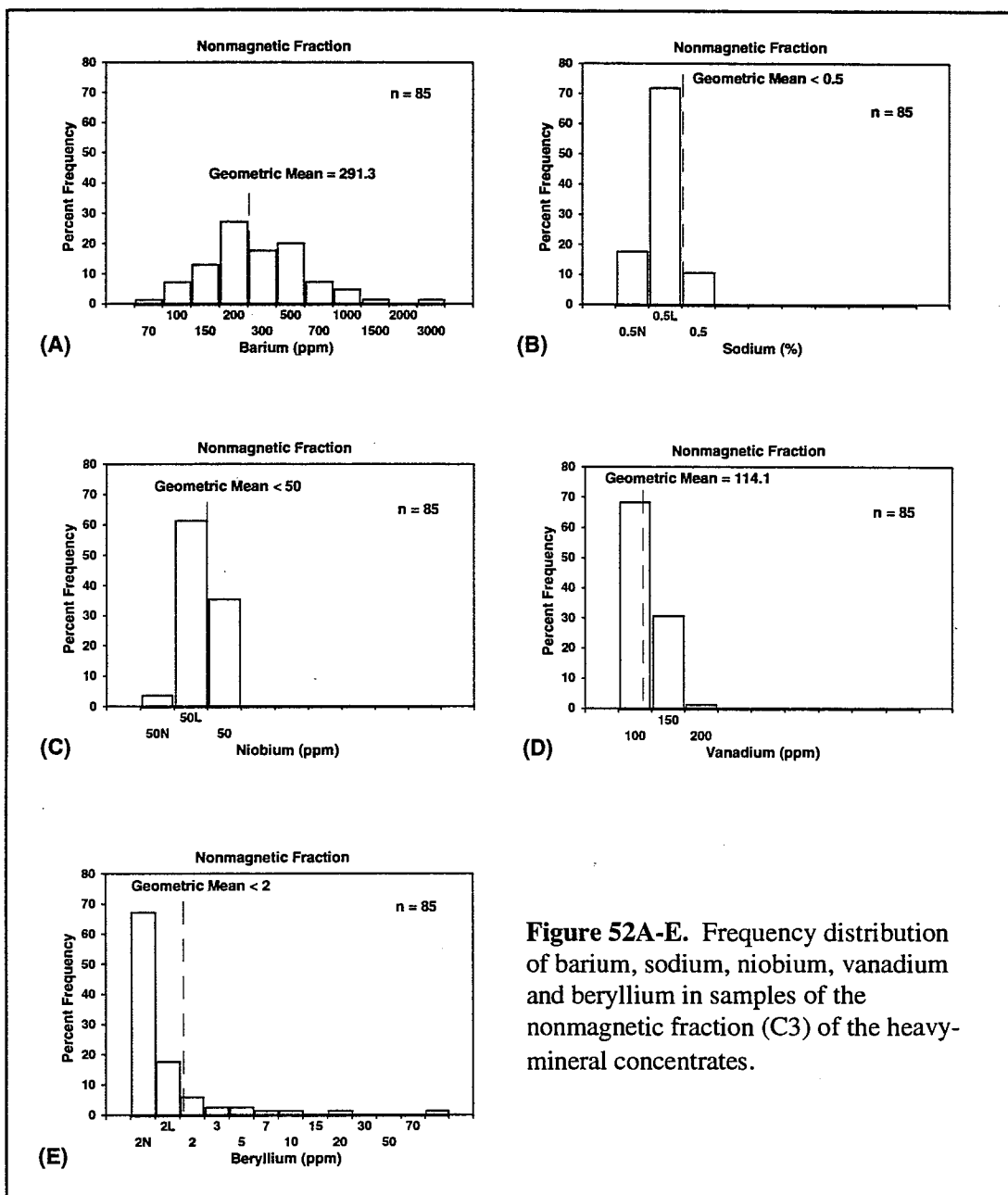


Figure 52A-E. Frequency distribution of barium, sodium, niobium, vanadium and beryllium in samples of the nonmagnetic fraction (C3) of the heavy-mineral concentrates.

Figures 53 and 54 show the geographic distribution of selected tin and beryllium values, respectively. The two extreme tin values (1000 ppm) are isolated occurrences, located west of the Mississippi River in samples from the Rainy and Wadena lobes. Mid-range tin values (100 to 300 ppm) start in the Duluth Complex and continue southwest to west of the Mississippi River, occurring predominantly in samples from the Superior lobe. Beryllium concentrations of 2 ppm or greater predominantly cluster in central Minnesota west of the Mississippi River and occur in samples from all four glacial lobes.

[See Table 3 for a summary of the frequency distribution data for the 35 elements analyzed in the samples of the nonmagnetic fraction (C3) of the heavy-mineral concentrates].

NONMAGNETIC FRACTION

TIN

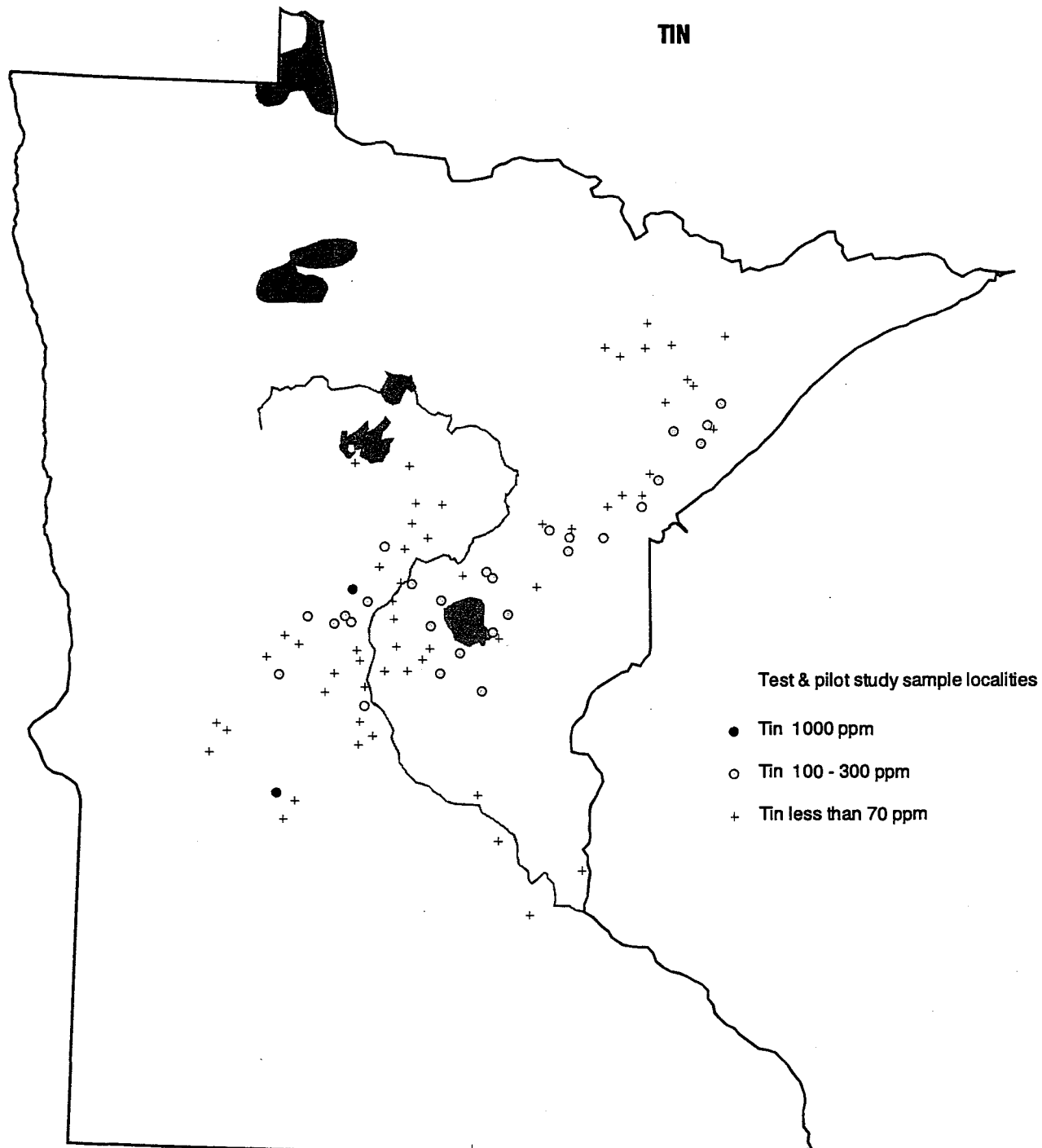


Figure 53. Geographic distribution of tin in samples of the nonmagnetic fraction (C3) of the heavy-mineral concentrates.

NONMAGNETIC FRACTION BERYLLIUM

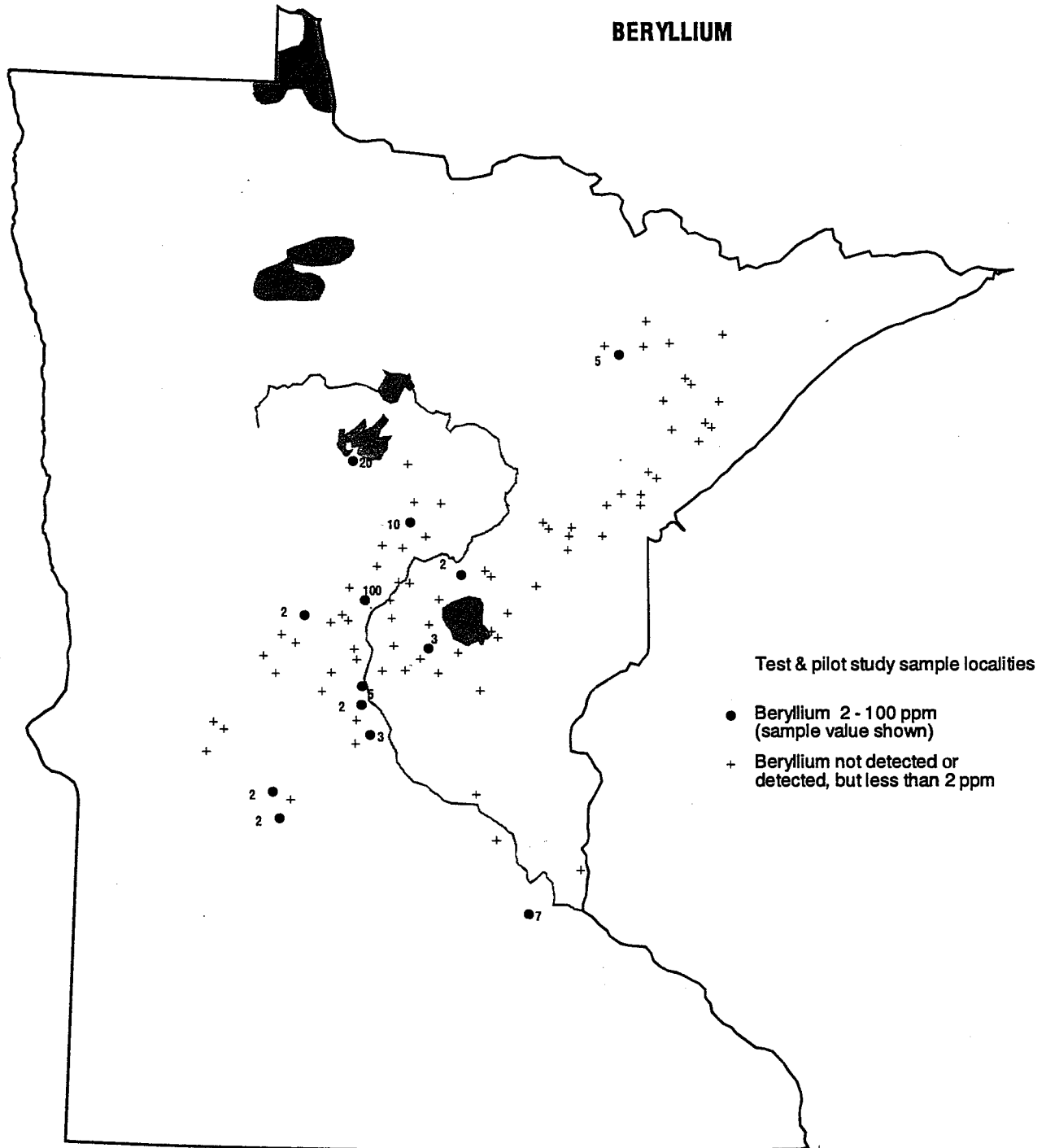


Figure 54. Geographic distribution of beryllium in samples of the nonmagnetic fraction (C3) of the heavy-mineral concentrates.

Table 3. Summary of frequency distribution data for 35 elements analyzed in samples of the nonmagnetic fraction (C3) of the heavy-mineral concentrates. [n = 85 samples; elements with many valid observations are in the shaded boxes; elements with a limited number of valid observations are in italic type; elements that were not detected are in standard type]

Element	See Histogram	Lower Limit of Determination 5mg sub-sample	% of Samples Element was Detected In	Range of Values Reported	Comments
<i>Antimony (Sb)</i>		200 ppm	1 % (n = 83)	200 ppm	
Arsenic (As)		500 ppm	0 %		Not detected at 500 ppm
Barium (Ba)	Fig. 52A	50 ppm	100 %	70 - 3000 ppm	Majority of values are ≤ 500 ppm
<i>Beryllium (Be)</i>	Fig. 52E	2 ppm	33 %	< 2 - 100 ppm	> 50 % of values are < 2 ppm
<i>Bismuth (Bi)</i>		20 ppm	5 %	< 20 - 100 ppm	
Boron (B)	Fig. 48C	20 ppm	100 %	20 - 500 ppm	> 70 % of values are ≤ 100 ppm
Cadmium (Cd)		50 ppm	0 %		Not detected at 50 ppm
Calcium (Ca)	Fig. 49B	0.1 %	100 %	5 - 50 %	> 50 % of values are ≤ 20 %
Chromium (Cr)	Fig. 51B	20 ppm	100 %	100 - 500 ppm	> 80 % of values are ≤ 200 ppm
<i>Cobalt (Co)</i>		20 ppm	14 %	< 20 - 30 ppm	
Copper (Cu)	Fig. 46	10 ppm	96 % (n=83)	< 10 - 300 ppm	Most values at or near 10 ppm
Gallium (Ga)	Fig. 51C	10 ppm	100 %	< 10 - 50 ppm	> 80 % of values are ≤ 20 ppm
Germanium (Ge)		20 ppm	0 %		Not detected at 20 ppm
<i>Gold (Au)</i>		20 ppm	8 %	< 20 - 300 ppm	
Iron (Fe)	Fig. 50C	0.1 %	100 %	0.2 - 2 %	> 70 % of values are ≤ 0.5 %
Lanthanum (La)	Fig. 49D	100 ppm	100 %	150 - 700 ppm	> 60 % of values are ≤ 300 ppm
<i>Lead (Pb)</i>	Fig. 47	20 ppm	100 % (n=79)	20 - 2000 ppm	Majority of values < 100 ppm
Magnesium (Mg)	Fig. 50A	0.05 %	100 %	0.2 - 3 %	> 60 % of values are ≤ 0.7 %
Manganese (Mn)	Fig. 50B	20 ppm	100 %	200 - 1500 ppm	> 65 % of values are ≤ 500 ppm
<i>Molybdenum (Mo)</i>		10 ppm	5 %	< 10 - 15 ppm	
<i>Nickel (Ni)</i>		10 ppm	16 %	< 10 - 100 ppm	
Niobium (Nb)	Fig. 52C	50 ppm	96 %	< 50 - 50 ppm	Most of values < 50 ppm
Phosphorus (P)	Fig. 49A	0.5 %	100 %	2 - 20 %	50 % of values are ≤ 10 %
Scandium (Sc)	Fig. 48B	10 ppm	100 %	10 - 100 ppm	> 50 % of values are ≤ 20 ppm
<i>Silver (Ag)</i>		1 ppm	7 %	< 1 - 7 ppm	
Sodium (Na)	Fig. 52B	0.5 %	82 %	< 0.5 - 0.5 %	Most of values are < 0.5 %
Strontium (Sr)	Fig. 51A	200 ppm	99 %	200 - 3000 ppm	60 % of values are ≤ 500 ppm
<i>Thorium (Th)</i>		200 ppm	1 %	< 200 ppm	
Tin (Sn)	Fig. 48A	20 ppm	100 %	< 20 - 1000 ppm	47 % of values are ≤ 30 ppm
Titanium (Ti)		0.005 %	100 %	> 2 %	All values > 2 % upper determination limit
<i>Tungsten (W)</i>		50 ppm	4 %	< 50 - 100 ppm	
Vanadium (V)	Fig. 52D	20 ppm	100 %	100 - 200 ppm	Majority of values are 100 ppm
Yttrium (Y)	Fig. 49C	20 ppm	100 %	150 - 500 ppm	> 70 % of values are ≤ 300 ppm
<i>Zinc (Zn)</i>		500 ppm	1 % (n=84)	500 ppm	
Zirconium (Zr)		20 ppm	100 %	≥ 2000 ppm	All values ≥ 2000 ppm upper determin. limit

For these same eighteen elements (see page 70), we looked at the frequency distribution of the single-element data in the nonmagnetic-fraction (C3) samples grouped by glacial lobe (not illustrated). T-tests measured the significance of any differences in the element means between samples from the various glacial lobes. Results showed significantly more ($\alpha .01$) sodium, yttrium, magnesium, boron, and ($\alpha .05$) gallium in the Superior lobe compared with the Wadena lobe; and significantly more ($\alpha <.01$) magnesium, ($\alpha .01$) boron, and ($\alpha .05$) yttrium in the Superior lobe compared with the Rainy lobe. Differences in the element means between the lobes also showed significantly more ($\alpha .01$) sodium and gallium in the Rainy lobe compared with the Wadena lobe. Significantly more ($\alpha .01$) scandium and ($\alpha .05$) beryllium occur in the Wadena lobe compared with the Superior lobe; and significantly more ($\alpha .01$) scandium occurs in the Wadena lobe compared with the Rainy lobe. Overall, the number of significant results is quite small, suggesting that element occurrences in the nonmagnetic fraction (C3) of the concentrate are not closely related to glacial lobe. See Table 4 for a summary of the elements in the nonmagnetic fraction that show a significant difference in their means between samples from the various glacial lobes.

Table 4. Summary of elements that show a significant difference in their means between the samples from the various glacial lobes in the nonmagnetic fraction (C3) of the concentrates. [n=18 elements; element listed below the significance level measured]

Significantly more of the element listed is found in samples in the:	Higher Significance.....Lower Significance		
	$\alpha <.01$	$\alpha .01$	$\alpha .05$
Wadena lobe sediments compared w/ Superior		Sc	Be
Wadena lobe sediments compared w/ Rainy		Sc	
Superior lobe sediments compared w/ Wadena		Na, Y, Mg, B	Ga
Superior lobe sediments compared w/ Rainy	Mg	B	Y
Rainy lobe sediments compared w/ Superior			
Rainy lobe sediments compared w/ Wadena		Na, Ga	

Paired-element Correlations in the Nonmagnetic Fraction

Paired-element correlation coefficients that represent the correlations between the twenty-five elements observed in the nonmagnetic-fraction (C3) samples are shown in Figure 55. The seven elements with few valid observations are included in the correlations because they do not affect the correlations among the other elements. Although the correlation coefficients are significant at 0.2 when $\alpha = .05$ and at 0.28 when $\alpha = .01$, only the stronger paired-element correlation coefficients of $\geq +0.4$ and ≤ -0.4 are highlighted on the matrix.

The positive correlations between phosphorus and lanthanum of .43 and between phosphorus and yttrium of .48 suggest a rare-earth element association. We calculated the normalized sum of phosphorus, lanthanum and yttrium values and looked at the geographic distribution of the high and low sum values (not illustrated). The nonmagnetic-fraction (C3) samples that show a high association among phosphorus, lanthanum, and yttrium are clustered in and near the Duluth Complex. Samples with the lowest associations among these elements predominantly occur in a north-south trending line along the west side of the Mississippi River. These results represent only the element concentrations in the nonmagnetic fraction (C3), not the complete heavy-mineral concentrate.

Other positive paired-element correlations include: (1) phosphorus with: calcium, scandium, and boron; (2) manganese with: magnesium, boron, and chromium; (3) boron with scandium and magnesium; (4) gallium with sodium; and (5) iron with strontium (see Fig. 55). The elements with few valid observations have several strong positive correlations of interest, including the correlation of molybdenum with tungsten at .68; nickel with cobalt at .65; iron with nickel at .64; and iron with cobalt at .52 (see Fig. 55). The geographic distribution of the normalized sum values of cobalt, nickel, and iron (not illustrated) shows that samples with either a high or a low association among these elements are randomly distributed across the study area.

A few strong negative correlations also occur between elements in the nonmagnetic fractions (C3) (see Fig. 55). The correlation coefficients suggest that the nickel, iron or cobalt content of a sample is inversely related to the phosphorous content (Note: nickel and cobalt are elements with few valid observations). The coefficients also suggest that the niobium or iron content of a sample is inversely related to the yttrium content.

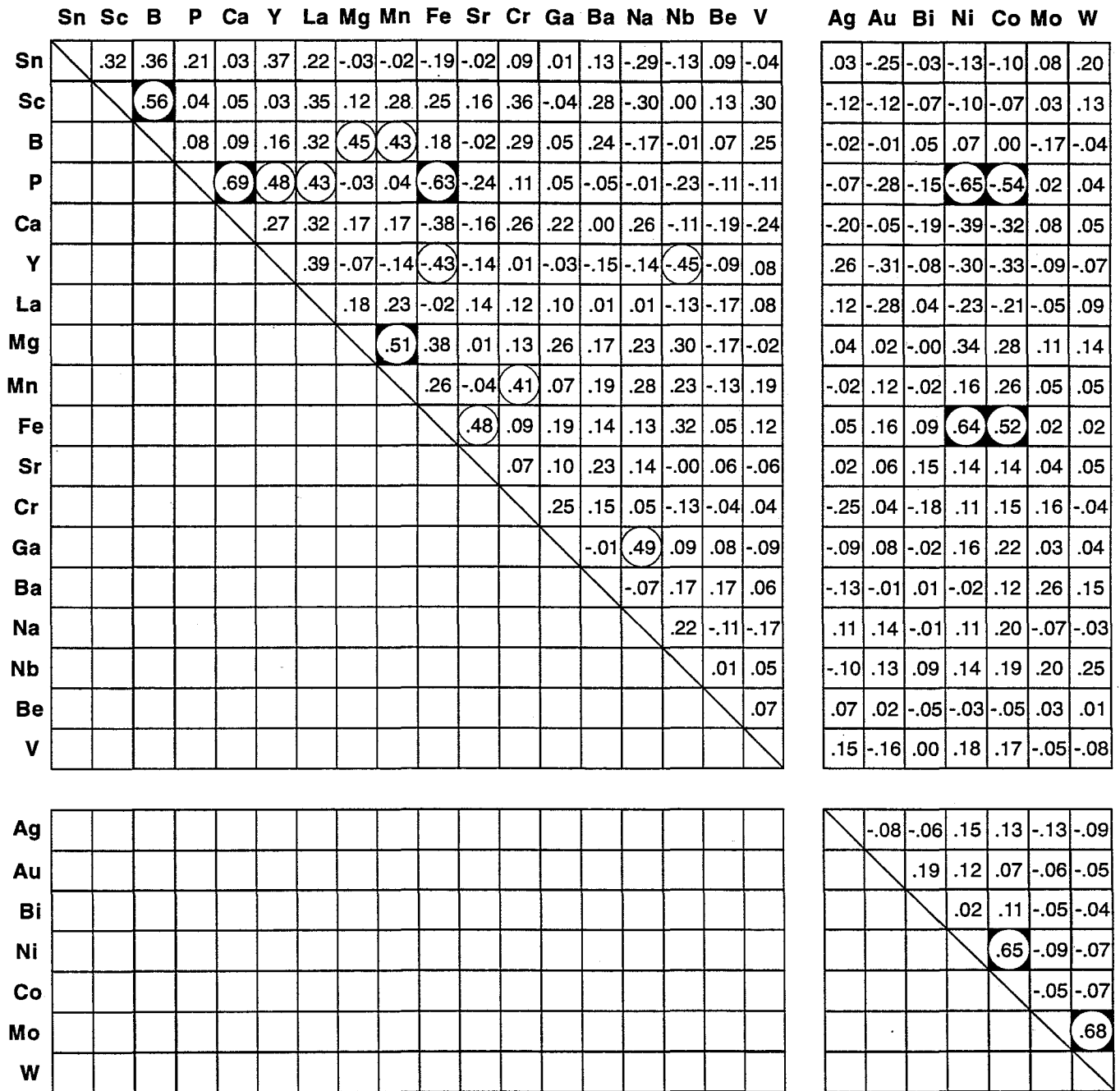
The nonmagnetic-fraction (C3) samples were also grouped by glacial lobe type and examined for paired-element correlations. These results (not illustrated) show many paired-element correlations within samples from the Wadena lobe, slightly less within samples from the Rainy lobe, and markedly less within samples from the Superior lobe.

Multi-element Associations in the Nonmagnetic Fraction

R-mode factor analysis, using two- to ten-factor models, examined the multi-element associations among the fourteen elements observed (Ba, B, Ca, Cr, Ga, Fe, La, Mg, Mn, P, Sc, Sr, Sn, and Y) in the nonmagnetic-fraction (C3) samples. The eight elements with few valid observations (Ni, Co, Au, Ag, Mo, W, Bi, Th), the four elements with some contaminated samples (Sb, Zn, Cu, Pb), and the four elements with inadequate data variation (Na, Nb, V, Be) were excluded from this analysis. The six-factor model was selected as the most reasonable factor model because it clearly shows the strongest factor—a phosphorus-calcium rare earth assemblage—and contains most of the other element associations seen in the other factor models.

Elements most strongly correlated with factor I of the six-factor model are the positive correlations of tin, yttrium, scandium, and boron. Although tin with yttrium and boron could represent tin mineralization, this is not a strong factor because scandium is not usually associated with these elements. Samples showing the strongest associations (factor scores >1)

elements with few
valid observations





 Correlation coefficient $\geq +0.4$ or ≤ -0.4
 Correlation coefficient $\geq +0.5$ or ≤ -0.5

Figure 55. Paired-element correlation coefficients for 25 elements in samples of the nonmagnetic fraction (C3) of the heavy-mineral concentrates.

among these four elements are geographically distributed from the south edge of the Duluth Complex to the southwestern part of the study area, but cluster in the central part of the study area on both sides of the Mississippi River (Fig. 56). The samples with a low association (factor scores <-1) among these elements are distributed in a tight cluster in the northeast greenstone-granite terrane and in a second looser cluster in the southwestern part of the study area (see Fig. 56). Histograms of the factor I scores grouped by glacial sediment type (not illustrated) do not show any significant differences in the element associations among samples from the various lobes. The samples from the Wadena lobe have a bimodal distribution that suggests intra-lobe variation; the geographic distribution of these samples (not illustrated) switches from high to mid-low values at adjacent sites indicating a very local characteristic.

Elements most strongly correlated with factor II of the six-factor model are the positive correlations of phosphorous, calcium, yttrium, and lanthanum, and their inverse (negative) correlation with iron. This is the strongest factor in the six-factor model and suggests that the phosphorus-calcium rare earth assemblage would be apatite. Samples that show the strongest positive associations (factor scores >1) among these elements strongly cluster in the Duluth Complex area (Fig. 57). The samples that show a low association (factor score <-1) among these elements cluster in the central part of the study area just west of the Mississippi River (see Fig. 57). Histograms of the factor II scores grouped by glacial lobe (not illustrated) show that the samples with the strongest element associations are in the Rainy and Superior lobes (see Fig. 57), although differences in the element means between the lobes is not significant at $\alpha = .05$.

Magnesium, manganese, boron, and iron are the elements most strongly correlated with factor III of the six-factor model. Boron suggests that tourmaline is contributing to this factor. The strongest associations among these elements occur in samples clustered down ice from the Duluth Complex, extending to the central part of the study area where the lowest factor scores cluster along both sides of the Mississippi River (Fig. 58). The frequency distribution of the factor III scores grouped by glacial lobe (not illustrated) show that there is significantly more ($\alpha .05$) magnesium, manganese, boron, and iron in samples from the Superior lobe compared with samples from the Wadena or Rainy lobes.

Elements most strongly correlated with factor IV of the six-factor model are strontium and iron, which suggests a carbonate. The strongest associations (factor scores >1) between these elements occur in a small group of samples in the northeast greenstone-granite terrane near the iron formations, and in a group of samples scattered from the Animikie Basin to just west of the Mississippi River (Fig. 59); these samples were collected in the Rainy and Superior lobe sediments. Samples that show a low association (factor score <-1) between strontium and iron form a tight cluster in the Duluth Complex area and in samples scattered predominantly west of the Mississippi River (Fig. 59); these samples are from three glacial lobes.

The elements most strongly correlated with factor V of the six-factor model are chromium, gallium, scandium, and manganese. Samples with the strongest associations (factor scores >1) among these elements form a strong cluster in the central part of the study area along and near the Mississippi River (Fig. 60). This cluster contains samples from all four lobes, which seems to suggest an association of local character. The samples that show the lowest associations (factor scores <-1) among these elements are randomly scattered throughout the study area; these samples were collected in Superior and Wadena lobe sediments.

**NONMAGNETIC FRACTION
FACTOR SCORES FOR
FACTOR I OF SIX-FACTOR MODEL**

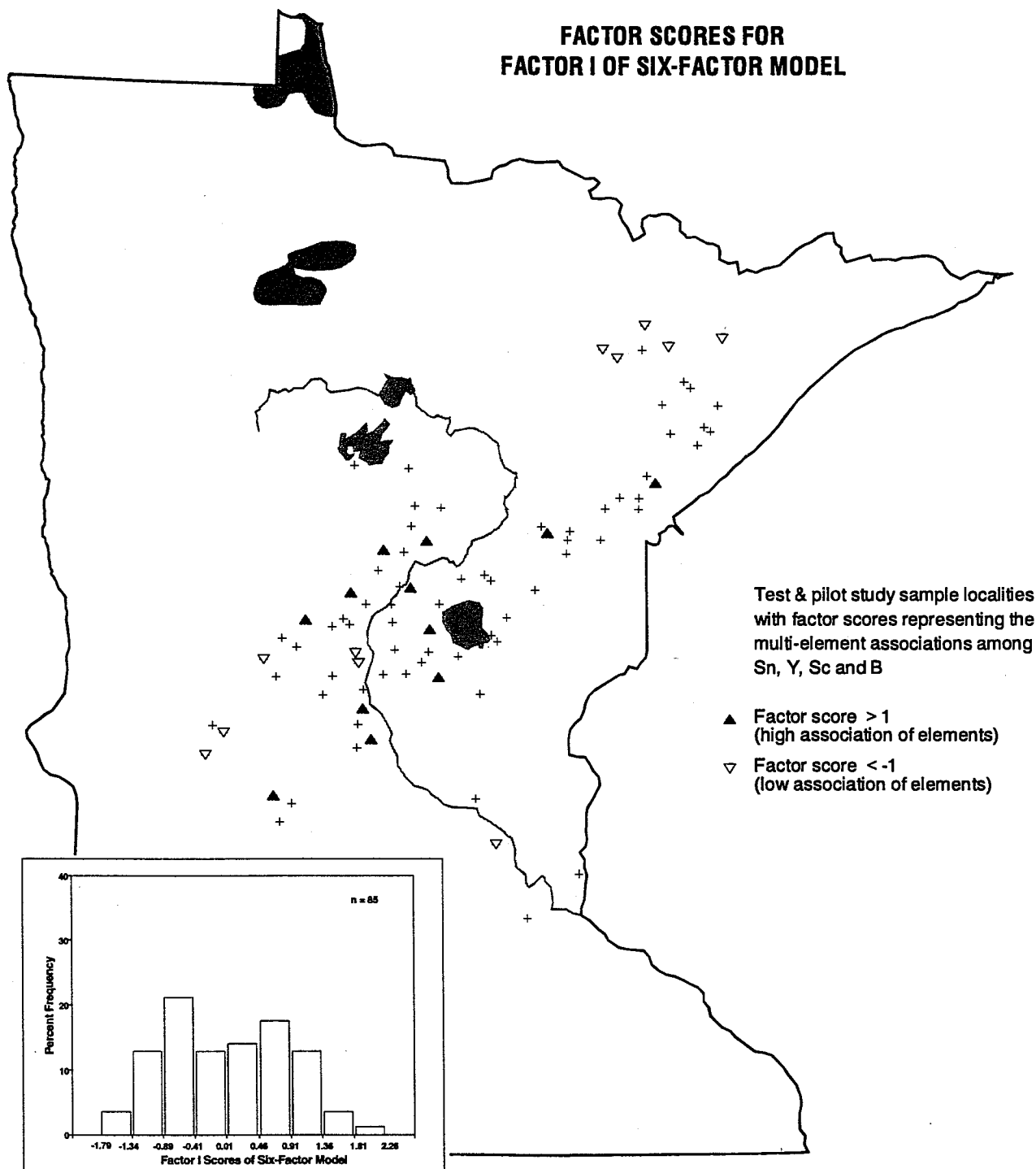


Figure 56. Frequency and geographic distribution of the high and low factor scores for Factor I of the six-factor model, which represents the multi-element associations among Sn, Y, Sc and B in samples of the nonmagnetic fraction (C3) of the heavy-mineral concentrates.

**NONMAGNETIC FRACTION
FACTOR SCORES FOR
FACTOR II OF SIX-FACTOR MODEL**

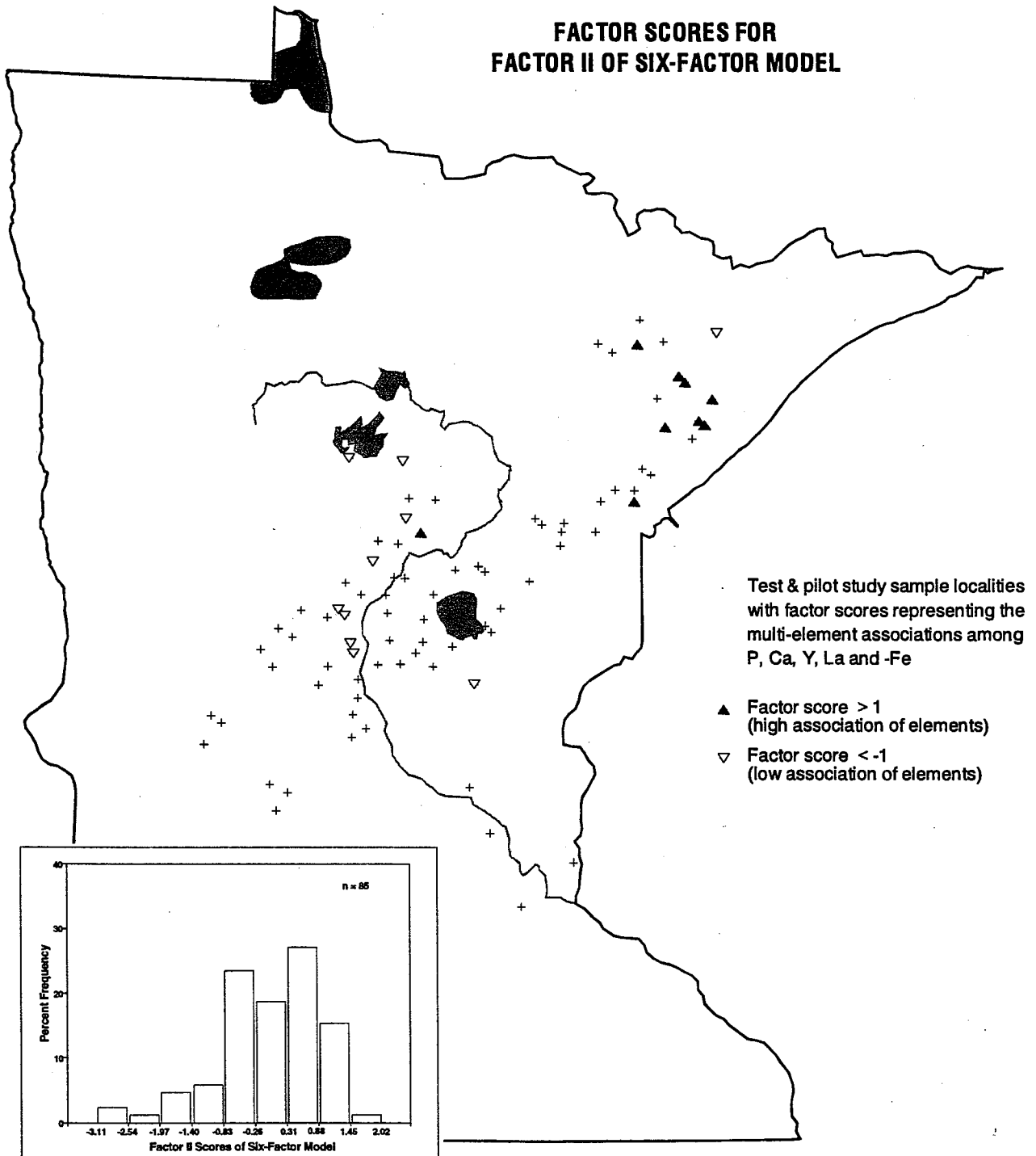


Figure 57. Frequency and geographic distribution of the high and low factor scores for Factor II of the six-factor model, which represents the multi-element associations among P, Ca, Y, La and -Fe in samples of the nonmagnetic fraction (C3) of the heavy-mineral concentrates.

**NONMAGNETIC FRACTION
FACTOR SCORES FOR
FACTOR III OF SIX-FACTOR MODEL**

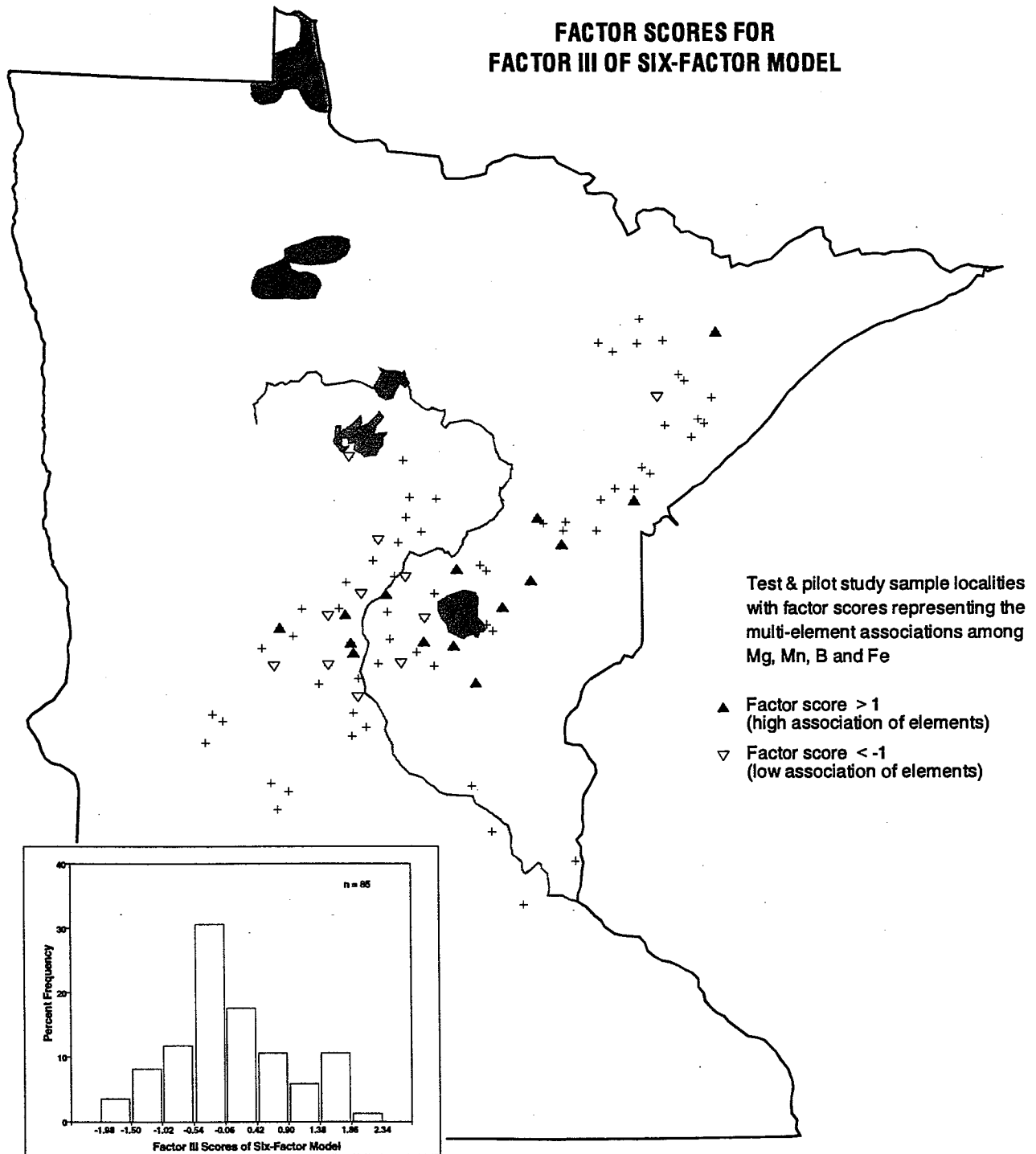


Figure 58. Frequency and geographic distribution of the high and low factor scores for Factor III of the six-factor model, which represents the multi-element associations among Mg, Mn, B and Fe in samples of the nonmagnetic fraction (C3) of the heavy-mineral concentrates.

Gallium and chromium are the most strongly correlated with factor VI of the six-factor model. This gallium-chromium association occurs along the Mississippi River—although not as strongly as in factor V—and with a second association in the northeastern part of the study area (Fig. 61). Two general groups of samples have a negative association with this factor—one in the southwestern part of the study area and another around Mille Lacs Lake; these samples are from three glacial lobes. The frequency distribution of the factor VI scores grouped by glacial lobe (not illustrated) shows significantly more gallium and chromium in samples from the Rainy ($\alpha < .01$) and Superior ($\alpha .05$) lobes than in samples from the Wadena lobe.

Several of the strong element associations in the six-factor model are also seen in most of the other factor models, although not always as clearly. These associations include the phosphorous-calcium-rare earth (apatite) factor, the magnesium-manganese-boron (tourmaline) factor and the strontium-iron (carbonate) factor. The tin-yttrium-boron (tin mineralization) factor is also seen in several factor models. From the seven-factor model on, gallium and barium drop out as single factors suggesting a weak association with the other elements. Also characteristic of the other factor models is the occurrence of iron in several factors within most models.

Three elements included in the above factor analysis have data with a poor distribution range: chromium, yttrium, and lanthanum. These questionable elements were dropped and factor analysis was computed again for the remaining eleven elements. This did not change the results significantly, with essentially the same factors showing up but without the chromium, yttrium, or lanthanum. Since these three elements support the element associations in the factor models we included them in the factor analysis.

Factor analysis was also computed with the fourteen elements plus copper and lead, on a reduced data set of 77 samples. The eight samples excluded (numbers 22632, 22635, 23918, 23922, 23943, 23945, 23950, and 23951) contained copper or lead contamination (Nelson and others, 1992). This data set did not significantly change the factor results—copper occurred as a single element in four factor models, and lead occurred with the gallium-chromium association in two factor models before dropping out as a single element. These results suggests that copper and lead have little association with the other elements.

CORRELATIONS BETWEEN THE GEOCHEMICAL DATA SETS

We looked for correlations between platinum and (or) palladium occurrences in the bulk-concentrate samples and the occurrence of the magnesium-nickel-cobalt factor in the paramagnetic-fraction (C2) samples or the apatite factor in the nonmagnetic-fraction (C3) samples. The results showed an absence of any significant correlation between occurrences of platinum or palladium with either factor.

NONMAGNETIC FRACTION
FACTOR SCORES FOR
FACTOR IV OF SIX-FACTOR MODEL

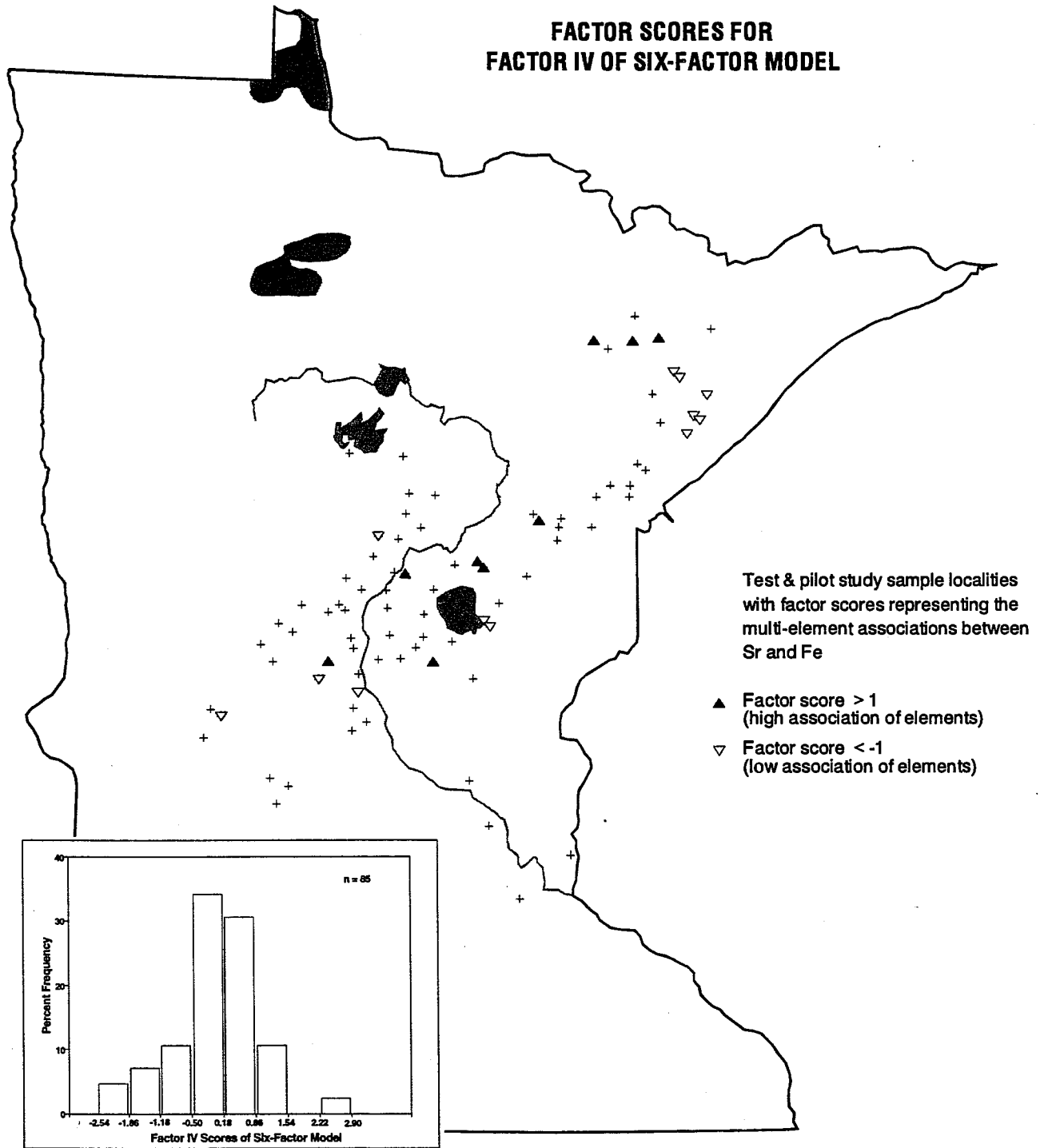


Figure 59. Frequency and geographic distribution of the high and low factor scores for Factor IV of the six-factor model, which represents the multi-element associations between Sr and Fe in samples of the nonmagnetic fraction (C3) of the heavy-mineral concentrates.

NONMAGNETIC FRACTION
FACTOR SCORES FOR
FACTOR V OF SIX-FACTOR MODEL

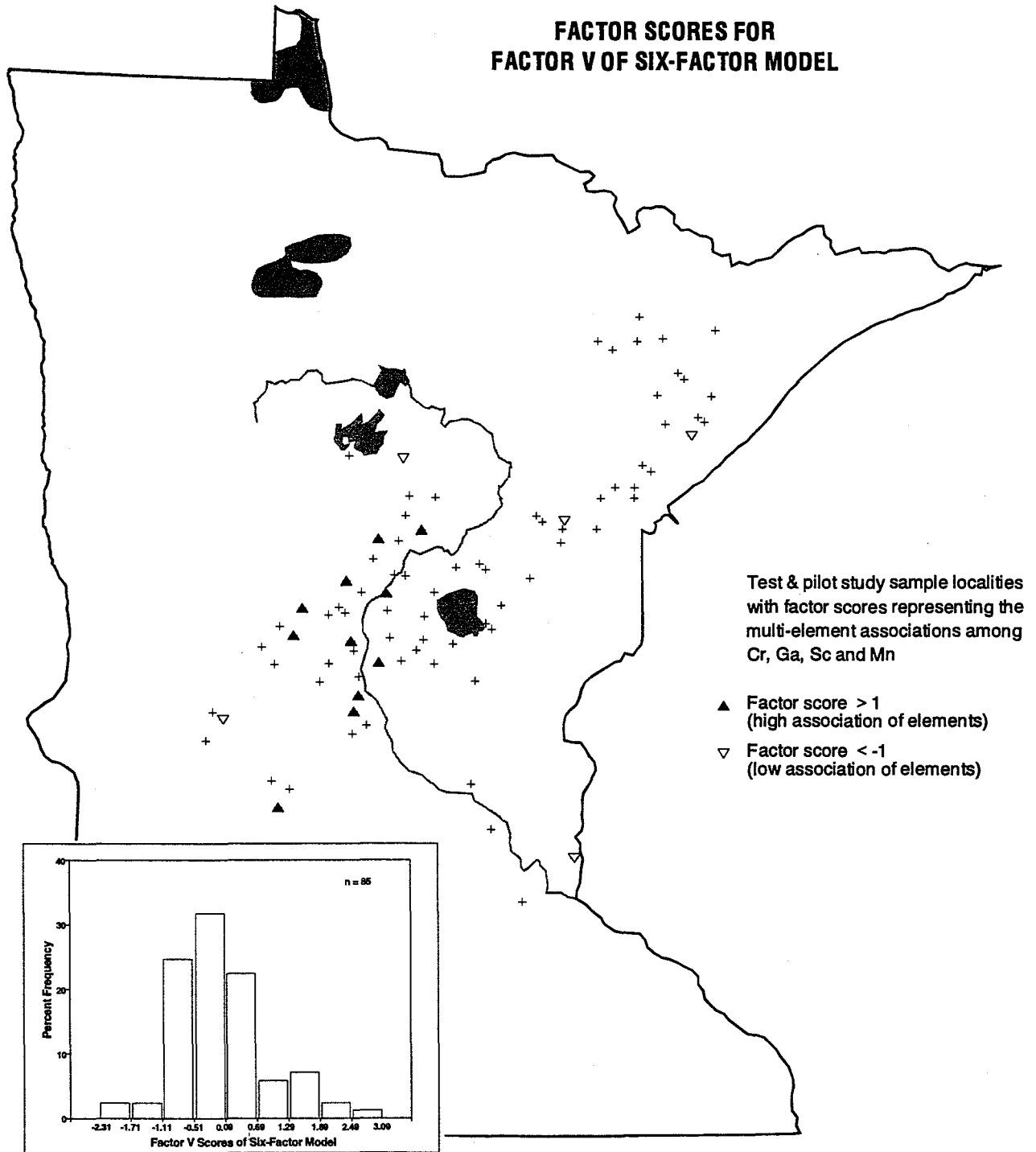


Figure 60. Frequency and geographic distribution of the high and low factor scores for Factor V of the six-factor model, which represents the multi-element associations among Cr, Ga, Sc and Mn in samples of the nonmagnetic fraction (C3) of the heavy-mineral concentrates.

NONMAGNETIC FRACTION
FACTOR SCORES FOR
FACTOR VI OF SIX-FACTOR MODEL

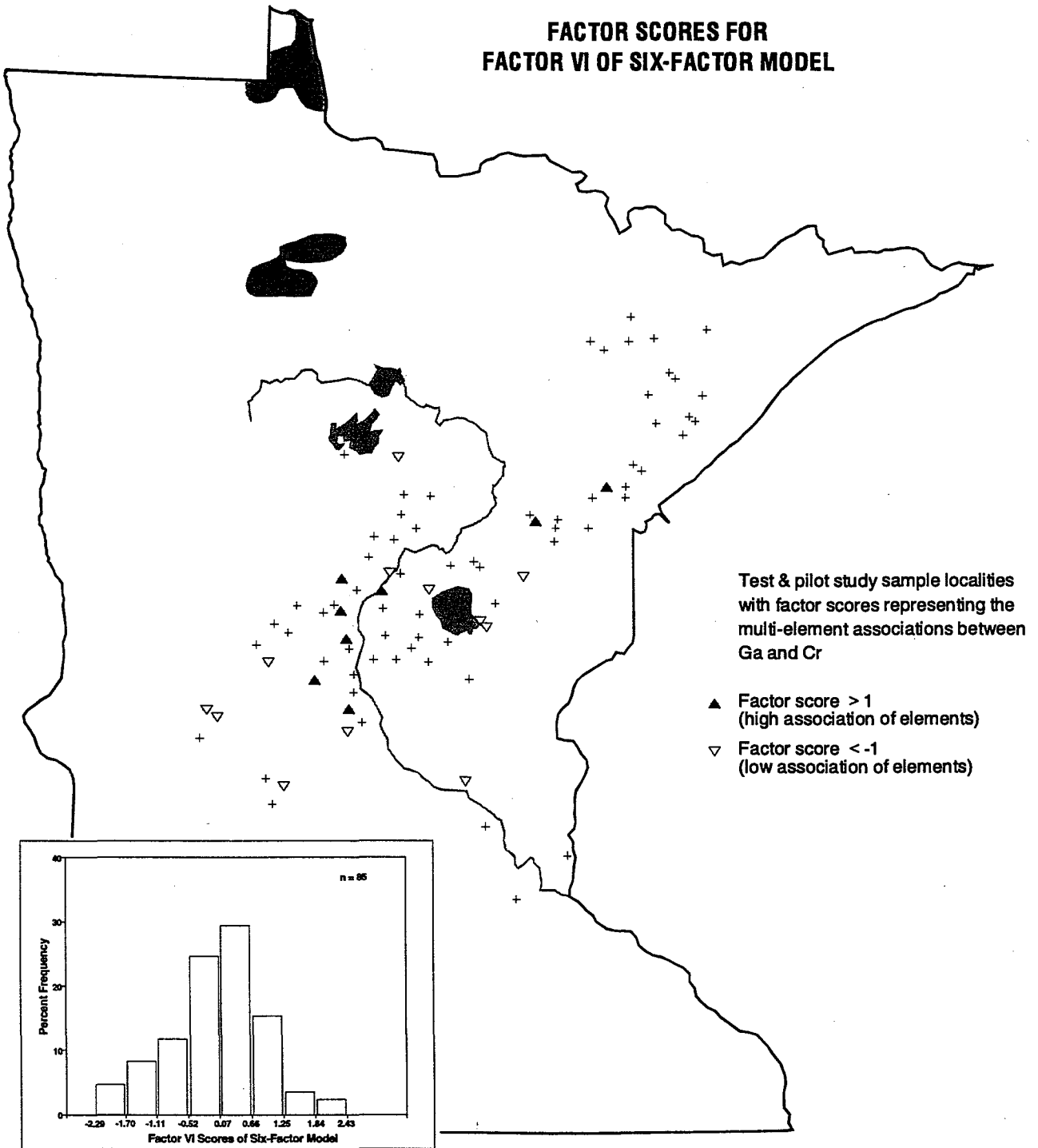


Figure 61. Frequency and geographic distribution of the high and low factor scores for Factor VI of the six-factor model, which represents the multi-element associations between Ga and Cr in samples of the nonmagnetic fraction (C3) of the heavy-mineral concentrates.

NONMAGNETIC FRACTION MINERALOGICAL RESULTS

The mineralogy of the samples in the nonmagnetic fraction (C3) of the concentrates was visually determined using binocular microscopy and shortwave ultraviolet light, and confirmed with x-ray diffraction techniques when necessary. Seventeen minerals were identified in the eighty-five nonmagnetic-fraction samples and are summarized below.

Gold was visually identified in nine samples, with observations ranging from one to three particles in each sample; these samples predominantly cluster along the Mississippi River (Fig. 62). Two isolated samples that contain two or more visible gold particles also contain several anomalous geochemical values. This includes sample number 23916, on the south edge of the Duluth complex, which contains extreme fire assay gold, platinum, and palladium values; and sample number 23960, in the southwestern part of the study area, which contains extreme base metal values and fire assay gold values. The visible gold particles were observed in samples from the Rainy, Wadena, and Superior lobes.

Scheelite (CaWO_4) was identified in 54 percent of the samples, with observations ranging from one to nine grains in each sample. Powellite (CaMoO_4) was identified in less than 4 percent of the samples, with one or two grains observed in each sample. Scheelite and powellite occurrences are scattered across the study area. Figure 63 shows the geographic distribution of samples that contain a combined value of four or more scheelite and powellite grains. These samples predominantly cluster in central Minnesota, with two isolated samples in the northeastern part of the study area. The sample (number 23960) that contains the most scheelite and powellite grains, is the same sample with the extreme gold and base metal values noted in the last paragraph.

Pyrite was identified in 20 percent of the samples, comprising less than 1 percent of each sample. Most of these samples are geographically distributed in two clusters; one cluster trails down ice from the south edge of the Duluth Complex and the other cluster occurs along the west side of the Mississippi River in central Minnesota (Fig. 64). Over 50 percent of the samples that contain pyrite are from the Superior lobe, with the remaining observations split between samples from the Rainy and Wadena lobes.

Cassiterite was identified in two samples, comprising less than 1 percent of each sample. Both samples were collected west of the Mississippi River, but are geographically isolated from each other; one sample is from the Rainy lobe and the other is from the Wadena lobe (Fig. 65).

Sillimanite was identified in 82 percent of the samples, and in most of these samples it comprises from 1 to 7 percent of the sample. Extreme sillimanite values of 20 and 30 percent were observed in sample numbers 23922 and 23926, respectively. Andalusite was identified in 80 percent of the samples, and in the majority of these samples it comprises from less than 1 to 30 percent of the sample. Extreme andalusite values of 40 and 50 percent were observed in sample numbers 23917 and 23922, respectively. The distribution of the samples with the extreme sillimanite and andalusite values geographically confirm each other; these four samples lie in the contact zone between the intrusive Duluth Complex and the Animikie Group sediments (overlay Appendix A on Fig. 65).

NONMAGNETIC FRACTION

VISIBLE GOLD

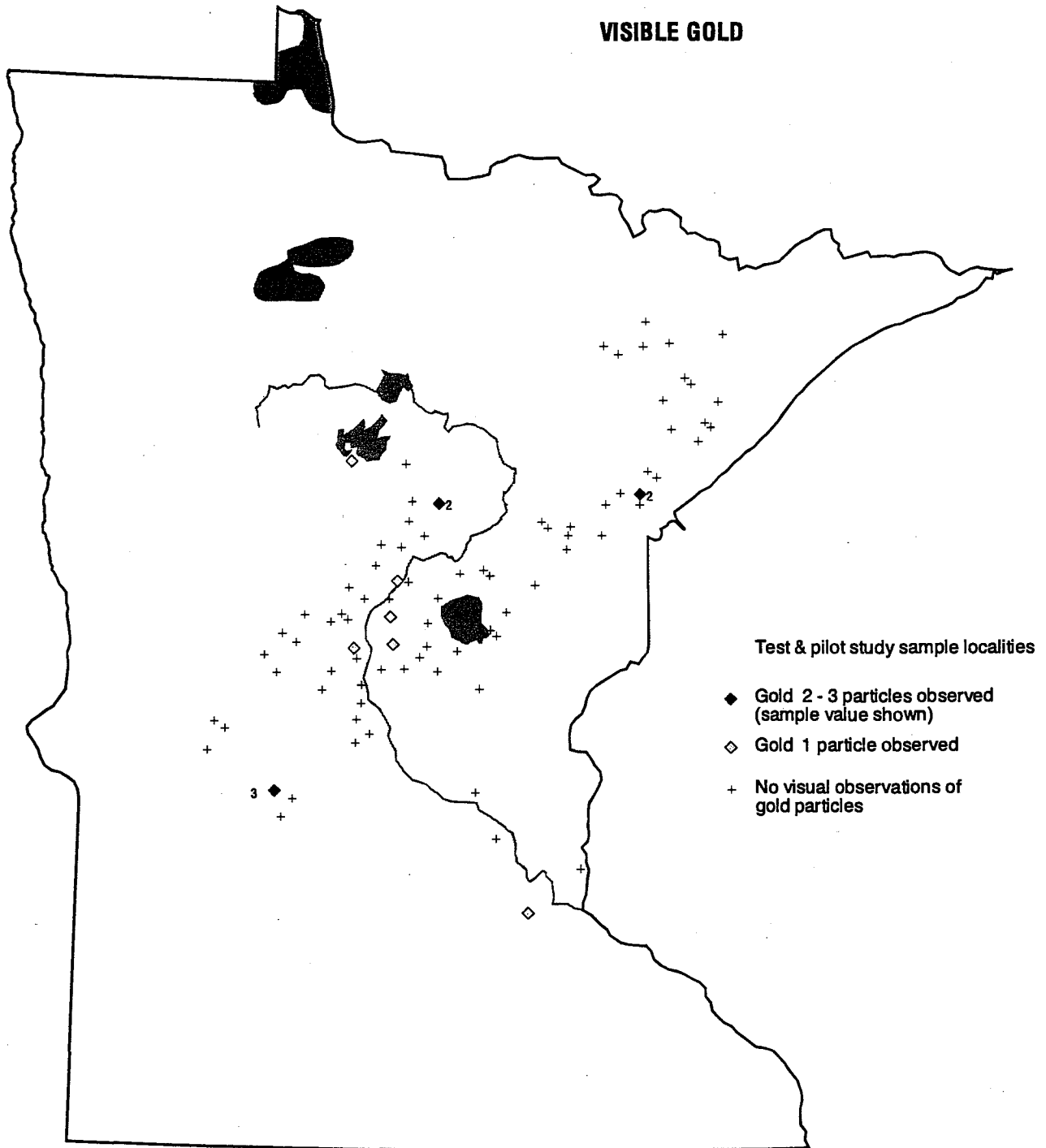


Figure 62. Geographic distribution of gold particles visually observed in samples of the nonmagnetic fraction (C3) of the heavy-mineral concentrates.

**NONMAGNETIC FRACTION
SCHEELITE AND POWELLITE**

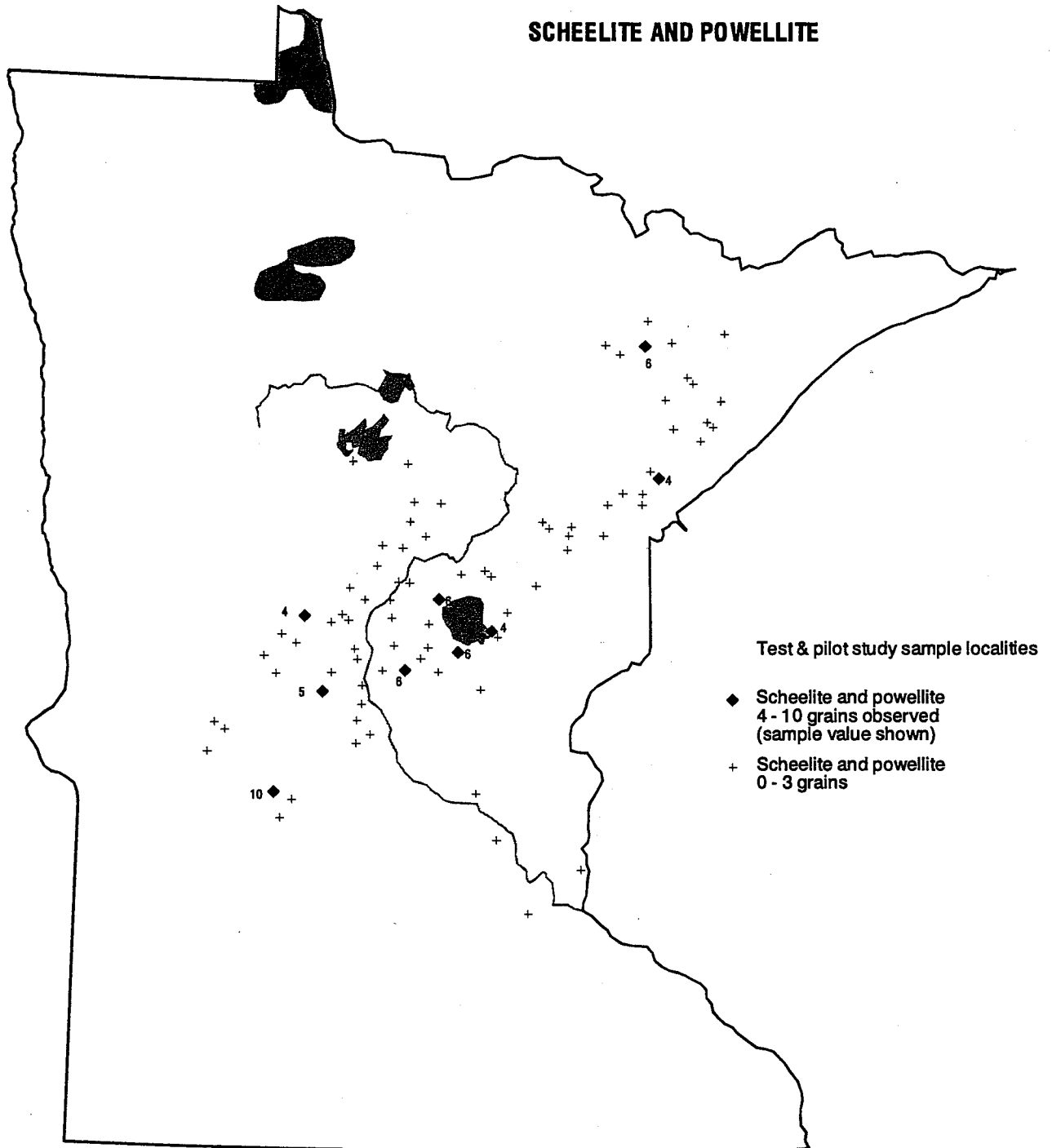


Figure 63. Geographic distribution of scheelite and powellite visually observed in samples of the nonmagnetic fraction (C3) of the heavy-mineral concentrates.

NONMAGNETIC FRACTION

PYRITE

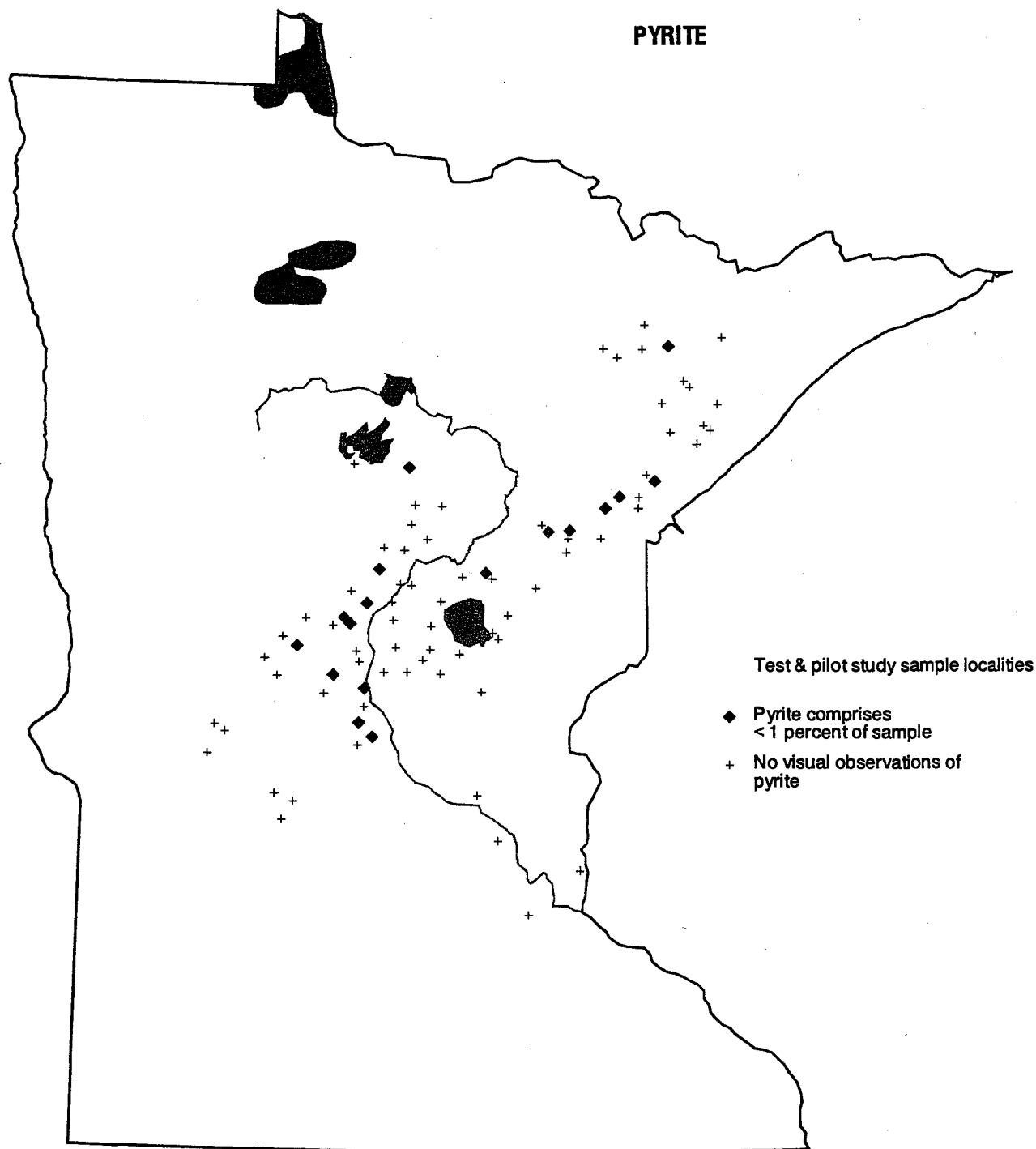


Figure 64. Geographic distribution of pyrite visually observed in samples of the nonmagnetic fraction (C3) of the heavy-mineral concentrates.

Apatite was identified in all samples, with values ranging from 3 to 50 percent of the sample. The samples where apatite is abundant, comprising 40 to 50 percent of the sample, are geographically scattered across the study area (Fig. 66). Those samples that contain less than 30 percent apatite are in a strong cluster in the Duluth Complex, and in a few isolated localities west of the Mississippi River (Fig. 66).

Tourmaline was identified in less than 25 percent of the samples, comprising less than 5 percent of each sample. These samples geographically extend from the Duluth Complex to just west of the Mississippi River (Fig. 67), and are about equally distributed in Superior and Rainy lobe sediments.

Sphene was identified in almost all samples, with values ranging from 2 to 40 percent of the sample. Although, the full range of sphene data values are geographically scattered throughout the study area, generally the higher values are in samples from the northeastern-most part of the study area (not illustrated).

Manganoan diopside was identified in 8 percent of the samples, comprising less than 1 percent of each sample. These samples are geographically scattered across the study area (not illustrated), with four samples from the Superior lobe and three samples from the Rainy or Wadena lobe. The occurrences of manganoan diopside did not show any obvious relationships to geologic features or the geochemical data.

Kyanite, rutile, and zircon were identified in more than 96 percent of the samples, but little variation in the data values was observed between samples. Kyanite values range from less than 1 to 10 percent of the sample; rutile values range from less than 1 to 30 percent of the sample; and zircon values range from 10 to 40 percent of the sample.

Barite, corundum, and spinel were identified in less than 6 percent of the samples. Barite was identified in sample numbers 23907, 23911, 23919, 23948, and 23965, and comprises less than 1 percent of each sample. These samples are geographically scattered from southwest of the Duluth Complex to west of the Mississippi River (not illustrated), with three samples from the Superior lobe and the other two from the Rainy and Wadena lobes. Corundum grains were identified in samples numbers 23927, 23944, and 23952, and comprise from less than 1 to 3 percent of each sample. Two corundum occurrences are in samples from the Superior lobe in central Minnesota, and the other occurrence is in a sample from the Rainy lobe in northeastern Minnesota (not illustrated). Spinel comprises less than 1 percent of sample number 23909. The spinel is in a sample from the Superior lobe in the central part of the study area (not illustrated). The occurrences of these three minerals did not show any obvious relationships to geologic features or the geochemical data.

NONMAGNETIC FRACTION

ANDALUSITE, SILLIMANITE AND CASSITERITE

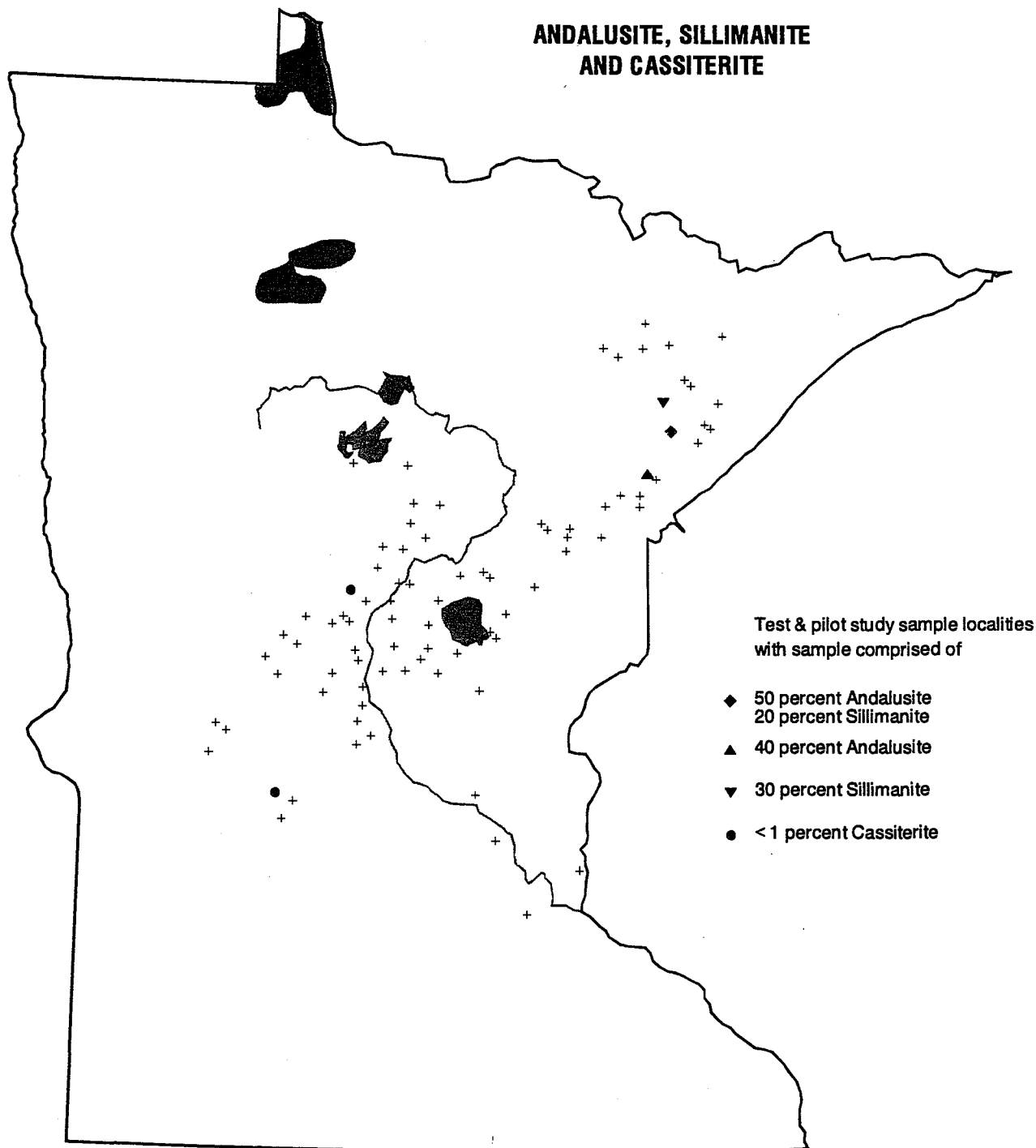


Figure 65. Geographic distribution of cassiterite and the extreme values of andalusite and sillimanite visually observed in samples of the nonmagnetic fraction (C3) of the heavy-mineral concentrates.

NONMAGNETIC FRACTION

APATITE

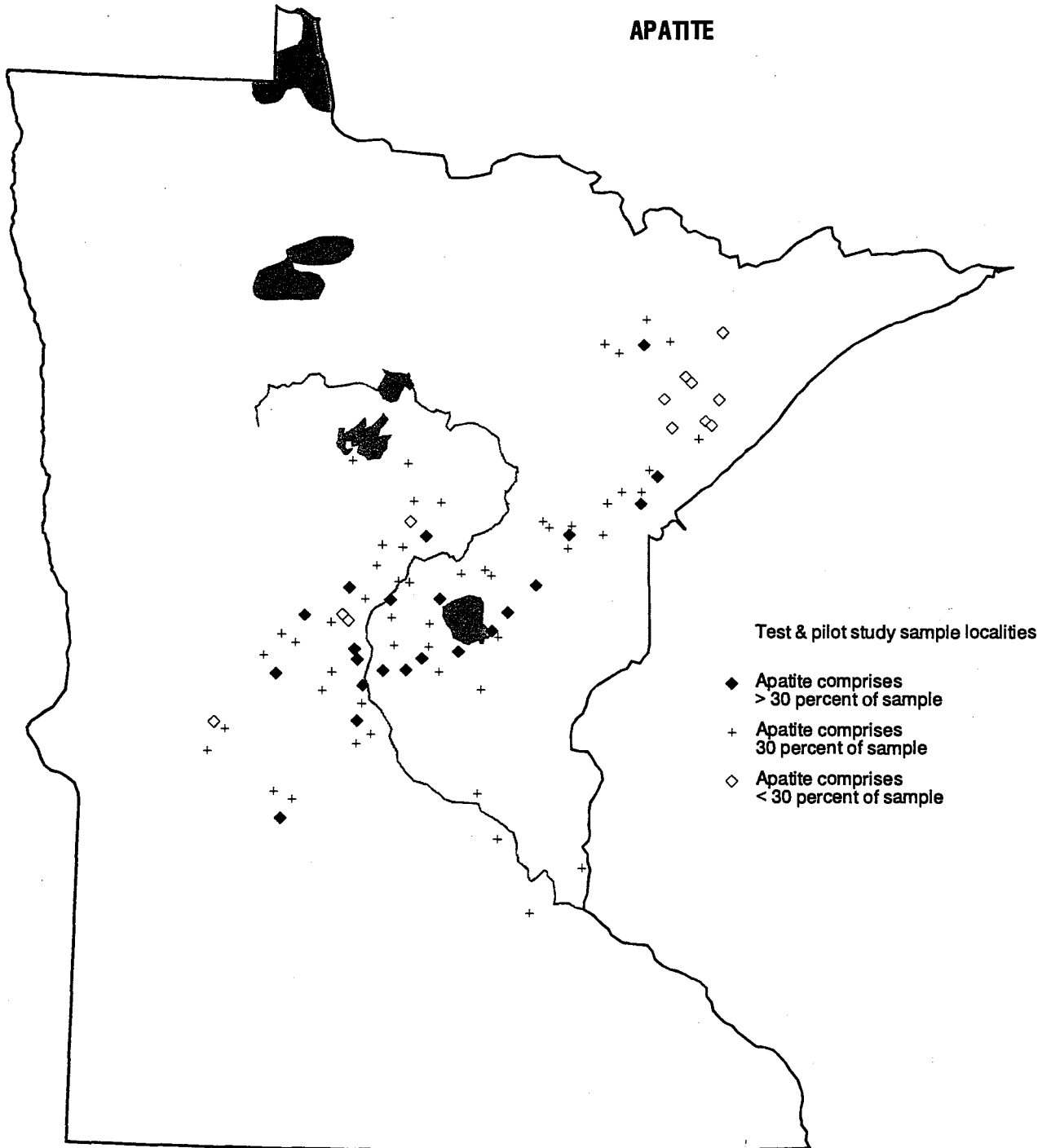


Figure 66. Geographic distribution of apatite visually observed in samples of the nonmagnetic fraction (C3) of the heavy-mineral concentrates.

NONMAGNETIC FRACTION TOURMALINE

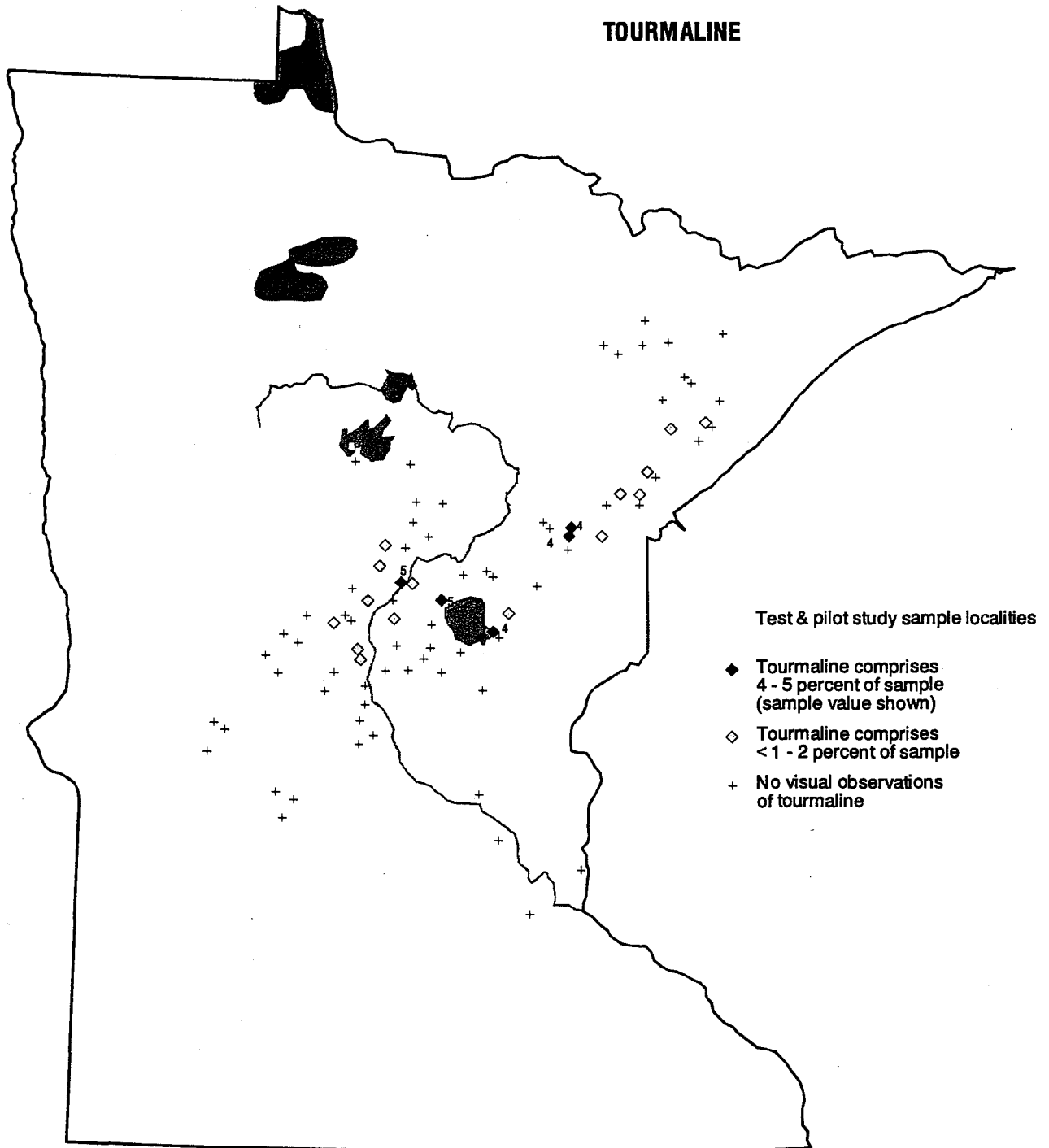


Figure 67. Geographic distribution of tourmaline visually observed in samples of the non-magnetic fraction (C3) of the heavy-mineral concentrates.

DISCUSSION

VARIATION

The range of values obtained for most of the measurements made on these samples exceeds what would be expected from sampling or analytical variation. For a few components the range of values is extreme. Unfortunately, many of these extreme values can be explained by contamination. Element associations in the samples with extreme values (for example: copper with zinc; and lead with antimony) suggest a specific form of contamination, such as brass and lead shot. The mineralogy of the concentrates confirms the presence of the contamination in the form of slivers of brass, lead, and aluminum. The gravel pits sampled are popular places for target shooting, and evidently the depth of penetration of both the bullets and the target materials exceeded the amount of cleaning of the pit wall prior to sampling. Fortunately, we can use a combination of chemistry and mineralogy to identify the contaminated samples and to specify the composition of the contamination. Other components of these samples are not affected by the contamination, and only a few of the samples are contaminated. Eliminating the contamination, the high and the low end of the range of values obtained for most of the components are in samples that are clustered geographically. This variation most likely reflects a natural variation.

VARIATION IN THE HEAVY MINERALS RELATED TO THE GLACIAL LOBE

Variation of the elemental composition of heavy minerals among samples from the various glacial lobes was less than expected. Indeed, in the nonmagnetic fraction (C3) of the concentrates, the chemical variation is largely independent of the lobe sampled. Of the 24 variables tested for the nonmagnetic fraction (18 elements and 6 factors) only seven, Mg, Na, B, Be, Ga, Sc, and Y, exhibit variation that can be related to the lobe sampled (see Table 4). Within these seven variables, the results seem contradictory. High magnesium in samples from the Superior lobe, for example, could be related to the abundance of mafic rocks (the Duluth Complex). Why, then, would the yttrium be high in the Superior lobe while scandium is high in the Wadena lobe? Similarly, the low concentrations of boron in the Rainy lobe and of sodium in the Wadena lobe are difficult to explain. Low gallium in samples from the Wadena lobe is reflected in the low scores for the unusual association of gallium and chromium in factor VI (see Fig. 61).

The paramagnetic fraction (C2) of the concentrates yield chemical characteristics more easily related to the glacial lobes. Of the 19 elements with adequate data to test sample variability between the lobes, 15 yield a significant difference for one or more of the lobe types (see Table 2). Sediment from the Wadena lobe is richest in the elements commonly associated with felsic rocks (B, Ga, La, Nb, Pb, Sr, and Y) and is poorest in elements commonly associated with mafic rocks [nickel and factor I of the two-factor model (Mg, Ni, and Co) (see Fig. 36)]. Sediment from the Superior lobe is poorest in the felsic components (B, Ga, La, Pb, and Y) and in complex factor II of the two-factor model (see Fig. 37). Sediment from the Rainy lobe is

poorest in zirconium but is generally intermediate in composition between the other two lobes, most similar to the Superior lobe. This intermediate composition blurs the distinction among the lobes.

The fire assay data for the bulk concentrates follow the general pattern seen in the nonmagnetic concentrates. Those elements of the platinum group for which adequate data are available (Pt, Pd, and Ru) are most abundant in samples from the Superior lobe (see Figs. 19 to 23). Gold-rich samples are about equally distributed among the lobes (compare Fig. 18 to Fig. 17).

This comparison among the glacial lobes does not yield a set of criteria that could be used to distinguish the lobe types. Although the means for some variables are different enough to signify a specific lobe, the overlap of the data is too great to allow confident assignment of individual sampling sites based on concentrate geochemistry. The generally intermediate character of the sediment from the Rainy lobe precludes its identification, and further blurs the distinction of the Superior and Wadena lobes. Those overall characteristics that could be used to distinguish the lobe indicate a Superior lobe sediment derived from a relatively mafic rock terrane, and a Wadena lobe sediment derived from a relatively felsic rock terrane. These characteristics are compatible with underlying bedrock geology and do not necessarily reflect a more distant provenance.

PATTERNS OF ANOMALOUS VALUES

The distinctive regional patterns of unusually high or unusually low values for the constituents of the heavy-mineral concentrates are evidently related to regional patterns in the bedrock geology. The distribution of high and low factor scores for factor I of the two-factor model for the chemistry of the paramagnetic fraction (C2) of the concentrates best defines the overall character of the patterns. High values for this factor are in the northeastern part of the area (see Fig. 36), mostly in samples from the Rainy lobe, in drift resting on or adjacent to the Duluth Complex. Only one of these samples is from the Superior lobe (sample number 23924) and only one is "down ice" from the Duluth Complex (sample number 23931 from the Rainy lobe) in an area underlain by the granite and greenstone terrane north of the Animikie Basin (Morey, 1994).

Low values for factor I of this two-factor model are more scattered, but all are in samples west of the Mississippi River (see Fig. 36), mostly from the Wadena lobe, in areas underlain by Archean rocks. A single sample (number 22632) is from the Rainy lobe, and sample 22631 is from drift resting on Proterozoic sediments at the northwest edge of the Animikie Basin where the sediments rest on Archean granite (Southwick and others, 1988). The composition of this factor, Mg, Ni, Co at the positive end and La, Y, Pb, B at the negative end, defines the distinction between mafic rocks, positive, and felsic rocks, negative. The geographic distribution of the factor scores indicates that the greatest mass of mafic rocks is in the east end of the study area and the greatest mass of felsic rocks is in the west, in accord with the bedrock geology (Morey, 1994).

Two additional patterns that emerge from the data reflect the mafic character in the east. Zirconium is unusually low in the paramagnetic fraction (C2) of the concentrates from drift

above the Duluth Complex (Rainy lobe sediments) (see Table 2). The nonmagnetic fraction (C3) of the concentrates over the Duluth Complex is also low in the mineral apatite compared with drift over the metamorphic and felsic igneous rocks to the west (see Fig. 66).

The Duluth Complex is clearly delineated by the aluminum silicate minerals andalusite and sillimanite in the nonmagnetic fraction (C3) of the concentrates. Andalusite ranges from less than 1 to 30 percent throughout most of the data set, but is most abundant in samples 23917 (40 percent) and 23922 (50 percent). Sillimanite is uniformly less than 10 percent of the nonmagnetic fraction of the concentrates except for samples 23922 (20 percent) and 23926 (30 percent). These three samples are on the contact of the Duluth Complex with the metamorphosed sedimentary rocks of the Animikie Basin (overlay Appendix A on Fig. 65). One likely explanation is that these two minerals reflect contact metamorphism where host rocks were thermally pushed to slightly higher grades than elsewhere.

Platinum, palladium, and ruthenium could be quantified in a sufficient number of the bulk concentrates to define patterns, although the absolute values are not high. The patterns for these elements appear to bear only an indirect relation to the Duluth Complex. A few scattered samples from drift over the Duluth Complex have anomalous platinum and palladium, as would be expected from the sporadic distribution of known occurrences of the platinum group in the Complex (Morton and Hauck, 1991; MN DNR, General Assessment Files). The major pattern of anomalous values for all three of the platinum-group elements begins at the western contact of the Duluth Complex and extends southwestward to the vicinity of Mille Lacs Lake (see Figs. 19, 20, and 23). The tightest clustering and the highest values in this pattern are immediately to the southwest of the contact (overlay Appendix A on figures). The samples defining this pattern are derived from the Superior lobe sediment where it overlies the sedimentary rocks along the southern edge of the Animikie Basin or somewhat older rocks of the Mille Lacs group (overlay Appendixes A and B on Figs. 19, 20, and 23) (Southwick and others, 1988).

The patterns of distribution of several other elements and minerals are similar to those of the platinum group. (1) Anomalous gold in the bulk concentrate is coincident with high platinum and (or) palladium in several samples (compare Figs. 18 with Figs. 19 and 20). Only one of these samples contained visible gold in the nonmagnetic fraction (C3) of the concentrate (see Fig. 62), and none of these had chemically detected gold in the nonmagnetic fractions. (2) Pyrite was found in the nonmagnetic fraction of the concentrates where the samples are rich in platinum-group elements (compare Fig. 64 with Figs. 19, 20, and 23). (3) Tourmaline is more abundant in the general platinum-rich area than it is elsewhere (compare Fig. 67 with Fig. 19). High values for tourmaline correlate better with platinum values than with pyrite. (4) The two samples richest in copper in the nonmagnetic fraction, after contamination is excluded (23908 and 23913 with 100 and 300 ppm respectively), are within the area of platinum-rich samples (see Fig. 46). One of these (23913) appears to be enriched in lead and zinc also.

The mafic-rich samples thus divide into two distinct assemblages. The Duluth Complex is clearly defined by the magnesium-dominated assemblage with scattered suggestions of platinum and palladium. This assemblage is appropriate to the mafic to ultramafic igneous rocks of the Complex. Samples of mafic character from the Superior lobe sediments to the southwest of the Duluth Complex are in an area underlain by sedimentary rocks along the southeastern edge of the Animikie Basin. The association of consistently high values for the

platinum group with tourmaline, pyrite, and occasionally gold or base metals suggests a more classical style of hydrothermal activity.

The felsic assemblage of elements (La, Y, Pb, and B), reflected in the negative component of the factor I scores for the two-factor model in the paramagnetic fraction (C2) of the concentrates, appears to be a weaker and geographically more diffuse grouping than the mafic (positive) component of this factor (see Fig. 36). In large part this is because the felsic component is overshadowed by the extreme contrast exhibited by the mafic component. Other features of the heavy minerals suggest a stronger and more coherent felsic signature along and to the west of the Mississippi River.

Factor scores for factor II of the six-factor model for the nonmagnetic fraction (C3) of the concentrates are strongly positive over the Duluth Complex and strongly negative in a north-trending belt west of the Mississippi River (see Fig. 57). This factor reflects the close association of phosphorus, calcium, and the rare-earth elements, most likely in the mineral apatite. Apatite is less abundant in samples from the vicinity of the Duluth Complex than in samples from west of the Mississippi River (see Fig. 66), but in the vicinity of the Duluth Complex apatite is the only presently known rare-earth accumulator. West of the Mississippi River, the rare-earth minerals monazite, florencite, and cheralite contain a major portion of the rare-earth elements in the samples. These rare-earth minerals are paramagnetic and appear in the C2 fraction of the concentrates rather than in the nonmagnetic fraction (C3). These are minerals found almost exclusively in felsic igneous and metamorphic rocks. Thus, the strong negative anomaly for the phosphorus, calcium, and the rare-earth element factor west of the Mississippi River (see Fig. 57), a feature of the nonmagnetic fraction of the concentrates, most likely reflects the partitioning of the rare earths away from apatite into paramagnetic minerals in the felsic terrane. The strong positive anomaly for this factor over the Duluth Complex (see Fig. 57) reflects the partitioning of nearly all of the rare-earth elements into relatively less abundant apatite.

The correlation of chromium with gallium in factor V of the six-factor model for the nonmagnetic fraction (C3) and lanthanum in the paramagnetic fraction (C2) is also related to changes in the host minerals for chromium between mafic to ultramafic rocks to the east and felsic igneous and metamorphic rocks west of the Mississippi River (see Figs. 60 and 35). These correlations are strongest along and to the west of the Mississippi River. Chromium is selectively enriched in oxide minerals in the mafic and ultramafic rocks, and these are concentrated in the magnetic fraction (C1) of the concentrates in the separation procedure used. Chromium is selectively enriched in the amphiboles along and to the west of the Mississippi River. These amphiboles are primarily found in the paramagnetic fraction and secondarily in the nonmagnetic fraction of the concentrates. Gallium is most abundant in aluminum minerals in felsic igneous and aluminous metamorphic rocks. These aluminum silicate minerals are concentrated in the nonmagnetic fraction of the heavy minerals. The rare-earth elements are in apatite (nonmagnetic fraction) in the mafic terrane and in the rare-earth phosphates (paramagnetic fraction) in felsic terrane. Thus, the strong correlation of chromium and lanthanum in the paramagnetic fraction, and of chromium and gallium in the nonmagnetic fraction, are to be expected from the separation procedure and from the mineralogic hosts for these elements. High concentrations of these elements in the appropriate fractions of samples along and to the west of the Mississippi River confirm the felsic nature of the source rocks in this area. The association of chromium with gallium, or chromium with lanthanum, do not

occur in the same samples (compare Figs. 60 and 35). Therefore, these two measures may provide independent, possibly mutually exclusive, evidence for the felsic terrane.

A number of elements and minerals common in deposits associated with felsic igneous rocks are enriched in the felsic terrane west of the Mississippi River. In the paramagnetic fraction (C2) of the concentrates, all of the detectable values for molybdenum, tin, and thorium, and most of those for beryllium, are in samples from the felsic terrane (see Figs. 29 and 30). In the nonmagnetic fraction (C3), most of the detectable values and the highest values for tungsten and beryllium, the measurable values for molybdenum, and the single detectable value for thorium are all in samples from the felsic terrane (see Figs. 43, 44, 46 and 54). Two of the minerals commonly associated with granite-related ore deposits are most frequently encountered in the nonmagnetic fraction (C3) of the concentrates from the felsic terrane. Both confirmed occurrences of cassiterite are in this terrane (see Fig. 65), as well as the broad, northerly aligned cluster of pyrite-rich concentrates just to the west of the Mississippi River (see Fig. 64).

Visible gold and analytically detectable gold in the nonmagnetic fraction (C3) of the concentrates are essentially confined to a northerly trending belt along the Mississippi River, in the felsic terrane (see Figs. 41 and 62). Gold determined in the bulk concentrate is more abundant and at a generally higher concentration in the felsic terrane (see Fig. 18). In the bulk concentrate, gold is also found in a group of samples from the platinum-rich terrane, where gold is generally not detected either analytically or mineralogically in the nonmagnetic fraction of the concentrates (compare Fig. 19 with Figs. 18, 41, and 62). Thus, it appears that free gold is a feature of the felsic terrane, whereas "no-see-em" gold is a feature of the platinum-rich terrane.

The cluster of samples in the northeastern part of the area, north of the Animikie Basin and northwest of the Duluth Complex, is generally intermediate in character between the mafic rocks to the south and southeast and the felsic rocks to the west. The lack of a cohesive alliance of these samples with the extremes represented by the other terranes lends a lackluster character to the terrane. However, several individual instances of anomalous characteristics suggest that the area has some potential. In the paramagnetic fraction (C2), four of these samples have detectable beryllium and one has detectable silver (see Figs. 29 and 30). In the nonmagnetic fraction (C3), two of these samples have detectable molybdenum, and one of these is beryllium-rich while the other is tungsten-rich (see Figs. 43, 54 and 44). The bulk concentrate is rich in gold at two of these sites (see Fig. 18). This area is generally regarded as a granite-greenstone terrane, although most of the greenstones are north of the sample sites (Morey, 1994; Southwick, 1993). This is in agreement with the characteristics outlined above, which are most suited to a granitic terrane.

INDIVIDUAL SITES WITH EXTREME CHARACTERISTICS

Four sites, samples 23960, 23935, 23908 (24111) and 23931 (see Fig. 68 for site locations), stand out as extreme. Each has characteristics reflecting a different source material. Sample 23960, from Wadena lobe sediment over Middle Archean bedrock (Morey, 1994), has the most extreme granite-like characteristics. The nonmagnetic fraction (C3) of the concentrate

HEAVY-MINERAL STUDY

SAMPLE SITES WITH EXTREME CHARACTERISTICS

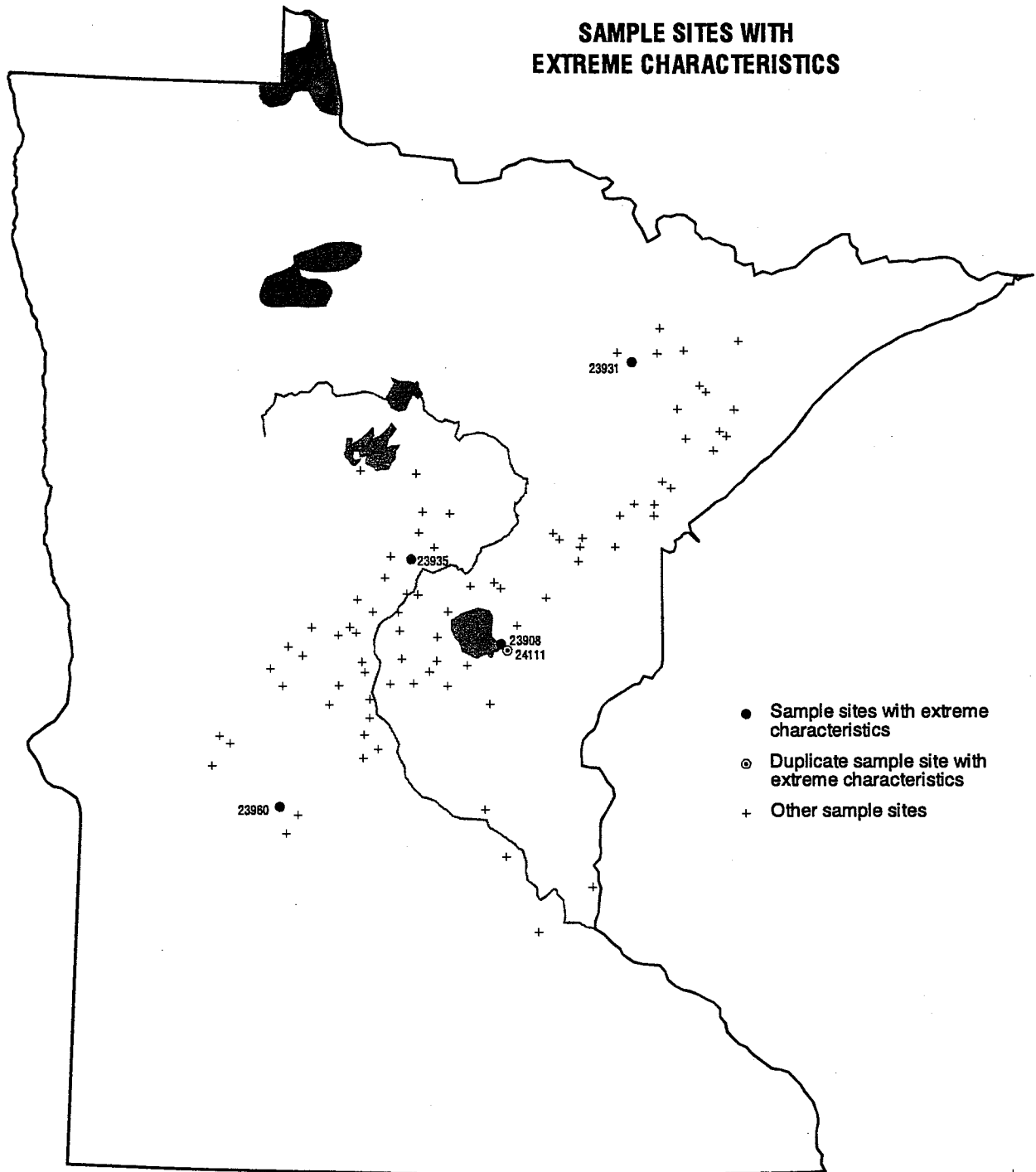


Figure 68. Geographic location of the individual sample sites with extreme characteristics.

has the maximum reported values for molybdenum, tin, and tungsten, the maximum number of scheelite/powellite grains, the maximum number of gold particles and cassiterite grains (see Figs. 43, 53, 44, 63, 62, and 65). This fraction also has high values for lead and beryllium (see Figs. 47 and 54). The paramagnetic fraction (C2) has the only detected values for thorium and tin and the bulk concentrate is gold-rich (see Figs. 30 and 18).

Sample 23935, from Rainy lobe sediment over metamorphosed late Archean volcanic and sedimentary rocks (Southwick and others, 1988), has extreme characteristics that would be attributed to base-metal deposits. The nonmagnetic fraction (C3) of the concentrates has high values for silver, gold, and antimony (see Fig. 46). It has the maximum value for lead (see Fig. 47) among those samples determined to be uncontaminated. The bulk concentrate yielded the maximum value for gold (see Fig. 18). These values are one to three orders of magnitude above background, reflecting major enrichment.

Samples 23908 and 24111 were collected from the same gravel pit on the east side of Mille Lacs Lake. The samples are from Superior lobe sediments over Early Proterozoic granite (Southwick and others, 1988). The two samples are similar, although not identical, and exhibit anomalous characteristics typical of the platinum-rich assemblage. The bulk concentrate is rich in platinum (4.1 and 3.2 ppb) (see Fig. 19) and palladium (2.2 and 2.1 ppb) for both samples, and sample 24111 also has detectable osmium, rhodium, and ruthenium (see Figs. 24 and 23). In addition, sample 23908 is anomalous for copper (100 ppm) in the nonmagnetic fraction (C3), both samples contain scheelite (3 or 4 grains), and 23908 has abundant tourmaline (see Figs. 46, 63 and 67).

Sample 23931, from Rainy lobe sediment over granitic rocks of Archean age (Morey, 1994), exemplifies the nondistinctive nature of the northeastern cluster of samples. On the basis of factor I of the two-factor model for the paramagnetic fraction (C2) of the concentrates, it has mafic affinities similar to those of samples from drift over the Duluth Complex (see Fig. 36). The nonmagnetic fraction (C3) for this sample is relatively rich in beryllium and molybdenum, similar to samples from the felsic terrane in the western part of the areas sampled (see Figs. 54 and 43). Thus, it exhibits dual characteristics, perhaps suitable to a "granite-greenstone" terrane; hence, does not stand out in comparison with the more pure felsic and mafic terranes.

Extreme values, like those described above, are usually interpreted to reflect proximity to the source. Yet, three of the four sites are presumably underlain by 100 feet or more of glacial drift (Olsen and Mossler, 1982). Sample 23931, which was collected from a site with less than 100 feet of drift and abundant outcrop, is the weakest of extreme sites. Direct proximity to the source seems unlikely to explain these extreme values both from the lack of relation to the thickness of the drift and the apparent incompatibility of the two southern extremes (23960 and 23908) with present knowledge of the immediately underlying geology at these sites. The reproducibility of the extreme values at 23908 (24111) argues against a fluke of concentration or of sampling bias at least at this site. The amount of lateral and vertical transport in the drift is unknown, but we suspect that it is short lateral transport that allows preservation of the extremes.

SUMMARY AND SPECULATION

The range in mineralogical and chemical parameters measured in these heavy-mineral concentrates is sufficient to allow reproducible recognition of regional geochemical patterns. Although some of the patterns are developed largely within the sediment of a single glacial lobe, the predominant cause of the patterns appears to reflect the local bedrock geology at the regional scale represented by the samples. In detail, individual samples do not appear to reflect immediately underlying rock types, so some lateral displacement is suggested. The amount of lateral displacement of the anomalies is not known, but it does not appear to be sufficient to overcome regional geochemical patterns.

Recognition of the geochemical patterns as being related to underlying regional geology allows speculation on the regional patterns and their relationship to mineral resource potential. Three large areas deserve special attention.

1. No source is presently known for the platinum-rich samples along the southeastern edge of the Animikie Basin (overlay Appendix A on Fig. 19). These samples are associated with tourmaline and some copper and gold. Considering the sporadic platinum associated with the Duluth Complex in our samples, this coherent pattern to the southwest would seem to warrant more attention. A classic hydrothermal type of mineralization is suggested.
2. In the northern part of the felsic terrane, in the general vicinity of the extreme sample 23935 (see location Fig. 68), the chemical and mineralogic characteristics suggests base and precious metal deposits. The pattern, particularly for gold (see Fig. 18), is much more coherent and stronger than would be expected for extensively reworked drift.
3. The extremely anomalous value for sample 23960 (see location Fig. 68) in the southwest part of the felsic terrane suggests a granite-related deposit—stockwork, skarn, greisen, etc. Elements such as tungsten, molybdenum, or tin may be sufficiently enriched to justify additional exploration for a bedrock source in this area.



REFERENCES

- Adrian, B.M., and Carlson, R.R., 1990, A method for semiquantitative spectrographic analysis of fire assay doré beads for the platinum-group elements and gold, *in* Zientek, M.L., and Page, N.J., Consultancy services in platinum-group mineral exploration for the Directorate of Mineral Resources (Indonesia): U.S. Geological Survey Open-File Report 90-527, p. 196-202.
- Alminas, H.V., McHugh, J.B., and Perry, E.C., Jr., 1992, Precious-and base-metal mineralization in the west-central Vermilion district, portions of St. Louis, Lake, and Cook counties, northeastern Minnesota: U.S. Geological Survey Bulletin 1984, 37 p.
- Boerboom, T., 1994, Minnesota at a glance: Precambrian geology: Minnesota Geological Survey, 4 p.
- Cleland, J.M., Morey, G.B., and McSwiggen, P.L., 1996, Significance of tourmaline-rich rocks in the north range group of the Cuyuna iron range, east-central Minnesota: *Economic Geology*, v. 91, p. 1282-1291.
- Dahlberg, E.H., Peterson, D., and Frey, B.A., 1989, 1988-1989 drill core repository sampling projects: Minnesota Department of Natural Resources, Division of Minerals Reports 255-1, 265, and 266, 316 p.
- Davis, J.C., 1986, *Statistics and data analysis in geology*: John Wiley & Sons, New York, 2nd ed., 646 p.
- Dyke, A.S., Vincent, J.S., Andrews, J.T., Dredge, L.A., and Cowan, W.R., 1989, The Laurentide Ice Sheet and an introduction to the Quaternary geology of the Canadian Shield, *in* Fulton, R.J., ed., *Quaternary geology of Canada and Greenland*: Geological Survey of Canada, Ottawa, p. 178-189.
- Eyles, N., 1983a, Glacial geology: A landsystem approach, *in* Eyles, N., ed., *Glacial geology: An introduction for engineers and earth scientists*: Oxford, Pergamon Press, p. 1-18.
- Eyles, N., 1983b, The supraglacial landsystem, *in* Eyles, N., ed., *Glacial geology: An introduction for engineers and earth scientists*: Oxford, Pergamon Press, p. 71-90.
- Frey, B.A., and Lawler, T.L., 1993, Reconnaissance mineral potential evaluation, Central Minnesota: Minnesota Department of Natural Resources, Division of Minerals, Hibbing, Open-File Report 295, 56 p. plus appendixes.
- Geerts, S., Barnes, R.J., and Hauck, S., 1990, Geology and mineralization in the Dunka Road copper-nickel mineral deposit, St. Louis County, Minnesota: Natural Resources Research Institute, University of Minnesota-Duluth, Technical Report NRRI/GMIN-TR-89-16, 69 p.
- Gilbertson, J.P., 1990, Quaternary geology along the eastern flank of the Coteau Des Prairies, Grant County South Dakota [MS thesis]: University of Minnesota-Duluth, 108 p.

Gowan, A.S., 1993, Sedimentology and geochemistry of selected glacial sediments from central Minnesota as a method for correlation and provenance studies of glacial stratigraphic units [M.S. thesis]: University of Minnesota-Duluth, 121 p.

Gravenor, C.P., 1975, Erosion by continental ice sheets: *American Journal of Science*, v. 275, p. 594-604.

Hauck, S.A., and Barnes, R.J., 1989, Precious metals (Pt-Pd-Au-Ag) in three copper-nickel deposits in the Duluth Complex: Natural Resources Research Institute, University of Minnesota- Duluth, Technical Summary Report NRRI/GMIN-TSR-89-1, 19 p.

Hobbs, H.C., and Goebel, J.E., 1982, Geologic map of Minnesota, Quaternary geology: Minnesota Geological Survey State Map Series S-1, scale 1:500,000.

Howarth, R.J., and Sinding-Larsen, R., 1983, Multivariate analysis, *in* Howarth, R.J., ed., *Handbook of exploration geochemistry—Volume 2, Statistics and data analysis in geochemical prospecting*: Elsevier Scientific Publishing Company, New York, p. 207-289.

Keighin, C.W., Morey, G.B., and Goldich, S.S., 1972, East-central Minnesota, *in* Sims, P.K., and Morey, G.B., eds., *Geology of Minnesota: A centennial volume*: Minnesota Geological Survey, University of Minnesota, St. Paul, p. 240-255.

Lawler, T.L., 1997, Field trip: Arrowhead Mine, Silver Creek, Anderson Farm, Carlton County, June 25, 1996 *in* Project Notebook 120-299: Minnesota Department of Natural Resources, Division of Minerals Open-File Report 203-13.

Lehr, J.D., and Hobbs, H.C., 1992, Glacial geology of the Laurentian divide area, St. Louis and Lake counties, Minnesota, *in* Field trip guidebook for the glacial geology of the Laurentian divide area, St. Louis and Lake counties, Minnesota: Minnesota Geological Survey Guidebook Series No. 18, p. 1-54.

Lilliesköld, M., 1990, Lithology and transport distance of glaciofluvial material, *in* Kujansuu, R., and Saarnisto, M., eds., *Glacial indicator tracing*: Rotterdam, Balkema, p. 151-164.

Listerud, W.H., and Meineke, D.G., 1977, Mineral resources of a portion of the Duluth Complex and adjacent rocks in St. Louis and Lake counties, northeastern Minnesota: Minnesota Department of Natural Resources, Division of Minerals Report 93, 49 p.

Marsden, R.W., 1968, Geology of the iron ores of the Lake Superior Region in the United States, *in* Ridge, J.D., ed., *Ore deposits of the United States, 1933-1967*: A.I.M.E. Inc., Graton-Sales Volume, v. 1, p. 489-506.

Martin, D.P., 1985, A compilation of ore mineral occurrences, drill core, and testpits in the State of Minnesota: Minnesota Department of Natural Resources, Division of Minerals Report 231, 266 p.

Martin, D.P., Meyer, G.N., Lawler, T.L., Chandler, V.W., and Malmquist, K.L., 1988, Regional survey of buried glacial drift geochemistry over Archean terrane in northern Minnesota: Minnesota Department of Natural Resources, Division of Minerals Report 252, v. I, 74 p., v. II, 386 p.

Martin, D.P., Meyer, G.N., Cartwright, D.F., Lawler, T.L., Pastika, J.T., Jirsa, M.A., Boerboom, T.J., and Streitz, A.R., 1989, Regional geochemical survey of glacial drift drill samples over Archean granite-greenstone terrane in the Effie area, northeastern Minnesota: Minnesota Department of Natural Resources, Division of Minerals Report 263, v. I, 59 p., v. II, 323 p.

Martin, D.P., Dahl, D.A., Cartwright, D.F., and Meyer, G.N., 1991, Regional survey of buried glacial drift, saprolite and Precambrian bedrock in Lake of the Woods County, Minnesota: Minnesota Department of Natural Resources, Division of Minerals Report 280, 75 p.

Matsch, C.L., and Schneider, A.F., 1987, Stratigraphy and correlation of the glacial deposits of the glacial lobe complex in Minnesota and northwestern Wisconsin: Quaternary Science Reviews, v. 5, p. 59-64.

McSwiggen, P.L., 1987, Geology and geophysics of the Denham-Mahtowa area, east-central Minnesota: Minnesota Geological Survey Miscellaneous Map Series M-63, scale 1:48,000.

Meier, A.L., Carlson, R.R., and Taggart, J.E., 1991, The determination of the platinum-group elements in geologic materials by inductively-coupled plasma/mass spectrometry, abstract and poster: The Sixth Annual International Platinum Symposium.

Meyer, G.N., 1986, Subsurface till stratigraphy of the Todd County area, central Minnesota: Minnesota Geological Survey Report of Investigations 34, 40 p.

Miall, A.D., 1983, Glaciofluvial transport and deposition, *in* Eyles, N., ed., *Glacial geology: An introduction for earth scientists and engineers*: Oxford, Pergamon Press, p. 168-183.

Minnesota Department of Natural Resources, Division of Minerals, Assessment Files: Minnesota Department of Natural Resources, Division of Minerals, Hibbing, Minnesota.

Mooers, H.D., 1988, Quaternary history and ice dynamics of the late Wisconsin Rainy and Superior lobes, central Minnesota [Ph.D. dissert.]: University of Minnesota, 200 p.

Morey, G.B., 1972, Pre-Mt. Simon regolith, *in* Sims, P.K., and Morey, G.B., eds., *Geology of Minnesota: A centennial volume*: Minnesota Geological Survey, p. 506-508.

Morey, G.B., 1976, The basis for a continental drilling program in Minnesota: Minnesota Geological Survey Information Circular 11, 25 p.

Morey, G.B., compiler, 1993, Geologic map of Minnesota: Bedrock geology: Minnesota Geological Survey State Map Series S-19, scale 1:3,000,000.

- Morey, G.B., compiler, 1994, Geologic map of Minnesota: Bedrock geology: Minnesota Geological Survey State Map Series S-20, scale 1:1,000,000.
- Morey, G.B. and Dahlberg, H., 1995, Geology of Minnesota: A guide for teachers: Minnesota Department of Natural Resources, Division of Minerals, 32 p.
- Morton, P., and Hauck, S.A., 1991, A review of the economic significance of the Duluth Complex, NE Minnesota *in* Ojakangas, R.W., ed., Precambrian geology of the southern Canadian shield and the eastern Baltic shield: Minnesota Geological Survey Information Circular 34, p.73-74.
- Nelson, S.L., Sutley, S.J., and Tripp, R.B., 1992, Chemical and mineralogical analyses and geological characteristics of heavy minerals from glaciofluvial sediments in Minnesota: test and pilot study data: Minnesota Department of Natural Resources, Division of Minerals Open-File Report 284, (A cooperative project with the U.S. Geological Survey), 100 p.
- Ojakangas, R.W., and Matsch, C.L., 1982, Minnesota's geology: University of Minnesota Press, Minneapolis, 255 p.
- Olsen, B.M., and Mossler, J.M., 1982, Geologic map of Minnesota: Depth to bedrock: Minnesota Geological Survey State Map Series S-14, scale 1:1,000,000.
- Parham, W.E., 1972, A possible peneplain of early late Cretaceous age in Minnesota, *in* Field trip guidebook for geomorphology and Quaternary stratigraphy of western Minnesota and eastern South Dakota: Minnesota Geological Survey Guidebook Series No. 7, p. 58-68.
- Pennington, J.W. and Davis, V.C., 1953, Investigations of iron sulfide deposits in south central Aitkin County and Carlton County, Minnesota: U.S. Bureau of Mines Report of Investigations 4937, 33 p.
- Setterholm, D.R., 1990, Geologic maps of the Late Cretaceous rocks, southwestern Minnesota: Minnesota Geological Survey Miscellaneous Map Series M-69, scale 1:750,000.
- Severson, M.J. and Barnes, R.J., 1991, Geology, mineralization, and geostatistics of the Minnamax/Babbitt CU-NI deposit (Local Boy Area), Minnesota, Part II: Mineralization and geostatistics: Natural Resources Research Institute, University of Minnesota-Duluth, Technical Report NRR/ITR-91/13b
- Severson, M.J., 1995, Geology of the southern portion of the Duluth Complex: Natural Resources Research Institute, University of Minnesota-Duluth, Technical Report NRR/ITR-95/26.
- Shettel, D.L., Jr., and O'Hara, P.F., 1992, Reevaluation of geochemical data from east central Minnesota: Prepared for the Minnesota Department of Natural Resources, Division of Minerals, Hibbing, 69 p.
- Shilts, W.W., and Kaszycki, C.A., 1986, Depth of glacial erosion: Ottawa, Atomic Energy of Canada Limited, 31 p.

- Sims, P.K., and Morey, G.B., eds., 1972, *Geology of Minnesota: A centennial volume*: Minnesota Geological Survey, 632 p.
- Sinclair, A.J., 1983, Univariate analysis *in* Howarth, R.J., ed., *Handbook of exploration geochemistry, Volume 2, Statistics and data analysis in geochemical prospecting*: Elsevier Scientific Publishing Company, New York, p. 68-69.
- Smith, N.D., 1985, Proglacial fluvial environment, *in* Ashley, G.M., Shaw, J., and Smith, N.D., eds., *Glacial sedimentary environments*: Tulsa, S.E.P.M., p. 85-134.
- Southwick, D.L., Meyer, G.N., and Mills, S.J., 1986, *Scientific core drilling in central Minnesota: Summary of lithologic and geochemical results*: Minnesota Geological Survey Information Circular 23, 186 p.
- Southwick, D.L., Morey, G.B., and McSwiggen, P.L., 1988, *Geologic map of the Penokean orogen, central Minnesota*: Minnesota Geological Survey Report of Investigations 37, 25 p., map scale 1:250,000.
- Southwick, D.L., 1989, An introduction to Minnesota's geologic framework and its implications for mineral exploration, *in* Morey, G.B., ed., *Workshop on the applicability of gold and platinum-group-element models in Minnesota*: Minnesota Geological Survey Information Circular 30, p. 1-6.
- Southwick, D.L., Setterholm, D.R., and Boerboom, T.J., 1990, *Scientific test drilling in west-central Minnesota: Summary of lithologic and stratigraphic results 1987-1988, and some preliminary geological conclusions*: Minnesota Geological Survey Information Circular 31, 98 p.
- Southwick, D.L., and Morey, G.B., 1991, *Precambrian geologic framework in Minnesota* *in* Ojakangas, R.W., ed., *Precambrian geology of the southern Canadian Shield and the eastern Baltic Shield: U.S.A.-U.S.S.R.—Canada Joint Seminar, August 21-23, 1990, Duluth, Minnesota*: Minnesota Geological Survey Information Circular 34, p. 49-57.
- Southwick, D.L., compiler, 1993, *Geologic map of Archean bedrock, Soudan-Bigfork area, northern Minnesota*: Minnesota Geological Survey Miscellaneous Map Series 79, scale 1:100,000.
- Spector, A., 1992, *Report on aeromagnetic data interpretation Shephard Area, Minnesota: Prepared for Minnesota Department of Natural Resources, (Division of Minerals)*: Allan Spector and Associates Ltd., Toronto, Canada, 18 p., 9 pl.
- Spector, A., 1993, *Report on aeromagnetic data interpretation Shephard Area extension (Minnesota): Prepared for the Minnesota Department of Natural Resources, (Division of Minerals)*: Allan Spector and Associates Ltd., Toronto, Canada, 15 p., 7 pl.
- Spector, A., 1994, *Report on aeromagnetic data interpretation Long Prairie area (Minnesota): Prepared for the Minnesota Department of Natural Resources, (Division of Minerals)*: Allan Spector and Associates Ltd., Toronto, Canada, 13 p., 7 pl.

Spector, A., 1995a, Report on aeromagnetic data interpretation Camp Ripley area (Minnesota): Prepared for the Minnesota Department of Natural Resources, Division of Minerals: Allan Spector and Associates Ltd., 12 p., 7 pl.

Spector, A., 1995b, Report on aeromagnetic data interpretation western Duluth Complex (Minnesota): Prepared for the Minnesota Department of Natural Resources, Division of Minerals: Allan Spector and Associates Ltd., 15 p., 19 pl.

Sugden, D.E., 1978, Glacial erosion by the Laurentide Ice Sheet: *Journal of Glaciology*, v. 20, p. 367-391.

VanTrump, G., Jr., and Miesch, A.T., 1977, The U.S. Geological Survey RASS-STATPAC system for management and statistical reduction of geochemical data: *Computers and Geosciences*, v. 3, p. 475-488.

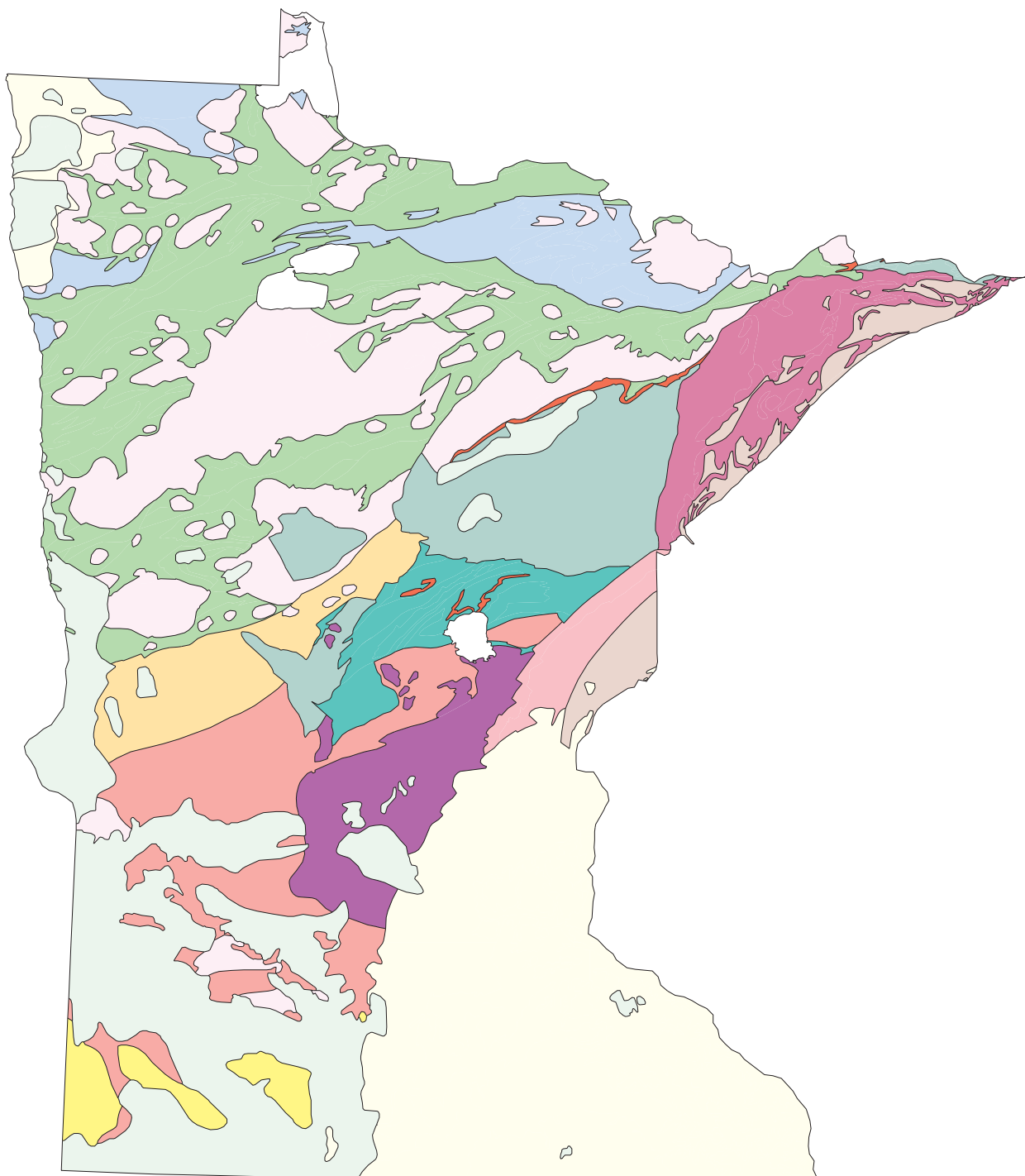
Winter, T.C., Cotter, R.D., and Young, H.L., 1973, Petrography and stratigraphy of glacial drift, Mesabi Iron Range area, northeastern Minnesota: U.S. Geological Survey Bulletin 1331-C, 41 p.

Witzke, B.J., Ludvigson, G.A., Poppe, J.R., and Ravn, R.L., 1983, Cretaceous paleogeography along the eastern margin of the western interior seaway, Iowa, southern Minnesota, and eastern Nebraska and South Dakota, *in* Reynolds, M.W., and Dolly, E.D., eds., *Mesozoic paleogeography of west-central United States*: Denver, S.E.P.M., Rocky Mountain Section, p. 225-252.

Wright, H.E., Jr., 1972, Quaternary history of Minnesota, *in* Sims, P.K., and Morey, G.B., eds., *Geology of Minnesota: A centennial volume*: Minnesota Geological Survey, p. 515-547.

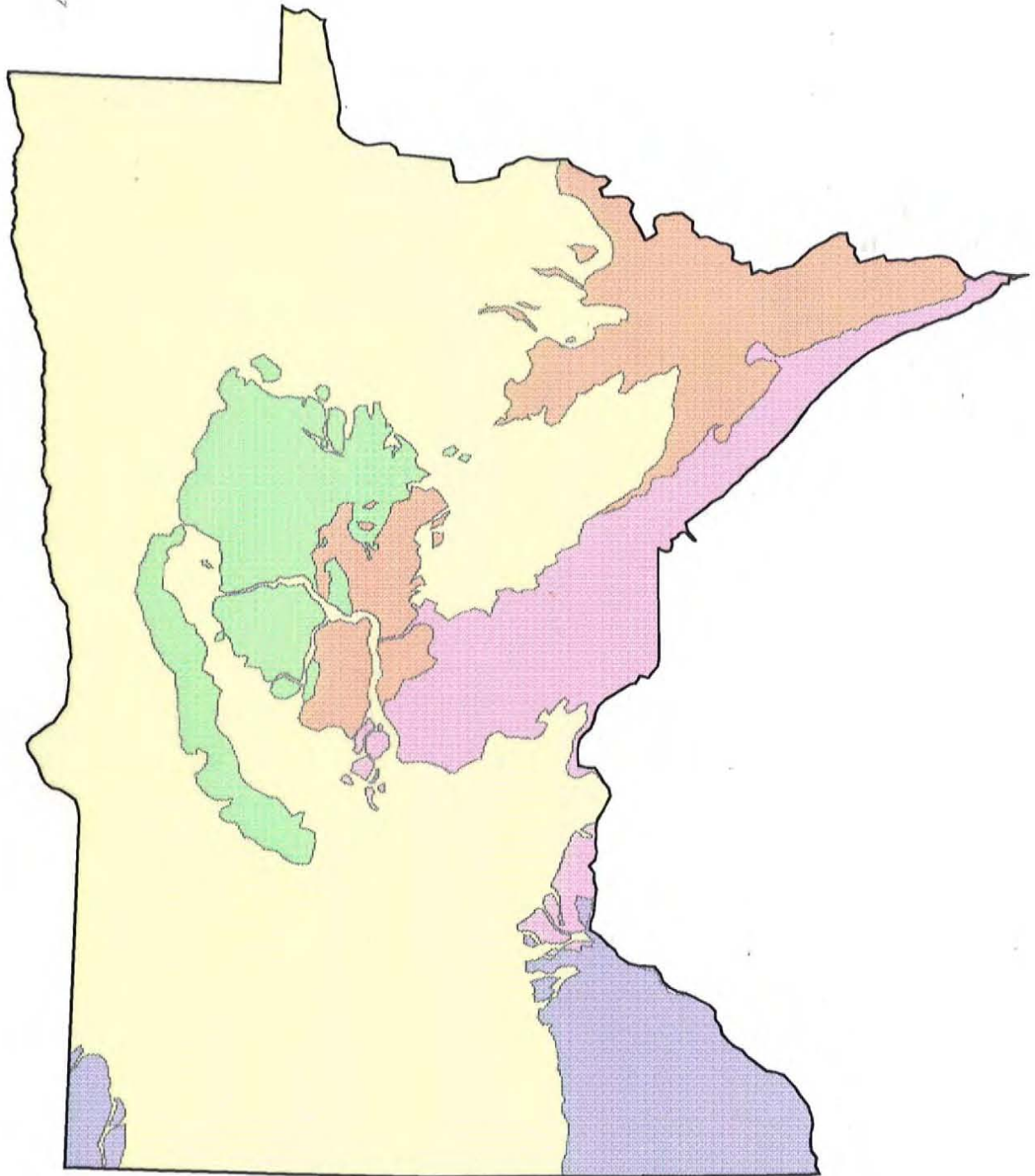
APPENDIX A

GENEALOGY OF GEOLGYN





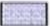


Mesozoic	Middle Proterozoic	Early Proterozoic	Later Archean	Middle Archean gneiss
Paleozoic	Sediments	Intrusions	Migmatite	
	Intrusives	Animikie Group	Greenstone belts	
		Iron Formation	"Quiet zone"	
		Fold and thrust belt		

APPENDIX B
GENERALIZED QUATERNARY GEOLOGY



LOBE SEDIMENTS

- | | | | | |
|---|--|--|--|--|
|  Rainy |  Superior |  Wadena |  Des Moines |  Undifferentiated |
|---|--|--|--|--|